

EFFECT OF VISCOSITY-COMPRESSIBILITY PRODUCT VARIATION ON THE
ANALYSIS OF FRACTURED WELL PERFORMANCES IN TIGHT
UNCONVENTIONAL RESERVOIRS

by

Caglar Komurcu

A thesis submitted to the Faculty and the Board of Trustees of the Colorado School of Mines in partial fulfillment of the requirements for the degree of Master of Science (Petroleum Engineering).

Golden, Colorado

Date _____

Signed: _____

Caglar Komurcu

Signed: _____

Dr. Erdal Ozkan

Thesis Advisor

Golden, Colorado

Date _____

Signed: _____

Dr. Ramona M. Graves

Professor, Petroleum Engineering

Dean, College of Earth Resource Sciences and Engineering

ABSTRACT

This research study for a Master of Science degree has been conducted under the Unconventional Reservoir Engineering Project (UREP) at the Marathon Center of Excellence for Reservoir Studies (MCERS) in the Petroleum Engineering Department of Colorado School of Mines. The main objective of the research is to investigate the effect of pressure-dependent viscosity-compressibility product on the analysis of fractured, tight-gas well performances.

Pressure drops required to economically produce fractured, tight-gas wells may be in the thousands of psi. Under these conditions, the gas compressibility-viscosity product may exhibit variations 3 to 10 times greater than the initial values in the vicinity of the fracture and have a significant impact on the observed rate-time behavior. Consequently, solutions and procedures used in conventional gas-well performance evaluation, which assume negligible variation of the viscosity-compressibility product, yield lower than expected permeability values. Further, since most of the property variation occurs very close to the fracture surface, accurately modeling their effects using finite difference methods is difficult due to severe time-step restrictions to ensure numerical stability and/or accuracy.

In this research, analytical, semianalytical, and numerical models are used. The spectral solution was developed by Thompson (2014), but has not been reported earlier. It is verified and used to observe the effects of variable viscosity-compressibility product in the analysis of fractured, tight-gas well performances in this thesis. In addition, a new perturbation solution is developed to discuss the validity of the superposition time in the analysis of nonlinear, tight-gas well performances. Data obtained from a commercial simulator (Eclipse) and numerical results from existing fully analytical solutions for constant viscosity-compressibility product are used for the verification of the new solutions. A similarity solution for infinite-acting reservoirs, provided by Thompson (2014), is also used in the verifications. Comments are made on the advantages and disadvantages of the numerical solutions.

The new solutions presented in this thesis demonstrate the shortcomings of the existing solutions and procedures in the analysis of fractured, tight-gas well performances. It is shown that the conventional definition of the superposition time is not accurate enough for tight-gas wells. Based on the new solutions, guidelines are provided to improve the analysis of fractured, tight-gas well performances.

TABLE OF CONTENTS

ABSTRACT.....	iii
LIST OF FIGURES	vii
LIST OF TABLES	ix
LIST OF SYMBOLS	x
ACKNOWLEDGEMENTS	xii
CHAPTER 1 INTRODUCTION	1
1.1 Motivation.....	2
1.2 Objectives	3
1.3 Method of Study	4
CHAPTER 2 BACKGROUND AND LITERATURE REVIEW	5
2.1 Analytical Modeling	6
2.2 Numerical Modeling.....	8
2.2.1 Finite Difference Methods	8
2.2.2 Finite-Element Methods.....	9
2.2.3 Boundary-Element Methods	9
2.2.4 Spectral Methods	9
2.3 Specialized solutions for Tight-Gas Reservoirs.....	10
2.3.1 Constant rate solution	11
2.3.2 Constant pressure solution	12
2.3.3 Superposition Solution.....	13
2.3.4 Rate Normalization	15
2.3.5 Superposition time	16
2.3.6 Material Balance time	17

CHAPTER 3 CONVENTIONAL FORMULATION AND SOLUTION OF GAS-FLOW IN POROUS MEDIA	19
3.1 Problem Formulation	19
3.2 Analytical Solution using Laplace Transforms.....	23
3.2.1 General Solution	23
3.2.2 Infinite Systems	24
3.2.3 Bounded Systems.....	25
3.3 Similarity Solution	26
3.4 Solution Procedure.....	31
CHAPTER 4 SPECTRAL SOLUTION OF 1D GAS FLOW IN POROUS MEDIA	33
4.1 Problem Formulation	33
4.2 Solution.....	36
CHAPTER 5 A PERTURBATION SOLUTION	39
5.1 Problem Formulation	39
5.2 Solution of the Perturbation Problem	40
5.3 Computational Procedure.....	54
CHAPTER 6 VERIFICATION OF THE SPECTRAL SOLUTION AND APPLICATIONS	57
6.1 Comparison of the Analytical (Similarity) and Spectral Solutions	59
6.2 Comparison of the Spectral Solution with a Commercial Simulator.....	60
6.3 Comparison of Constant and Variable Viscosity-Compressibility product.....	63
6.4 Correction Factors for Square-Root-of-Time and Superposition-Time Analyses	66
6.4.1 Correction Factors for Infinite-Acting Reservoirs	66
6.4.1.1 Correction Factor for Square Root of Time Analysis.....	66
6.4.1.2 Correction Factor for Superposition-Time Analysis.....	69
6.4.2 Correction Factors for Bounded Reservoirs	72

6.5	Validity of Spectral Solution for Variable Pressure Production.....	74
6.6	Sensitivity Analysis of Spectral Solution	76
CHAPTER 7 APPLICATIONS OF THE NEW SUPERPOSITION TIME		79
7.1	Case 1 - Linear Pressure Decline Based on the Rational Model	79
7.2	Case 2 – Nonlinear Decline	82
CHAPTER 8 CONCLUSIONS AND RECOMMENDATIONS.....		85
8.1	Conclusions.....	85
8.2	Recommendations for Future Work.....	86
WORKS CITED		87

LIST OF FIGURES

Figure 2.1: Constant vs. Variable Viscosity-Compressibility product (Thompson, 2012).	7
Figure 2.2: Constant-rate solution.....	11
Figure 2.3: Rate-normalized pseudo-pressure vs. square root of time.	13
Figure 2.4: Material Balance time.	17
Figure 6.1: Gas property correlations used in this work.....	57
Figure 6.2: Spectral Solution Algorithm.....	58
Figure 6.3: Spectral and Analytical Models match.....	59
Figure 6.4: Gas flow rate vs. time obtained from the spectral and analytical solutions.	60
Figure 6.5: Logarithmic grid sizes of the Eclipse model.....	61
Figure 6.6: Eclipse vs. spectral model results for constant pressure production.	61
Figure 6.7: Bottomhole pressures for the variable-pressure-production scenario generated by the Weibull regression model.	62
Figure 6.8: Comparison of the results of Eclipse and the spectral model for variable- pressure production with skin.	63
Figure 6.9: Constant vs. variable viscosity-compressibility product comparison for constant pressure production ($p_{wf} = 1000$ psia).....	64
Figure 6.10: Rate-normalized pseudo-pressure vs. square root of time for constant and variable viscosity-compressibility product scenarios: Constant pressure production ($p_{wf} = 1000$ psia).	64
Figure 6.11: Square root of time plot to calculate $\sqrt{k}x_f$ for constant $p_{wf,c}$ values of 1000, 2000, 3000 and 4000 psia.	67
Figure 6.12: Correlation for the new correction factor for the square-root-of-time analysis.....	68
Figure 6.13: Superposition time plot to calculate $\sqrt{k}x_f$ for constant $p_{wf,c}$ values of 1000, 2000, 3000 and 4000 psia.	70

Figure 6.14: Calculation of new correction value for superposition time slope.	71
Figure 6.15: Boundary effects on square root of time plot.	72
Figure 6.16: Boundary effects on superposition time plot.	73
Figure 6.17: Boundary effects on square root of time plot.	74
Figure 6.18: Square root of time plot for variable pressure production.	75
Figure 6.19: Superposition time plot variable pressure production.	75
Figure 6.20: Variable Pressure production with Weibull regression model to analyze Spectral Solution sensitivity.	76
Figure 6.21: Constant viscosity-compressibility solution for 10, 75, and 150 collocation points for variable-pressure production case.	77
Figure 6.22: Variable viscosity-compressibility solution for 10, 75, and 150 collocation points for variable-pressure production.	77
Figure 7.1: Wellbore pressure and flow rate as a function of time for Case 1.	80
Figure 7.2: Square-root-of-time analysis of Case 1.	80
Figure 7.3: Comparison of the conventional and new, gas superposition time analyses - Case 1.	81
Figure 7.4: The bottomhole pressures from the Weibull model and the corresponding flow rate trend - Case 2.	83
Figure 7.5: Comparison of the new and conventional superposition time solution - Case 283
Figure 7.6: Square root of time analysis - Case 2.	84

LIST OF TABLES

Table 6.1: Reservoir and Fluid Data	57
Table 6.2: Wellbore Boundary Condition Models.....	58
Table 6.3: Square root of time analysis of the four Variable Compressibility-Viscosity product scenarios	65
Table 6.4: Calculated kx_f values and error percentages with correction factor proposed by Ibrahim and Wattenbarger	68
Table 6.5: Calculated kx_f values with the new Square root of time correction factor.....	69
Table 6.6: Calculated kx_f values and error percentages with the correction factor proposed by Ibrahim and Wattenbarger (2006).....	70
Table 6.7: Calculated kx_f values with the new superposition time correction factor	71
Table 6.8: Square root of time analysis for the Bounded system	73
Table 7.1: Comparison of the specialized solutions and the new method - Case 1	82
Table 7.2: Comparison of the specilazed solutions and the new method - Case 2	84

LIST OF SYMBOLS

c_g	:	Gas compressibility, psia ⁻¹
c_{gi}	:	Initial gas compressibility, psia ⁻¹
C_k	:	Cardinal function
c_r	:	Rock compressibility, psia ⁻¹
c_t	:	Total compressibility, psia ⁻¹
$D_{i,k}$:	Chebyshev differentiation matrix
h	:	Reservoir height, ft
h_f	:	Fracture height, ft
k	:	Permeability, md
L_D	:	Dimensionless Length
L_e	:	Reservoir Length, ft
m_D	:	Dimensionless pseudo-pressure drop with constant reference rate
m_k	:	Pseudo-pressure at the Gauss-Lobatto point, psia ² /cp
$m(p)$:	Real gas pseudo-pressure, psia ² /cp
m_{wf}	:	Variable rate pseudo-pressure drop, psia ² /cp
m_{wcu}	:	Unit Constant rate pseudo-pressure drop, psia ² /cp
m'_{wcu}	:	Derivative of the Unit Constant rate pseudo-pressure drop, psia ² /cp
p	:	Pressure, psia
p_i	:	Initial reservoir pressure, psia
p_{\min}	:	Minimum bottomhole pressure, psia
p_{\max}	:	Maximum bottomhole pressure, psia
p_{wf}	:	Bottomhole pressure, psia
Q	:	Cumulative gas production, scf
q	:	Variable rate, scf/day

q_D	:	Dimensionless rate
q_{sf}	:	Sandface rate, scf/day
s	:	Dimensionless skin factor
T	:	Reservoir Temperature, °R
t	:	Time, day
t_D	:	Dimensionless time
T_k	:	Chebyshev polynomial of degree k
t_{MB}	:	Material balance time, day
u_D	:	Dimensionless Laplace variable
x_f	:	Fracture half length, ft
x_{max}	:	Pressure influence distance in reservoir, ft
x_n	:	n^{th} collocation point
Z	:	Gas Deviation Factor

Greek Symbols

γ_g	:	Specific gas gravity
Δm_{su}	:	Unit rate skin pseudo-pressure drop, psia ² /cp
Δm_w	:	Real gas Pseudo-pressure for variable flow rate production
Δm_{wc}	:	Real gas Pseudo-pressure for constant flow rate production
ζ	:	Spatial coordinate system coefficient
η	:	Diffusivity constant
μ	:	Viscosity, cp
μ_i	:	Initial viscosity, cp
ξ	:	Unique function
ρ_g	:	Gas density, lbm/ft ³
ϕ	:	Porosity
φ_n	:	Pseudospectral test function

ACKNOWLEDGEMENTS

I would like to express my deepest appreciation and thanks to my advisor Dr. Erdal Ozkan, for his valuable guidance, intellectual contributions and patience. Without his supervision and mentorship this thesis study would not have been possible. Furthermore, I would like to thank Dr. Leslie Thompson for introducing me this topic, helping me with my study and providing valuable input and solutions throughout the entire research. I would also like to thank Dr. Azra Tutuncu, chair of the committee, for her time and useful comments, remarks and suggestions. All of you have been there to guide me from beginning to end of this study.

This research and Master of Science education is sponsored by the Turkish Petroleum Company. I would like to thank the TPAO for providing me this opportunity.

I am also grateful to my father, Kasim Komurcu, my mother, Cemile Komurcu and my sisters Pinar and Damla Komurcu for always being there for me and making their presences felt even if they are many miles away from me. I would also like to express my special thanks to Afitap Kutluhan for her motivational support, being beside me and believing me for the last year during my study at Colorado School of Mines.

I would like to say thanks to my friends for their contribution and support to this study, namely: Basar Basbug, Sinan Oz, Ozlem Ozcan and Filiz Geren.

Finally, I would like to thank those closest to me, whose presence made this journey enjoyable every other day in Golden. Special thanks to Onur Conger, Hakan Corapcioglu, Ezgi Karasozen, Sarp Ozkan, Mehmet Ali Torcuk, Max Willis, Caglar Yesiltepe and the Kaya family. Their unconditional support has been essential all these years.

CHAPTER 1

INTRODUCTION

This thesis has been prepared for the partial fulfillment of the requirements for a Master of Science degree in the Petroleum Engineering Department of the Colorado School of Mines. The research work has been conducted under the Unconventional Reservoir Engineering Project (UREP) at the Marathon Center of Excellence for Reservoir Studies (MCERS). The main objective of the research is to investigate the effect of pressure-dependent viscosity-compressibility product on the analysis of hydraulically fractured well performances in tight, unconventional, gas reservoirs and provide guidelines to improve the analysis and interpretation of pressure and production data.

Hydraulic fracture technology is a must to have economical flow rates in tight, unconventional, gas reservoirs. Despite hydraulic fracturing, large pressure gradients are required to produce the gas stored in the small pore spaces of the tight matrix causing considerable pressure drop during production. The most notable consequence of high-pressure drop in gas wells is to decrease the reservoir pressure to levels where the viscosity-compressibility product becomes highly dependent on pressure. Both analytical and numerical solutions used to model flow of real gases in porous media have shortcomings under these conditions. Consequently, conventional models predict inaccurate production rates and the conventional analysis approaches infer unrealistic reservoir conditions.

This thesis will investigate the effect of pressure-dependency of the gas viscosity-compressibility product in five chapters. This first chapter provides an introduction to the research topic, which presents the motivation, objectives, and the method of the research. Chapter 2 provides the background of the study together with a literature review. In Chapter 3, the conventional formulation of the gas-flow problem in porous media is documented and the transformations and solutions used for the conventional gas-well performance analysis are introduced. Chapters 4 and 5 introduce the spectral and perturbation solutions of the fractured, tight-gas wells, respectively, which are the central new contributions of this thesis work. The verification of the spectral solution and its applications are documented in Chapter 6. Chapter 7 discusses the use of the perturbation solution explained in Chapter 5 for the development of a

new gas superposition time. Finally, Chapter 8 sums up the results of this work and presents the conclusions and recommendations for future research.

1.1 Motivation

Multi-fractured tight-gas-well performances can be analyzed by numerical or analytical methods according to the complexity of conditions. Analytical methods are the most frequently used tools because of their relative simplicity and less data requirement; however the nonlinearity of the problem when the viscosity-compressibility product becomes a considerable function of pressure complicates or deters the analytical solution efforts. Numerical solutions, which discretize the space-time domain to approximate the problem, may be an option to handle the nonlinearity of the problem at the expense of numerical errors caused by the restrictive grid and time-step requirements.

Moreover, analytical methods provide a closed-form solution, which is the preferred form for the investigation of the functional dependencies of the parameters involved, whereas numerical simulations represent the model behavior in terms of the distribution of the parameter values over a pre-assigned space-time grid, which usually limits the ability to make explicit observations of functional behaviors. In principle, both procedures may provide acceptable solutions under certain conditions, but the approximations and assumptions used in the solutions make the applicability of these solutions to most tight gas well cases questionable.

The improvements required to make numerical models more accurate for the prediction of tight-gas reservoir performances are mostly related to grid and time step selection issues. These improvements usually result in computationally less efficient and practically less desirable simulation models. On the other hand, the realities of the field applications, regarding data needs and ease of application, impose the use of analytical tools more often, at least for initial investigations. Furthermore, the computational efficiency of numerical models is an area of research by itself and outside the scope of this thesis.

Therefore, the motivation of this research is the need to improve the analytical tools of performance prediction and data analysis for tight-gas wells and to provide guidelines regarding the application ranges and interpretations. To this end, the nonlinearity of the real-gas flow equation has always been one of the most fundamental problems. Linearization of the gas-diffusion equation by pseudo-pressure transformation does not provide an adequate practical

solution when the viscosity-compressibility product becomes a strong function of pressure, which is the most common condition in tight, unconventional gas fields.

A related problem is the analysis of variable-pressure, variable-rate data, which is the most common type of tight gas-well data. Traditionally, variable-pressure, variable-rate data are handled by superposition, which requires a linear problem. This makes the application of the common procedures such as superposition time moot. Therefore, a rigorous investigation of the variable-pressure, variable-rate problem in tight, unconventional gas wells is expected to shed light to the ranges of applicability of the superposition time analyses.

1.2 Objectives

The general objective of this research is to improve the analysis of tight-gas well performances under the effect of highly variable viscosity-compressibility product. Specifically, it addresses the problems caused by the nonlinearity of the diffusion equation at relatively low pressures, which cannot be handled by the conventional pseudo-pressure transformation. Because the source of the problem is the strong pressure dependency of the viscosity-compressibility product at low pressures, obtaining more rigorous analytical or semianalytical solutions of the nonlinear gas-flow equation is a key objective. The improved solutions are used to delineate the problems encountered when unconventional gas-well performances are analyzed by the conventional techniques and to provide guidelines to improve the analysis of tight-gas well data.

The specific objectives of this study are the following:

- 1) Document the problems encountered and errors incurred in the analysis of tight-gas well performances by pseudo-pressure linearization
- 2) Present more rigorous semianalytical solutions to account for the nonlinearity caused by pressure-dependent viscosity-compressibility product
- 3) Verify the accuracy of the solutions by comparing with the results of a commercial numerical simulator.
- 4) Demonstrate the application of the improved analytical solutions

1.3 Method of Study

Although analytical and numerical solutions are also used, the general method of this research is semianalytical. In general, the semianalytical methods find a more rigorous solution of an approximate or idealized problem, whereas the numerical methods attempt to obtain an approximate solution for the more rigorous problem. In this study, numerical results are obtained from a commercial finite-difference simulator (Eclipse) (Schlumberger, 2013) and used for the comparison of the semianalytical solutions. Also, the computation of the semianalytical solutions may require some numerical techniques; however these do not change the fundamentally analytical nature of the solutions.

Several solutions are presented and used in this work. The solutions based on pseudo-pressure linearization and constant-rate production are standard and presented for convenience in comparisons. These solutions are derived either in real-time or Laplace-transform domain. For the solution of the nonlinear gas-flow problem, three methods are used. One of the methods uses a commercial numerical simulator. For this case, only the input data and information required to reproduce the results are presented. The other two solutions are semianalytical and documented in this thesis for the first time.

The first of the semianalytical solutions is courtesy of Thompson (2014) and uses spectral methods. The solution has not been published or documented earlier; the details of the derivation, in addition to the practical use and interpretations, are presented in this thesis for the first time. The second solution uses a perturbation approach for the solution of the 1D, nonlinear diffusion equation, which is similar to the method suggested by Baretto et al. (2012). This new solution forms the basis of the discussions on superposition time.

CHAPTER 2

BACKGROUND AND LITERATURE REVIEW

Modeling flow of real gases in porous media and the analysis of gas-well performance pose a challenge because of the nonlinearity of the governing flow equations. Common approaches to obtain solutions for gas-flow in porous media include numerical or analytical approximations. Numerical methods based on finite-difference approximations of the gas diffusion equation are usually used to handle complex reservoir conditions if data are available to characterize the reservoir and formation fluids in reasonable detail. When the reservoir complexity permits the use of simplifying assumptions, the data requirements hinder the use of numerical simulators, or a quick estimate or analysis of the well performances is intended, analytical solutions become the tools of choice. However, nonlinear problems are not amenable to analytical solutions unless some assumptions are made or some transformations are used.

The most common approach in the petroleum industry to obtain analytical solutions to real-gas flow in porous media is the use of pseudo-pressure transformation suggested by Al-Hussainy et al. (1966). With the additional assumption of negligible variation of the viscosity-compressibility product during production, the pseudo-pressure transformation linearizes the gas diffusion equation and permits the use of the standard solution techniques of oil diffusion equation. The original implementation of this approach was intended for the analysis of gas-well-test data or transient flow periods during which the reservoir pressure does not significantly deviate from the initial pressure.

Although it is well known (Raghavan, 1996) that the pseudo-pressure approach does not sufficiently linearize the gas diffusion equation during boundary-dominated flow, or in general, when large pressure drops are observed during production, it has been widely used in the analysis of tight, unconventional gas-reservoir performances where long production periods need to be considered and the corresponding pressure drop precludes the assumption of negligible variation of the viscosity-compressibility product. Some discrepancies in the literature have been noted in the analysis of the multi-fractured, tight, unconventional gas-well data based on the conventional pseudo-pressure linearization of the diffusion equation and the use superposition principle. However, a detailed discussion of the causes and consequences of these discrepancies has not been presented.

Below, the conventional gas-well flow models, assumptions, and transformations are presented and difficulties encountered in the analysis of gas-well data by the conventional models are highlighted. The basis of the superposition and material balance time concepts are also presented. Then, the backgrounds of the new analytical solutions presented in this thesis are given. This chapter also serves as a literature review for the thesis work.

2.1 Analytical Modeling

Classical analytical methods are based on the continuity equation for flow of real gases in porous media. Muskat (1937) developed the first solution by the method of successions of steady states. Al-Hussainy et al. (1966) obtained approximate analytical solutions for real gases by linearizing the flow equation. The following continuity equation for flow of real gases in porous media is obtained by combining the mass conservation equation, Darcy's law and the real-gas equation of state.

$$\frac{1}{r} \frac{\partial}{\partial r} \left(r \frac{p}{\mu Z} \frac{\partial p}{\partial r} \right) = \frac{\phi}{2.637 \times 10^{-4} k} \frac{\partial(p/Z)}{\partial t} \quad (2.1)$$

This equation is nonlinear and not amenable to analytical solutions unless some simplifying assumptions are made or the dependent variable is transformed to a new one, in which the partial differential equation becomes linear or weakly nonlinear.

Al-Hussainy et al. (1966) introduced the following “real gas pseudo-pressure” transformation, which accounts for the variation of viscosity and Z-factor with pressure to linearize the continuity equation.

$$m(p) = 2 \int_{p_i}^p \frac{p'}{\mu Z} dp' \quad (2.2)$$

Substituting Eq. 2.2 into Eq. 2.1 yields:

$$\frac{1}{r} \frac{\partial}{\partial r} \left(r \frac{\partial m}{\partial r} \right) = \frac{\phi c_t \mu}{2.637 \times 10^{-4} k} \frac{\partial m}{\partial t} \quad (2.3)$$

In terms of pseudo-pressure, Eq. 2.3 is still nonlinear because the compressibility and viscosity in the right hand side are functions of pressure. However, at relatively high pressures and when the pressure change is relatively small throughout the application, as in the pressure-

transient analysis during infinite-acting period, the change in the viscosity-compressibility product may be neglected and its value at the highest (initial) pressure may be used as a constant. Then, Eq. 2.3 is written as follows:

$$\frac{1}{r} \frac{\partial}{\partial r} \left(r \frac{\partial m}{\partial r} \right) = \frac{\phi c_{ii} \mu_i}{2.637 \times 10^{-4} k} \frac{\partial m}{\partial t} \quad (2.4)$$

Equation 2.4 has been successfully used for the analysis of pressure-transient behavior and short-term performances of conventional gas reservoirs. When there is a steep pressure decline, as in the boundary dominated flow periods, or when the transient flow lasts long to cause considerable pressure drop, as in fractured horizontal wells in shale, the constant compressibility-viscosity product assumption is not readily justifiable. In Fig. 2.1, the red continuous line depicts an example of the normalized variable viscosity-compressibility product changing by pressure. The dashed line in Fig. 2.1 is the value of the viscosity-compressibility product at the initial pressure and indicates the error caused by the constant viscosity-compressibility product assumption when pressure drops significantly over time.

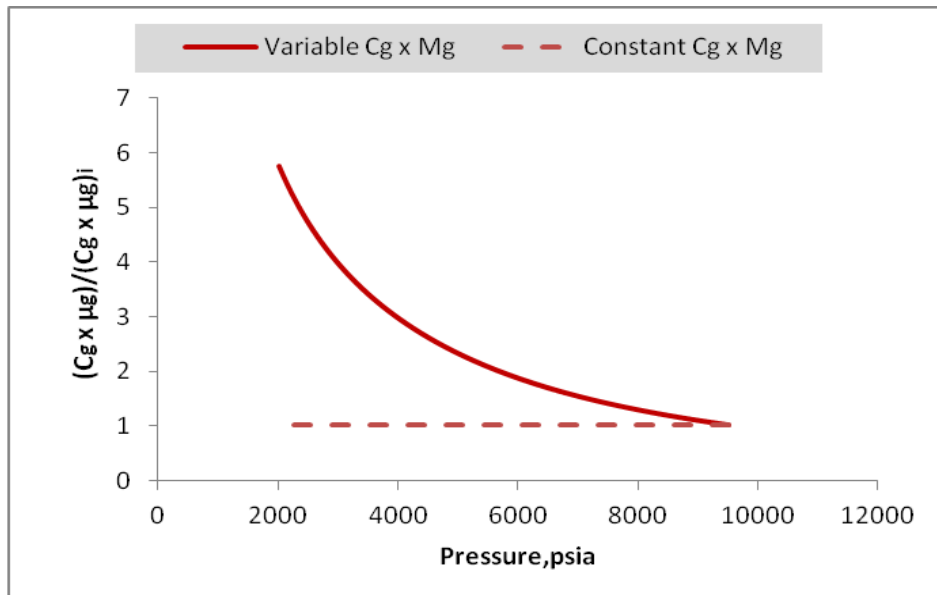


Figure 2.1: Constant vs. Variable Viscosity-Compressibility product (Thompson, 2012).

To obtain analytical solutions for Eq. 2.1, some other techniques have also been applied. Kale and Mattar (1980) presented an approximate constant rate solution for radial gas flow by the method of perturbation. Later, Peres et al. (1989) derived the exact solution for constant rate production in an infinite reservoir.

Gupta and Andsager's (1967) work was the first paper about superposition time for the analysis of variable-gas-rate data. In 1991, Samaniego and Cinco-Ley presented a method, which incorporates the effects of skin and high-velocity flow in the radial variable-rate-production solution for an infinite acting system. They used the step-function approximation of the flow rate for the derivation. More recently, Barreto et al. (2012) proposed a solution for variable rate and pressure-dependent fluid properties by using the Green's function method.

2.2 Numerical Modeling

Another approach used in the analysis of multi-fractured tight-gas well performance is numerical modeling. In petroleum industry, the most common approach for numerical modeling is the use of finite-difference approximations of flow equations. Although not as common, finite-element and boundary-element techniques are also used for the numerical solution of special problems of interest. In this research, a finite-difference simulator and a spectral method, which may be considered as a variant of finite-element techniques, will be used to obtain numerical solutions of the nonlinear gas-flow equation.

2.2.1 Finite Difference Methods

Finite-difference methods are one of the most common numerical solution methods used in petroleum engineering. The finite-difference simulators are commercially available or may be built in house for specific purposes. Despite their great capabilities, commercial simulators are not intended to capture all the physics because most of them are designed to solve more general problems. Furthermore, by nature, they provide an approximate solution because they approximate the partial differential equations by local algebraic difference equations (Press, W.H., Teukolsky, S.A., Vetterling, W.T. et al., 2007). To improve the accuracy of finite-difference solutions, very fine grids and very small time steps need to be used; however, all these features eventually extend the runtime and may increase the round-off errors. Also, available data, time and cost limitations, and the type of the analysis may sometimes restrict the use of detailed finite-difference simulators.

2.2.2 Finite-Element Methods

Finite-element techniques have also been used in petroleum engineering (e.g., Dalen, 1979; Young, 1981; Forsyth, 1990; and Fung et al., 1991; Durlofsky and Chien, 1993; Krogstad et al., 2011) parallel to their increased popularity in general engineering applications (Divo and Kassab, 2003). Although the bases of the finite-difference and finite-element approaches are different, their common feature is the discretization of the solution domain. The finite-element formulations can be derived from a statement of weighted residual for the solution of a field equation by successively weakening the derivative continuity requirement, which corresponds to the successive integration of the weighted residual statement (Cartwright, 2001). The first weak form provides the basis for the finite-element approach, which is equivalent to Green's second identity.

2.2.3 Boundary-Element Methods

Similar to the finite-element formulations, the boundary-element methods can be derived from a weighted residual solution of a field equation by successively weakening the derivative continuity requirement (Cartwright, 2001). While the first weak form provides the basis for the finite-element approach, the second weak form leads to the boundary element formulations. Despite their potential to provide near-analytical accuracy, these methods are less commonly used for reservoir flow modeling in petroleum engineering (Kikani and Horne, 1992; Sato and Horne, 1993a and 1993b; Zhou et al., 2013).

2.2.4 Spectral Methods

Spectral methods are another means of solving partial differential equations numerically. These methods are very powerful for smooth functions (exponential convergence) and derivatives. The most significant difference between spectral methods and finite-difference methods (FDMs) is that spectral methods approximate the solution, while FDMs approximate the equation that needs to be solved. The fact that the spectral methods approximate the solution is similar to finite-element methods (FEMs). However, the spectral methods' advantage over FEMs is that they approximate the solution as a linear combination of continuous functions that are generally nonzero throughout the domain (sinusoids or Chebyshev polynomials), whereas FEMs approximate the solution locally (Press, W.H., Teukolsky, S.A., Vetterling, W.T. et al., 2007).

Another benefit is that; it's very easy to incorporate nonlinear terms, which can represent fluid properties, pressure dependent permeability and non-darcy flow (Thompson, L., 2012).

Trefethen (2000) sums up concisely the strong sides of the spectral methods as follows: “If one wants to solve an ODE or PDE to high accuracy on a simple domain, and if the data defining the problem are smooth, then spectral methods are usually the best tool. They can often achieve 10 digits of accuracy where a finite difference (or finite element) method would get 2 or 3. At lower accuracies, they demand less computer memory than the alternatives.”

The main approach behind spectral methods is that the solution of nonlinear diffusion equations is given in the following form of an infinite series:

$$f(x) \approx f_N(x) = \sum_{n=0}^N a_n \phi_n(x) \quad (2.5)$$

A spectral method defines the solution as a truncated expansion in a set of basis functions as is expressed in Eq. 2.5. According to the solution type (periodic, non-periodic, or different types of domains), convenient basis functions need to be chosen and different choices of these basis functions give different flavors of spectral methods (Press, W.H., Teukolsky, S.A., Vetterling, W.T. et al., 2007).

2.3 Specialized solutions for Tight-Gas Reservoirs

Tight-gas fields generally show linear-flow behavior during their transient flow period. Muskat (1937) and Miller (1956) have done some of the earlier studies about this concept for different reservoir conditions. Linear-flow regime was investigated for both single and multiphase flow systems in Muskat's study. Later, Miller discussed the linear flow solutions for both infinite acting and bounded aquifer systems produced at constant rate or constant pressure. In 1982, Kohlhaas, del Giudice and Abbott claimed that linear flow can be seen in the early life of fractured wells, channel sands and wells between parallel faults. In addition to these studies, Stright and Gordon (1983) pointed out that linear flow regime can be seen for several years in the reservoirs with long narrow fractures, thin high permeability streaks, and long rectangular geometries. They also suggested that exponential-decline type curves could be used to understand boundary-dominated period.

Constant-rate solution and superposition-time approach are the bases of the most common methods for analyzing tight-gas well performances. Following sections discusses the shortcomings of these approaches for tight-gas systems.

2.3.1 Constant rate solution

Due to very low matrix permeability, tight-gas wells are usually stimulated to create high-conductivity hydraulic fractures with half-lengths reaching to the drainage boundary. Therefore, tight gas wells usually show linear flow behavior during the transient-flow period, which can last for several years. Constant-rate solutions are the bases of the approaches presented in literature to analyze these types of flows. Although gas wells' production data often show variable rate behavior, constant-rate solutions are useful for understanding how gas wells behave during the transient-flow period (Liang et al., 2011).

The solution for 1D linear flow toward an infinite conductivity fracture producing at constant rate is given by:

$$m_{wf} = \frac{200.5qT}{\sqrt{k(\phi c_i \mu)_i} h x_f} \sqrt{t} + \Delta m_s$$

where Δm_s is the pseudo-pressure drop in the skin zone. Eq. 2.6 indicates that gas pseudo-pressure plotted against square root of time on Cartesian coordinates should yield a straight line. As demonstrated in Figure 2.2, the slope of the straight line provides the formation permeability and its intercept yields the skin.

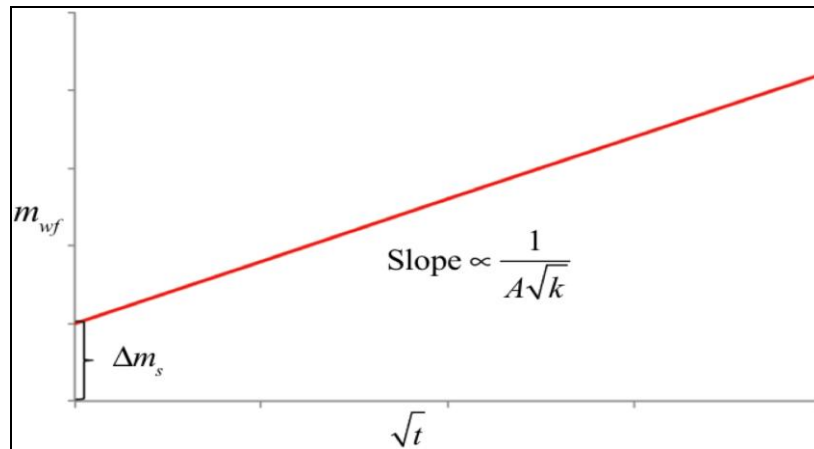


Figure 2.2: Constant-rate solution.

2.3.2 Constant pressure solution

Because of the field observations of approximately constant bottomhole flowing pressures during production from tight-gas wells, constant-pressure production solutions have also been of interest (in this case, the parameter of interest is the flow rate). Constant-pressure production solutions can be obtained from the formal solution of the initial-boundary-value-problem or by using the corresponding constant-rate solution in a superposition (or convolution) expression.

Wattenbarger et al. (1998) developed solutions and type curves for both constant-rate and constant-pressure production cases and pointed out that they are not the same. Then, they used the existing solutions to derive linear flow solutions for the constant-rate and constant-pressure production cases. Later, El-Banbi and Wattenbarger (1998) noted that the use of the constant-rate solution to analyze the performances of tight-gas wells producing at constant bottomhole pressure could cause up to 60% error.

In Fig. 2.3, the reciprocal flow rate is multiplied by the constant bottomhole pseudo-pressure drop $(m_{wf,c}/q)$ and plotted against the square root of time for an example constant-pressure production case.

Two straight lines with different slopes are displayed at early and late times in Fig. 2.3. The early time straight line follows the constant-rate production solution $(m_{wf,c}/q)$ and is given by:

$$\frac{m_{wf,c}}{q(t)} = \frac{200.5T}{\sqrt{k(\phi c_i \mu)_i h x_f}} \sqrt{t} \quad (2.6)$$

The late-time solution, on the other hand, deviates from the constant-rate solution and is given by (El-Banbi et al., 1998):

$$\frac{m_{wf,c}}{q(t)} \approx \frac{315T}{\sqrt{k\phi c_{ii} \mu_i h x_f}} \sqrt{t} \quad (2.7)$$

Thus, the slopes of the early- and late-time straight lines give the permeability value for constant pressure production as follows:

$$m = \frac{CT}{x_f \sqrt{k} h_f \sqrt{(\phi \mu c_t)_i}} \quad \text{where } C = \begin{cases} 200.5 & \text{for early time} \\ 315 & \text{for late time} \end{cases} \quad (2.8)$$

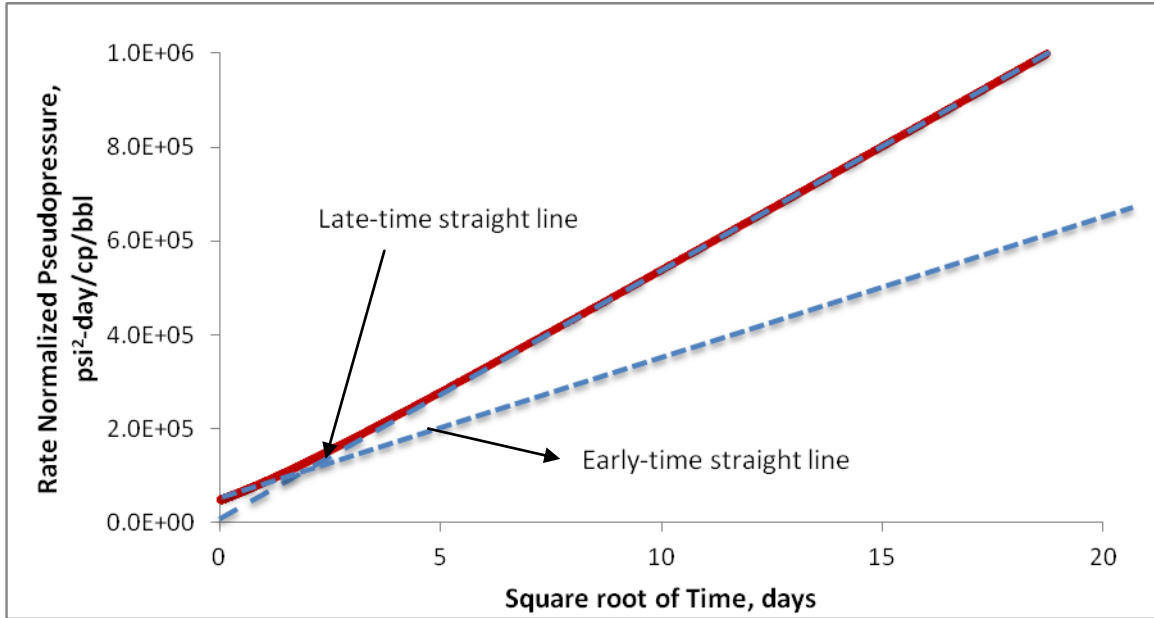


Figure 2.3: Rate-normalized pseudo-pressure vs. square root of time.

2.3.3 Superposition Solution

As mentioned earlier, tight gas wells mostly produce at variable-rate, variable-bottomhole-pressure condition. If the pseudo-pressure approach linearizes the real-gas continuity equation, then following convolution (Duhamel's equation/superposition) relation can be applied to develop solutions for the pseudo-pressure drop corresponding to a specified variable-rate production condition:

$$m_{wf}(t) = \int_0^t \frac{q(\tau)}{q_c} m'_{wf,q}(t-\tau) d\tau + \frac{q(t)}{q_c} \Delta m_s \quad (2.9)$$

where $m_{wf}(t)$ is the pseudo-pressure drop for the variable production rate of $q(t)$, $m'_{wf,q}(t-\tau)$ is the time derivative of the pseudo-pressure drop for the constant production rate of q_c , and Δm_s is the skin pseudo-pressure drop corresponding to the constant production rate of q_c .

q_c . Van Everdingen and Hurst (1949) discretized Eq. 2.10 to obtain the pressure drop for the variable-rate production problem (Δp_{wf}) from the summation of pressure drops for the constant-rate production problem ($\Delta p_{wf,q}$). Their approach is applied in terms of pseudo-pressure as follows:

Let us consider the sequence of time $0 = t_0 < t_1 < t_2 \cdots < t_n < t_{n+1} = t$ and write Eq. 2.10 as

$$m_{wf}(t) = \sum_{i=0}^n \int_{t_i}^{t_{i+1}} \frac{q(t')}{q_c} m'_{wf,q}(t-\tau) d\tau + \frac{q(t)}{q_c} \Delta m_s \quad (2.10)$$

For $t_i < t' < t_{i+1}$, if we approximate

$$q(t') \approx q(t_{i+1}) \equiv q_{i+1} \quad (2.11)$$

then, Eq. 2.11 becomes

$$m_{wf}(t) = \sum_{i=0}^n \frac{q(t')}{q_c} \int_{t_i}^{t_{i+1}} m'_{wf,q}(t-\tau) d\tau + \frac{q(t)}{q_c} \Delta m_s \quad (2.12)$$

or integrating

$$m_{wf}(t) \approx \sum_{i=0}^n \frac{q^{i+1}}{q_c} \left[m_{wf,q}(t-t^i) - m_{wf,q}(t-t^{i+1}) \right] + \frac{q^{n+1}}{q_c} \Delta m_s \quad (2.13)$$

Expanding and recalling that $t_0 = 0$ and $t_{n+1} = t$, we can rearrange Eq. 2.14 as follows:

$$\begin{aligned} m_{wf}(t) = & \frac{1}{q_c} \left\{ q^1 \left[m_{wf,q}(t) - m_{wf,q}(t-t^1) \right] \right. \\ & + q^2 \left[m_{wf,q}(t-t^1) - m_{wf,q}(t-t^2) \right] \\ & + q^3 \left[m_{wf,q}(t-t^2) - m_{wf,q}(t-t^3) \right] \\ & \vdots \\ & + q^n \left[m_{wf,q}(t-t^{n-1}) - m_{wf,q}(t-t^n) \right] \\ & \left. + q^{n+1} \left[m_{wf,q}(t-t^n) - m_{wf,q}(t-t^{n+1}) \right] + q^{n+1} \Delta m_s \right\} \end{aligned} \quad (2.14)$$

Because $m_{wf,q}(t-t^{n+1}) = m_{wf,q}(0) = 0$, we can rearrange Eq. 2.15 as follows:

$$m_{wf}(t) \approx q^1 \frac{m_{wf,q}(t)}{q_c} + \sum_{i=1}^n (q^{i+1} - q^i) \frac{m_{wf,q}(t-t^i)}{q_c} + q^{n+1} \frac{\Delta m_s}{q_c} \quad (2.15)$$

Van Everdingen and Hurst's solution has many applications in the literature. Walker (1968) defined transient rate behavior from the constant terminal pressure solution with superposition technique. His method calculated the reservoir pressure with the help of superposition principle from short shut-in period information for single-phase oil flow. His derivation was strictly limited to the undersaturated crude oil flow. Agarwal (1980) and Fetkovich and Vienot (1984) also developed variable-rate production solutions by using Van Everdingen and Hurst's approach. Later, Whitson and Sognesand (1986) investigated the limits of superposition by applying it to a well-test analysis with significant rate variation. Their study came up with recommendations of using pressure-transient and rate-time methods to estimate rock properties.

2.3.4 Rate Normalization

Rate normalization is an approximate procedure used in the analysis of variable-rate production problems. The basis of this approach is the approximation of the superposition solution given in Eq. 2.16 by making some assumptions.

Let us divide Eq. 2.16 by the last rate, $q(t) = q^{n+1}$. This yields:

$$\frac{m_{wf}(t)}{q(t)} \approx \frac{q^1}{q(t)} \frac{m_{wf,q}(t)}{q_c} + \sum_{i=1}^n \frac{(q^{i+1} - q^i)}{q(t)} \frac{m_{wf,q}(t-t^i)}{q_c} + \frac{\Delta m_s}{q_c} \quad (2.16)$$

If the rate varies smoothly, Eq. 2.13 may be approximated by (Raghavan, 1993)

$$\frac{m_{wf}(t)}{q(t)} \approx \frac{m_{wf,q}(t)}{q_c} + \frac{Dm_s}{q_c} \quad (2.17)$$

This indicates that the rate-normalized pseudo-pressure responses for variable flow rate can be approximated by the rate-normalized pseudo-pressure responses for constant flow rate. Because for linear flow,

$$\frac{m_{wf,q}(t)}{q_c} = \frac{200.5T}{\sqrt{k(\phi c_i \mu)_i} h x_f} \sqrt{t} \quad (2.18)$$

Eq. 2.18 yields

$$\frac{m_{wf}}{q} \approx \frac{200.5T}{\sqrt{k(\phi c_i \mu)_i h x_f}} \sqrt{t} + \frac{\Delta m_s}{q_c} \quad (2.19)$$

Eq. 2.20 indicates that a plot of rate-normalized pseudo-pressure vs. square root of time should yield a straight line with slope given by

$$m = \frac{200.5T}{\sqrt{k(\phi c_i \mu)_i h x_f}} \quad (2.20)$$

2.3.5 Superposition time

In order to analyze variable production rate data, constant rate solution can be used with the help of Duhamel's principle. If we substitute Eq. 2.19 into Eq. 2.17, we have

$$\frac{m_{wf}(t)}{q(t)} \approx \frac{200.5T}{\sqrt{k(\phi c_i \mu)_i h x_f}} \left[\frac{q^1}{q(t)} \sqrt{t} + \sum_{i=1}^n \frac{(q^{i+1} - q^i)}{q(t)} \sqrt{t - t^i} \right] + \frac{\Delta m_s}{q_c} \quad (2.21)$$

Therefore, a plot of rate-normalized pseudo-pressure $\left[m_{wf}(t)/q(t) \right]$ vs. the superposition time defined by

$$t_{\text{superposition}} = \left[\frac{q^1}{q(t)} \sqrt{t} + \sum_{i=1}^n \frac{(q^{i+1} - q^i)}{q(t)} \sqrt{t - t^i} \right] \quad (2.22)$$

yields a straight line with the slope

$$m_{\text{linear}} \approx \frac{200.5T}{\sqrt{k(\phi c_i \mu)_i h x_f}} \quad (2.23)$$

This is the basis of the analysis of variable flow rate tests by using the superposition time.

Cinco-Ley and Samaniego (1989) documented the advantages and limitations of the superposition time from the standpoint of flow regimes during the pressure build-up tests. In another application of superposition time, Ibrahim (2004) analyzed the long-term production data for different flow regimes using superposition time.

2.3.6 Material Balance time

In tight gas wells, production data generally consists of the change of the production rate in time for a constant or variable bottomhole pressure. On the other hand, constant flow rate solutions are the basis of the pressure-transient analysis theory and application. Palacio and Blasingame (1993) and later Agarwal et al. (1999) defined a material balance time, which converts the variable rate data to constant-pressure data. Physically, the material balance time is the time required for the well to flow at a constant rate to produce the actual amount of gas (Fig 2.4). Poe (2002) has also investigated the use of the material balance time especially for the linear flow regime using the constant pressure solution, rather than the constant rate solution, as a base model.

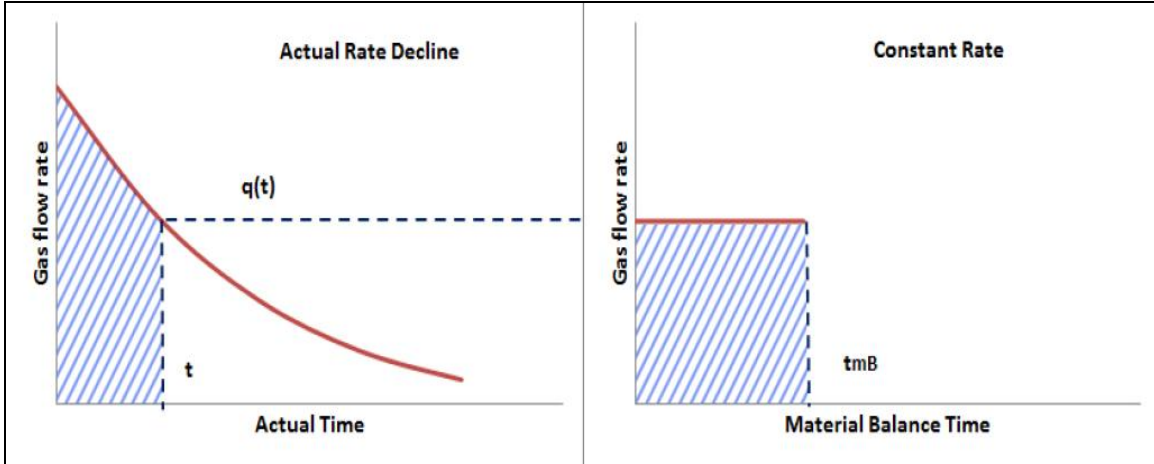


Figure 2.4: Material Balance time.

For liquid flow, material balance time can be defined as the ratio of cumulative production to instantaneous gas flow rate:

$$t_{MB} = \frac{Q}{q(t)} \quad (2.24)$$

For gas flow, because of the pressure-dependence of the viscosity-compressibility product, the material balance time is defined by (Palacio and Blasingame, 1993):

$$t_{MB} = \frac{(\mu_g c_g)_i}{q(t)} \int_0^t \frac{q(t)}{\mu_g c_g} dt \quad (2.25)$$

This definition requires the evaluation of the viscosity-compressibility product at the average reservoir pressure at time t . In turn, the estimation of the average pressure requires the knowledge of gas in place, which is usually one of the parameters of interest in the analysis. This leads to iterative procedures described by Palacio and Blasingame (1993) and Agarwal et al. (1998). In the later parts of this study, the material balance time is computed by using the viscosity-compressibility product at the wellbore pressure instead of the average reservoir pressure.

CHAPTER 3

CONVENTIONAL FORMULATION AND SOLUTION OF GAS-FLOW IN POROUS MEDIA

This chapter presents the classical formulation of the transient flow problem of real gases in porous media and introduces the common analytical solutions, which arise from assumptions under restricted conditions. The problem formulation and the solutions consider 1D linear flow of a real gas toward a fractured well. Following the problem formulation and the introduction of the pseudo-pressure transformation, first the solutions for infinite and bounded systems by Laplace transformation are presented. The Laplace-transformation solutions assume a linearized flow equation; that is, the variation of the viscosity-compressibility product is negligible. Then, a similarity-transformation solution is presented for infinite-acting systems, which takes into account the variation of the viscosity-compressibility product. This solution, however, is nonlinear and requires an iterative procedure for numerical computations.

3.1 Problem Formulation

Due to symmetry, considering half of the system, the gas diffusion equation and the boundary conditions are given as follows:

The real-gas diffusion equation:

$$C_1 \frac{\partial}{\partial x} \left(\rho_g \frac{k}{\mu_g} \frac{\partial p}{\partial x} \right) = \phi \rho_g c_g \frac{\partial p}{\partial t} \quad (3.1)$$

where $C_1 = (1.127 \times 10^{-3})(5.615)$ for the units on both sides of Eq.3.1 are $\frac{\text{lbm}}{\text{day-ft}^3}$.

The initial condition:

$$p(x, t = 0) = p_i \quad (3.2)$$

The outer boundary condition for an infinite-acting system:

$$\lim_{x \rightarrow \infty} p(x, t) = p_i \quad (3.3)$$

The outer boundary condition for a closed, finite (bounded system):

$$\left[\frac{\partial p}{\partial x} \right]_{x=L_x} = 0 \quad (3.4)$$

Finally, the prescribed constant-pressure inner boundary (production) condition is given by

$$p(x=0, t) = p_{wf}(t) \quad (3.5)$$

From the real gas equation of state, we know that,

$$\rho_g = \frac{pM}{zRT} \quad (3.6)$$

Then, Eq.3.1 can be written as follows:

$$C_1 \vec{\nabla} \left(\frac{p}{z} \frac{k}{\mu_g} \vec{\nabla} p \right) = \frac{\partial}{\partial t} \left(\phi \frac{p}{z} \right) \quad (3.7)$$

Consider the right hand side of Eq. 3.7:

$$\frac{\partial}{\partial t} \left(\phi \frac{p}{z} \right) = \frac{\partial}{\partial p} \left(\phi \frac{p}{z} \right) \frac{\partial p}{\partial t} = \left[\phi \frac{\partial}{\partial p} \left(\frac{p}{z} \right) + \left(\frac{p}{z} \right) \frac{\partial \phi}{\partial p} \right] \frac{\partial p}{\partial t} \quad (3.8)$$

and

$$\frac{\partial}{\partial p} \left(\frac{p}{z} \right) = \frac{z - p \frac{\partial z}{\partial p}}{z^2} \Rightarrow \left(\frac{1}{z} - \frac{p}{z^2} \frac{\partial z}{\partial p} \right) = \frac{p}{z} \left(\frac{1}{p} - \frac{1}{z} \frac{\partial z}{\partial p} \right) \quad (3.9)$$

We can write,

$$\frac{\partial}{\partial t} \left(\phi \frac{p}{z} \right) = \frac{p}{z} \left(\phi c_g + \frac{\partial \phi}{\partial p} \right) \frac{\partial p}{\partial t} = \frac{p}{z} \phi \left[c_g + \frac{1}{\phi} \frac{\partial \phi}{\partial p} \right] \frac{\partial p}{\partial t} \quad (3.10)$$

In Eq. 3.10, we have used the definition of gas compressibility given by

$$c_g = \left(\frac{1}{p} - \frac{1}{z} \frac{\partial z}{\partial p} \right) \quad (3.11)$$

Also using the definitions of the rock compressibility,

$$c_r = \frac{1}{\phi} \frac{\partial \phi}{\partial p} \quad (3.12)$$

and the total compressibility,

$$c_g + c_r = c_t \quad (3.13)$$

and we can write Eq. 3.7 as follows,

$$C_1 \vec{\nabla} \left(\frac{p}{z} \frac{k}{\mu_g} \vec{\nabla} p \right) = \phi c_t \frac{p}{z} \frac{\partial p}{\partial t} \quad (3.14)$$

To express the diffusion equation in Eq. 3.14 in terms of pseudo-pressure, we first multiply both sides by 2 to obtain,

$$C_1 \frac{\partial}{\partial x} \left(\frac{2p}{z} \frac{k}{\mu_g} \frac{\partial p}{\partial x} \right) = \phi \frac{2p}{z} c_t \frac{\partial p}{\partial t} \quad (3.15)$$

and then use the following real-gas pseudo-pressure (Al-Hussainy et al., 1966):

$$m(p) = \int_p^{p_i} \frac{2p'}{z\mu_g} dp' \quad (3.16)$$

The derivatives of the pseudo-pressure can be expressed as follows:

$$\frac{\partial m(p)}{\partial x} = - \frac{2p}{z\mu_g} \frac{\partial p}{\partial x} \quad (3.17)$$

that is,

$$\frac{\partial p}{\partial x} = \frac{\partial m(p)}{\partial x} \left(- \frac{z\mu_g}{2p} \right) \quad (3.18)$$

and

$$\frac{\partial p}{\partial t} = \frac{\partial m(p)}{\partial t} \left(- \frac{z\mu_g}{2p} \right) \quad (3.19)$$

Then, the diffusion equation is expressed in terms of pseudo-pressure as follows:

$$\frac{\partial^2 m(p)}{\partial x^2} = \frac{\phi c_t \mu_g}{C_1 k} \frac{\partial m(p)}{\partial t} \quad (3.20)$$

or

$$(3.21)$$

$$\frac{\partial^2 m(p)}{\partial x^2} = \frac{1}{\eta} \frac{\partial m(p)}{\partial t}$$

where the diffusivity, η , is defined by

$$\eta = \frac{C_1 k}{\phi c_i \mu_g} \quad (3.22)$$

If we convert the initial condition to pseudo-pressure, we have:

$$m[p(x, t = 0)] = m(p_i) \quad (3.23)$$

For an infinite-acting reservoir, the boundary conditions become:

$$\lim_{x \rightarrow \infty} m[p(x, t)] = m(p_i) \quad (3.24)$$

Similarly, for a finite system, the boundary condition is given by

$$\left[\frac{\partial m(p)}{\partial x} \right]_{x=L_x} = 0 \quad (3.25)$$

Finally, for the flowing wellbore pseudo-pressure, we have

$$m[p(x = 0, t)] = m[p_{wf}(t)] \quad (3.26)$$

Eq. 3.26 includes the pseudo-pressure drop, $\Delta m(p)_{skin}$, over a thin-skin zone on the surface of the fracture. We define a dimensionless thin-skin factor by

$$s = \frac{C_1 T_{sc} k h}{q_{sc} P_{sc} T z} \Delta m(p)_{skin} \quad (3.27)$$

From Darcy's Law, we have,

$$q_{sc} \rho_{sc} = q \rho = v A \rho = C_1 A \rho \frac{k}{\mu} \left(\frac{\partial p}{\partial x} \right)_{x=0} \quad (3.28)$$

where $A = 4x_f h$. Using Eqs. 3.6 and 3.18, we can write Eq. 3.28 as

$$q_{sc} = C_1 k A \frac{T_{sc}}{2 T P_{sc}} \left[\frac{\partial m(p)}{\partial x} \right]_{x=0} \quad (3.29)$$

Using Eqs. 3.29, Eq. 3.27 can be rearranged as follows:

$$\Delta m(p)_s = -\frac{As}{2h} \left[\frac{\partial m(p)}{\partial x} \right]_{x=0} \quad (3.30)$$

Finally, the wellbore flowing pseudo-pressure including skin effect, Eq. 3.26, can be written as follows,

$$m[p_{wf}(t)] = m[p(0,t)] - \frac{As}{2h} \left[\frac{\partial m(p)}{\partial x} \right]_{x=0} \quad (3.31)$$

3.2 Analytical Solution using Laplace Transforms

Laplace transformation is a common solution procedure for transient flow problems in porous media (Van Everdingen and Hurst, 1949; and Carslaw and Jaeger, 1959). However, the application of Laplace transformation is limited to linear problems. If the assumptions that $(c_g \mu_g)$ is constant and $(c_g \mu_g) \approx (c_g \mu_g)_i$ hold, then the solution of the gas diffusion equation in terms of pseudo-pressure can be obtained by Laplace transformation. The solutions obtained in the Laplace transform domain cannot be conveniently inverted into the time domain and numerical inversion is the preferred option. In this thesis, the numerical Laplace inversion algorithm proposed by Abate and Valko (2004) has been used.

Below, we first present the derivation of the general solution. The solutions for infinite and bounded reservoirs follow.

3.2.1 General Solution

Taking the Laplace transform of Eq. 3.21 subject to Eq. 3.23, we have:

$$\frac{\partial^2 \bar{m}(p)}{\partial x^2} = \frac{u}{\eta_i} \bar{m}(p) \quad (3.32)$$

where u is the Laplace transform parameter. Also, the Laplace transforms of Eqs. 3.24, 3.25, and 3.31 are given, respectively, by;

$$\lim_{x \rightarrow \infty} \bar{m}(x, u) = 0 \quad (3.33)$$

$$\left[\frac{\partial \bar{m}(x, u)}{\partial x} \right]_{x=L_x} = 0 \quad (3.34)$$

and

$$\bar{m}_{wf}(u) = \bar{m}(0, u) - \frac{As}{2h} \left(\frac{\partial \bar{m}}{\partial x} \right)_{x=0} \quad (3.35)$$

The general solution of Eq. 3.32 is given by:

$$\bar{m}(x, u) = \alpha(u) \exp\left(-\sqrt{\frac{u}{\eta_i}} x\right) + \beta(u) \exp\left(\sqrt{\frac{u}{\eta_i}} x\right) \quad (3.36)$$

Differentiating Eq. 3.36 yields:

$$\frac{\partial \bar{m}(x, u)}{\partial x} = -\alpha(u) \sqrt{\frac{u}{\eta_i}} \exp\left(-\sqrt{\frac{u}{\eta_i}} x\right) + \beta(u) \sqrt{\frac{u}{\eta_i}} \exp\left(\sqrt{\frac{u}{\eta_i}} x\right) \quad (3.37)$$

Then, from Eqs. 3.35 through 3.37, we have:

$$\bar{m}_{wf}(u) = \alpha(u) \left(1 + \frac{As}{2h} \sqrt{\frac{u}{\eta_i}}\right) + \beta(u) \left(1 - \frac{As}{2h} \sqrt{\frac{u}{\eta_i}}\right) \quad (3.38)$$

Thus, we can write:

$$\alpha(u) = \frac{\bar{\Delta m}_{wf}(u) - \beta(u) \left(1 - \frac{As}{2h} \sqrt{\frac{u}{\eta_i}}\right)}{\left(1 + \frac{As}{2h} \sqrt{\frac{u}{\eta_i}}\right)} \quad (3.39)$$

3.2.2 Infinite Systems

For infinite systems, the use of the outer boundary condition (Eq. 3.33) in Eq. 3.36 indicates:

$$\beta(u) = 0 \quad (3.40)$$

Then, from Eq. 3.39, we have:

$$\alpha(u) = \frac{\bar{m}_{wf}}{\left(1 + \frac{As}{2h} \sqrt{\frac{u}{\eta_i}}\right)} \quad (3.41)$$

The flow rate at the wellbore (Eq. 3.29) is given in Laplace domain by

$$\bar{q}_{sf}(u) = \frac{C_1}{2} \frac{kAT_{sc}}{Tp_{sc}} \left[\frac{\partial \bar{m}(p)}{\partial x} \right]_{x=0} \quad (3.42)$$

Using Eqs. 3.40 and 3.41 in Eq. 3.36 and substituting for $\left[\frac{\partial \bar{m}(p)}{\partial x} \right]_{x=0}$ in Eq. 3.42 yields:

$$\bar{q}_{sf}(u) = \frac{C_1}{2} \frac{kAT_{sc}}{Tp_{sc}} \sqrt{\frac{u}{\eta_i}} \frac{\bar{m}_{wf}}{\left(1 + \frac{As}{2h} \sqrt{\frac{u}{\eta_i}} \right)} \quad (3.43)$$

For constant pressure production, using

$$m_{wf} = m_c = \text{constant} \quad (3.44)$$

and taking the inverse Laplace transform of Eq. 3.43, we obtain

$$q_{sf}(t) = \frac{C_1 khT_{sc} m_c}{Tp_{sc}} \frac{1}{s} \exp\left(\frac{4\eta_i h^2 t}{A^2 s^2}\right) \text{erfc}\left(\frac{2h\sqrt{\eta_i t}}{As}\right) \quad \text{for } s > 0 \quad (3.45)$$

and,

$$q_{sf}(t) = \frac{C_1}{2} \frac{kAT_{sc} m_c}{Tp_{sc} \sqrt{\pi \eta_i t}} \quad \text{for } s = 0 \quad (3.46)$$

3.2.3 Bounded Systems

For a closed, bounded system from Eqs. 3.34 and 3.37, we have:

$$\alpha(u) = \beta(u) \exp\left(2\sqrt{\frac{u}{\eta_i}} L_x\right) \quad (3.47)$$

Substituting Eq. 3.47 into Eq. 3.39 yields:

$$\bar{m}_{wf} = \beta(u) \left[\exp\left(2\sqrt{\frac{u}{\eta_i}} L_x\right) + 1 + \frac{As}{2h} \sqrt{\frac{u}{\eta_i}} \left(\exp\left(2\sqrt{\frac{u}{\eta_i}} L_x\right) - 1 \right) \right] \quad (3.48)$$

Thus,

$$\beta(u) = \frac{\bar{m}_{wf}}{\left[\exp\left(2\sqrt{\frac{u}{\eta_i}} L_x\right) + 1 + \frac{As}{2h} \sqrt{\frac{u}{\eta_i}} \left(\exp\left(2\sqrt{\frac{u}{\eta_i}} L_x\right) - 1 \right) \right]} \quad (3.49)$$

Substituting Eq. 3.49 into Eq. 3.39 gives:

$$\alpha(u) = \frac{\bar{m}_{wf} \exp\left(2\sqrt{\frac{u}{\eta_i}} L_x\right)}{\left[\exp\left(2\sqrt{\frac{u}{\eta_i}} L_x\right) + 1 + \frac{As}{2h} \sqrt{\frac{u}{\eta_i}} \left(\exp\left(2\sqrt{\frac{u}{\eta_i}} L_x\right) - 1\right)\right]} \quad (3.50)$$

Using Eqs. 3.49 and 3.50 in Eq. 3.37 yields:

$$\frac{\partial \bar{m}(p)}{\partial x} = \frac{\bar{m}_{wf} \sqrt{\frac{u}{\eta_i}} \left[\exp\left(\sqrt{\frac{u}{\eta_i}} x\right) - \exp\left(\sqrt{\frac{u}{\eta_i}} (2L_x - x)\right)\right]}{\left[\exp\left(2\sqrt{\frac{u}{\eta_i}} L_x\right) + 1 + \frac{As}{2h} \sqrt{\frac{u}{\eta_i}} \left(\exp\left(2\sqrt{\frac{u}{\eta_i}} L_x\right) - 1\right)\right]} \quad (3.51)$$

Evaluating Eq. 3.51 as $x \rightarrow 0$ and using Eq. 3.42, we obtain

$$\bar{q}_{sf}(u) = \frac{C_1}{2} \frac{kAT_{sc}}{Tp_{sc}} \frac{\bar{m}_{wf} \sqrt{\frac{u}{\eta_i}} \left(-\exp\left(2\sqrt{\frac{u}{\eta_i}} L_x\right) + 1\right)}{\left[\exp\left(2\sqrt{\frac{u}{\eta_i}} L_x\right) + 1 + \frac{As}{2h} \sqrt{\frac{u}{\eta_i}} \left(\exp\left(2\sqrt{\frac{u}{\eta_i}} L_x\right) - 1\right)\right]} \quad (3.52)$$

3.3 Similarity Solution

It is also possible to use similarity transforms to obtain the solution for the variable viscosity-compressibility product case. A similarity solution provided by Thompson (2014) is used in this thesis. This solution is built for infinite systems with constant bottomhole pressure production.

Suppose that pressure (pseudo-pressure) is a unique function of $\xi = \frac{x}{\sqrt{t}}$. Then we can

write space and time derivatives of pseudo-pressure as follows:

$$\left(\frac{\partial m(p)}{\partial x}\right)_t = \frac{dm(p)}{d\xi} \left(\frac{\partial \xi}{\partial x}\right)_t = \frac{1}{\sqrt{t}} \frac{dm(p)}{d\xi} \quad (3.53)$$

$$\left(\frac{\partial}{\partial x} \left(\frac{\partial m(p)}{\partial x}\right)\right)_t = \left(\frac{\partial}{\partial x} \left(\frac{1}{\sqrt{t}} \frac{dm(p)}{d\xi}\right)\right)_t \quad (3.54)$$

$$\left(\frac{\partial m(p)}{\partial t}\right)_x = \frac{dm(p)}{d\xi} \left(\frac{\partial \xi}{\partial t}\right)_x = -\frac{x}{2t\sqrt{t}} \frac{dm(p)}{d\xi} = -\frac{\xi}{2t} \frac{dm(p)}{d\xi} \quad (3.55)$$

Substituting Eqs.3.66 and 3.67 in Eq.3.20, we obtain our transformed flow equation as:

$$\frac{1}{t} \frac{d^2 m(p)}{d\xi^2} = -\frac{\phi c_g \mu_g}{C_1 k} \frac{\xi}{2t} \frac{dm(p)}{d\xi} \quad (3.56)$$

Rearranging Eq. 56 yields:

$$\frac{d^2 m(p)}{d\xi^2} = -\frac{\xi}{2\eta} \frac{dm(p)}{d\xi} \quad (3.57)$$

We also need to express boundary conditions in terms of ξ :

$$\lim_{\xi \rightarrow \infty} m(p(\xi)) = m(p_i) \quad (3.58)$$

$$m(p(\xi = 0)) = m(p_c) \quad (3.59)$$

Let us now define;

$$g = \frac{dm(p)}{d\xi} \quad (3.60)$$

Then Eq. 3.57 can be written as follows;

$$C_1 \frac{dg}{d\xi} = -\xi \frac{\phi c_i \mu_g}{2k} g \quad (3.61)$$

Integrating Eq.3.61 from 0 to ξ we obtain:

$$g(\xi) = \alpha \exp\left(-\int_0^\xi \xi' \frac{\phi c_i \mu_g}{2C_1 k} d\xi'\right) \quad (3.62)$$

where α is a constant. Then,

$$\frac{dm(p)}{d\xi} = \alpha \exp\left(-\int_0^\xi \xi' \frac{\phi c_i \mu_g}{2C_1 k} d\xi'\right) \quad (3.63)$$

Integrating Eq. 3.63 from $\xi = 0$ to $\xi = \infty$ and using the boundary conditions (Eqs. 3.58 and 3.59) yields:

$$m(p_c) = -\alpha \int_0^\infty \exp\left(-\int_0^{\xi'} \xi'' \frac{\phi c_i \mu_g}{2C_1 k} d\xi''\right) d\xi' \quad (3.64)$$

Thus,

$$\alpha = -\frac{m(p_c)}{\int_0^\infty \exp\left(-\int_0^{\xi'} \xi'' \frac{\phi c_i \mu_g}{2C_1 k} d\xi''\right) d\xi'} \quad (3.65)$$

If we substitute Eq.3.65 into Eq.3.63 we obtain:

$$\frac{dm(p)}{d\xi} = -\frac{m(p_c) \exp\left(-\frac{1}{2} \int_0^\xi \frac{\xi'}{\eta} d\xi'\right)}{\int_0^\infty \exp\left(-\frac{1}{2} \int_0^\xi \frac{\xi'}{\eta} d\xi'\right) d\xi''} \quad (3.66)$$

To obtain the general solution for the pseudo-pressure distribution, Eq. 3.66 is integrated from ξ to ∞ as follows:

$$m[p(x,t)] = -\frac{m(p_c) \int_{x/\sqrt{t}}^\infty \exp\left[-\frac{1}{2\eta_i} \int_0^{\xi''} \xi' \frac{c_t \mu_g}{(c_t \mu_g)_i} d\xi'\right] d\xi''}{\int_0^\infty \exp\left[-\frac{1}{2\eta_i} \int_0^{\xi''} \xi' \frac{c_t \mu_g}{(c_t \mu_g)_i} d\xi'\right] d\xi''} \quad (3.67)$$

where,

$$\eta_i = \frac{C_1 k}{\phi(c_t \mu_g)_i} \quad (3.68)$$

Let,

$$\psi = \int_{x/\sqrt{t}}^\infty \exp\left(-\frac{1}{2\eta_i} \int_0^{\xi''} \xi' \frac{c_t \mu_g}{(c_t \mu_g)_i} d\xi'\right) d\xi'' \quad (3.69)$$

Note that if t is fixed and

$$x' = \sqrt{t} \xi'' \quad (3.70)$$

Then,

$$dx' = \sqrt{t} d\xi'' \quad (3.71)$$

and,

$$\psi = \frac{1}{\sqrt{t}} \int_x^\infty \exp\left(-\frac{1}{2\eta_i} \int_0^{\frac{x'}{\sqrt{t}}} \xi' \frac{c_t \mu_g}{(c_t \mu_g)_i} d\xi'\right) dx' \quad (3.72)$$

Similarly, let

$$x'' = \sqrt{t} \xi' \quad (3.73)$$

Then

$$dx'' = \sqrt{t} d\xi' \quad (3.74)$$

and,

$$\psi = \frac{1}{\sqrt{t}} \int_x^\infty \exp\left(-\frac{1}{2\eta_i t} \int_0^{x'} \frac{c_i \mu_g}{(c_i \mu_g)_i} dx''\right) dx' \quad (3.75)$$

Suppose that $\xi'' > \frac{x^*}{\sqrt{t}}$. For a system with negligible compressibility and viscosity variation with pressure.

$$\frac{x^*}{\sqrt{\eta_i t}} > 10 \quad (3.76)$$

ensures that the pressure at the time “t” is equal to the initial pressure. Then we can write Eq. 3.75 as:

$$\psi\left(\frac{x}{\sqrt{t}}\right) = \psi_1\left(\frac{x}{\sqrt{t}}\right) + \kappa \quad (3.77)$$

where,

$$\psi_1\left(\frac{x}{\sqrt{t}}\right) = \int_{\frac{x}{\sqrt{t}}}^{10\sqrt{\eta_i}} \exp\left(-\frac{1}{2\eta_i} \int_0^{\xi''} \frac{c_i \mu_g}{(c_i \mu_g)_i} d\xi'\right) d\xi'' \quad (3.78)$$

$$\kappa = \int_{10\sqrt{\eta_i}}^\infty \exp\left(-\frac{1}{2\eta_i} \int_0^{\xi''} \frac{c_i \mu_g}{(c_i \mu_g)_i} d\xi'\right) d\xi'' \quad (3.79)$$

where,

$$\chi(\xi'') = \int_0^{\xi''} \frac{c_i \mu_g}{(c_i \mu_g)_i} d\xi' \quad (3.80)$$

First, let us solve the integral $\chi(\xi'')$ in Eq. 3.80. We can write

$$\chi(\xi'') = \int_0^{10\sqrt{\eta_i}} \frac{c_i \mu_g}{(c_i \mu_g)_i} d\xi' + \int_{10\sqrt{\eta_i}}^{\xi''} \frac{c_i \mu_g}{(c_i \mu_g)_i} d\xi' \quad (3.81)$$

$$\chi(\xi'') = \int_0^{10\sqrt{\eta_i}} \xi' \frac{c_i \mu_g}{(c_i \mu_g)_i} d\xi' + \frac{(\xi'')^2 - 100\eta_i}{2} \quad (3.82)$$

$$\chi(\xi'') = C^* + \frac{(\xi'')^2}{2} \quad (3.83)$$

where,

$$C^* = \left(\int_0^{10\sqrt{\eta_i}} \xi' \frac{c_i \mu_g}{(c_i \mu_g)_i} d\xi' \right) - 50\eta_i \quad (3.84)$$

Then κ in Eq. 3.79 becomes,

$$\kappa = \int_{10\sqrt{\eta_i}}^{\infty} \exp \left[-\frac{1}{2\eta_i} \left(C^* + \frac{(\xi'')^2}{2} \right) \right] d\xi'' \quad (3.85)$$

We can write the Eq.3.85 in terms of Error function,

$$erf(z) = \frac{2}{\sqrt{\pi}} \int_0^z \exp(-t^2) dt \quad (3.86)$$

as follows:

$$\kappa = \sqrt{\pi\eta_i} \exp \left(-\frac{C^*}{2\eta_i} \right) [1 - erf(5)] \quad (3.87)$$

Because

$$erf(5) = 0.99 \quad (3.88)$$

We can assume

$$\kappa \approx 0 \quad (3.89)$$

Thus, our approximation to Eq. 3.67 is:

$$m[p(x,t)] = \frac{m(p_c) \psi_1 \left(\frac{x}{\sqrt{t}} \right)}{\psi_1(0)} \quad (3.90)$$

If $\frac{c_g \mu_g}{(c_g \mu_g)_i}$ ratio is constant with the pressure change, Eq. 3.67 becomes:

$$m[p(x,t)] = m(p_c) \left[1 - erf \left(\frac{x}{2\sqrt{\eta_i t}} \right) \right] \quad (3.91)$$

Differentiating Eq. 3.67 with respect to x , we have:

$$\frac{\partial m(p)}{\partial x} = \frac{1}{\sqrt{t}} \frac{dm(p)}{d\xi} = -\frac{1}{\sqrt{t}} \frac{m(p_c) \exp \left[-\frac{1}{2\eta_i} \int_0^{\frac{x}{\sqrt{t}}} \xi' \frac{c_i \mu_g}{(c_i \mu_g)_i} d\xi' \right]}{\psi_1(0)} \quad (3.92)$$

If we substitute Eq.3.92 into Eq. 3.29, we have the rate at any point in the reservoir by:

$$q(x,t) = -\frac{C_1 kAT_{sc}}{2} \frac{1}{Tp_{sc}} \frac{1}{\sqrt{t}} \frac{m[p(x,t)] \exp \left[-\frac{1}{2\eta_i} \int_0^{\frac{x}{\sqrt{t}}} \xi' \frac{c_i \mu_g}{(c_i \mu_g)_i} d\xi' \right]}{\psi_1(0)} \quad (3.93)$$

and the rate at the well $x=0$ is:

$$q(t) = -\frac{C_1 kAT_{sc}}{2Tp_{sc}} \frac{1}{\sqrt{t}} \frac{m(p_c)}{\psi_1(0)} \quad (3.94)$$

For a reservoir with constant viscosity-compressibility product, flow rate at the well would be:

$$q(t) = -\frac{C_1 kAT_{sc}}{2Tp_{sc}} \frac{m(p_c)}{\sqrt{\pi \eta_i t}} \quad (3.95)$$

Thus, rate normalized pseudo-pressure will be given by:

$$\frac{m(p_c)}{q(t)} = \frac{2Tp_{sc}\psi_1(0)}{C_1 kAT_{sc}} \sqrt{t} \quad (3.96)$$

3.4 Solution Procedure

The evaluation of the similarity solution is iterative:

- 1) As a first guess, evaluate $c_g \mu_g$ at initial conditions with the following pressure distribution equation,

$$m^0(p(x,t)) = m(p_c) \left(1 - \operatorname{erf} \left(\sqrt{\frac{1}{\eta_i}} \frac{x}{2} \right) \right) \quad (3.97)$$

- 2) Compute the first estimate of the pressure distribution with x at a given time, and a new first estimate of the $c_g \mu_g$ distribution with x .

3) Calculate Eq. 3.90 again and check whether the new pressure distribution is close enough to the last guess. If it is not close enough, update the guess for the pressure distribution and repeat the calculation until convergence.

CHAPTER 4

SPECTRAL SOLUTION OF 1D GAS FLOW IN POROUS MEDIA

As noted in the introduction, spectral methods provide a good alternative to finite difference or finite element methods when in relatively homogeneous reservoirs. In the spectral method introduced here (Thompson, 2014), the solution is approximated by using a truncated Chebyshev series in space and a backward Euler finite difference approximation in time. In addition, the system is solved on the truncated interval $0 < x < x_{max}$ where t is the time of interest and,

$$x_{max}(t) = \min(10\sqrt{\eta_i t}, L_x) \quad (4.1)$$

4.1 Problem Formulation

The spectral solution method will be applied to the following partial differential equation (PDE) and the boundary conditions:

$$\frac{\partial^2 m(p)}{\partial x^2} = \frac{1}{\eta} \frac{\partial m(p)}{\partial t} \quad (4.2)$$

$$m(p(x, t=0)) = m(p_i) \quad (4.3)$$

$$\left[\frac{\partial m(p)}{\partial x} \right]_{x=x_{max}} = 0 \quad (4.4)$$

and

$$m(p_{wf}(t)) = m(p(0, t)) - \frac{As}{2h} \left[\frac{\partial m(p)}{\partial x} \right]_{x=0} \quad (4.5)$$

An implicit solution is sought because explicit formulations are inordinate for spectral solutions due to timestep restrictions for stability (Press, W.H., Teukolsky, S.A., Vetterling, W.T. et al., 2007). First, the spatial domain of the problem is rescaled to $-1 < \zeta < 1$ where,

$$\zeta = \frac{(2x - x_{max}(t))}{x_{max}(t)} \quad (4.6)$$

and

$$x = \frac{1}{2} x_{max}(t)(\zeta + 1) \quad (4.7)$$

Then we can write,

$$\left(\frac{\partial m(p)}{\partial x}\right)_t = \frac{\partial m(p)}{\partial \zeta} \frac{\partial \zeta}{\partial x} \quad (4.8)$$

Because,

$$\frac{\partial \zeta}{\partial x} = \frac{2}{x_{\max}(t)} \quad (4.9)$$

We can write Eq. 4.8 as follows;

$$\left(\frac{\partial m(p)}{\partial x}\right)_t = \frac{2}{x_{\max}(t)} \frac{\partial m(p)}{\partial \zeta} \quad (4.10)$$

Thus, we also have,

$$\left(\frac{\partial^2 m(p)}{\partial x^2}\right)_t = \frac{4}{x_{\max}^2(t)} \left(\frac{\partial^2 m(p)}{\partial \zeta^2}\right)_t \quad (4.11)$$

Consider the total derivative of $m(p)$; we have:

$$dm(p) = \left(\frac{\partial m(p)}{\partial \zeta}\right)_t d\zeta + \left(\frac{\partial m(p)}{\partial t}\right)_\zeta dt \quad (4.12)$$

Differentiating the total derivative of pseudo-pressure (Eq. 4.12) with respect to time, keeping x fixed, gives:

$$\left(\frac{\partial m(p)}{\partial t}\right)_x = \left(\frac{\partial m(p)}{\partial \zeta}\right)_t \left(\frac{\partial \zeta}{\partial t}\right)_x + \left(\frac{\partial m(p)}{\partial t}\right)_\zeta \left(\frac{\partial t}{\partial t}\right)_x \quad (4.13)$$

Because,

$$\left(\frac{\partial \zeta}{\partial t}\right)_x = -\frac{1}{x_{\max}(t)} \frac{\partial x_{\max}(t)}{\partial t} - x_{\max}(t) \left[-\frac{1}{x_{\max}^2(t)} \frac{\partial x_{\max}(t)}{\partial t}\right] = 0 \quad (4.14)$$

Equation 4.13 can also be written as:

$$\left(\frac{\partial m(p)}{\partial t}\right)_x = \left(\frac{\partial m(p)}{\partial t}\right)_\zeta \quad (4.15)$$

Therefore, the system of equations to be solved (Eqs. 4.2 through 4.5) becomes:

$$\alpha(p) \left(\frac{\partial^2 m(p)}{\partial \zeta^2}\right)_t = \left(\frac{\partial m(p)}{\partial t}\right)_\zeta \quad (4.16)$$

$$m(p(\zeta, t=0)) = m(p_i) \quad (4.17)$$

$$\left[\frac{\partial m(p)}{\partial \zeta} \right]_{\zeta=1} = 0 \quad (4.18)$$

$$m(p_{wf}(t)) = m(p(-1,t)) - \frac{As}{hx_{max}(t)} \left[\frac{\partial m(p)}{\partial \zeta} \right]_{\zeta=-1} \quad (4.19)$$

where,

$$\alpha(p) = \frac{4\eta}{x_{max}^2(t)} \quad (4.20)$$

Let us now assume that pseudo-pressure variation with ζ and time is approximated by the following infinite series:

$$m[p(\zeta, t)] \approx \sum_{k=0}^N c_k(t) T_k(\zeta) \quad (4.21)$$

Here, $T_k(\zeta)$ is the Chebyshev polynomial of degree k given by

$$T_k(\zeta) = \cos(k \arccos \zeta) \quad (4.22)$$

Substituting Eq.4.21 in Eqs.4.16-4.19 transformed diffusivity equation and boundary conditions become,

$$\alpha[p(\zeta_j, t)] \sum_{k=0}^N c_k(t) \frac{d^2 T_k(\zeta_j)}{d\zeta^2} = \sum_{k=0}^N T_k(\zeta_j) \frac{\partial c_k(t)}{\partial t} \quad (4.23)$$

$$\sum_{k=0}^N c_k(0) T_k(\zeta_j) = m(p_i) \quad (4.24)$$

$$\sum_{k=0}^N c_k(t) \frac{dT_k(\zeta_0)}{d\zeta} = 0 \quad (4.25)$$

and

$$m[p_{wf}(t)] = \sum_{k=0}^N c_k(t) T_k(\zeta_N) - \frac{As}{hx_{max}} \sum_{k=0}^N c_k(t) \frac{dT_k(\zeta_N)}{d\zeta} \quad (4.26)$$

Eqs. 4.23 through 4.26 are evaluated at the Gauss-Lobatto points, ζ_j , where,

4.2 Solution

The system of equations given by Eqs. 4.23 through 4.26 may be solved for the coefficients $\{c_k\}_{k=0}^N$ however it is more common to express the Chebyshev polynomials in terms of Cardinal functions. In general, any interpolating polynomial for a function $f(x)$ can be written in terms of Cardinal functions, $C_k(\zeta_j)$ as follows.

$$f(x) \approx \sum_{k=0}^N f(x_k) C_k(x) \quad (4.27)$$

where

$$C_k(\zeta_j) = \delta_{k,j} = \begin{cases} 1 & \text{for } k = j \\ 0 & \text{for } k \neq j \end{cases} \quad (4.28)$$

Eq. 4.28 states that the Cardinal functions are 0 except at the n^{th} collocation point where they are 1. With the help of the Lagrange interpolation formula given by,

$$P(x) = \frac{(x-x_1)(x-x_2)\dots(x-x_{N-1})}{(x_0-x_1)(x_0-x_2)\dots(x_0-x_{N-1})} y_0 + \dots + \frac{(x-x_0)(x-x_2)\dots(x-x_{N-1})}{(x_1-x_0)(x_1-x_2)\dots(x_1-x_{N-1})} y_1 + \dots + \frac{(x-x_0)(x-x_1)\dots(x-x_{N-2})}{(x_{N-1}-x_0)(x_{N-1}-x_1)\dots(x_{N-1}-x_{N-2})} y_{N-1} \quad (4.29)$$

the following explicit representation of the Cardinal functions is obtained:

$$C_k(x) = \prod_{\substack{j=0 \\ j \neq i}}^{N_x} \frac{x-x_j}{x_k-x_j} \quad (4.30)$$

To follow this approach, we approximate the pseudo-pressure in terms of the Cardinal functions, $C_k(z_j)$ as follows.

$$m[p(\zeta, t)] \approx \sum_{k=0}^N m_k(t) C_k(\zeta) \quad (4.31)$$

Differentiating Eq. 4.31 with respect to ζ , we have:

$$\frac{\partial m[p(\zeta_i, t)]}{\partial \zeta} \approx \sum_{k=0}^N m_k(t) \frac{dC_k(\zeta_i)}{d\zeta} \quad (4.32)$$

and

$$\frac{\partial^2 m[p(\zeta_i, t)]}{\partial \zeta^2} \approx \sum_{k=0}^N m_k(t) \frac{d^2 C_k(\zeta_i)}{d^2 \zeta} \quad (4.33)$$

Chebyshev differentiation matrices, $D_{i,k}$, can be defined at the interior collocation points as follows:

$$D_{i,k} \equiv \frac{dC_k(\zeta_i)}{d\zeta} \quad (4.34)$$

According to Chebyshev differentiation matrix theorem, the entries of Chebyshev spectral differentiation matrix, D , for $N \geq 1$ are defined as follows (Trefethen, 2000).

$$D_{0,0} = \frac{2N^2 + 1}{6} \quad (4.35)$$

$$D_{N,N} = -\frac{2N^2 + 1}{6} \quad (4.36)$$

$$D_{j,j} = -\frac{\zeta_j}{2(1-\zeta_j^2)}, \text{ for } j = 1, 2, \dots, N-1 \quad (4.37)$$

and

$$D_{i,j} = \frac{c_i}{c_j} \frac{(-1)^{i+j}}{2(\zeta_i - \zeta_j)}, \text{ for } i \neq j; i, j = 0, 1, 2, \dots, N \quad (4.38)$$

where,

$$c_i = \begin{cases} 2 & \text{for } i = 0 \text{ or } N \\ 0 & \text{otherwise} \end{cases} \quad (4.39)$$

In terms of the notation of the differentiation matrix, we can write Eqs. 4.32 and 4.33 as follows:

$$\frac{\partial m[p(\zeta_i, t)]}{\partial \zeta} \approx \sum_{k=0}^N D_{i,k} m_k(t) \quad (4.40)$$

$$\frac{\partial^2 m[p(\zeta_i, t)]}{\partial \zeta^2} \approx \sum_{k=0}^N D_{i,k}^2 m_k(t) \quad (4.41)$$

Also, the system of equations, Eqs.4.23-4.26, are rearranged at the interior collocation points ($i = 1, 2, \dots, N - 1$) as follows:

$$\alpha_i \sum_{k=0}^N D_{i,k}^2 m_k^{n+1}(t) = \frac{m_i^{n+1} - m_i^n}{\Delta t} \quad (4.42)$$

$$m_i^0 = m(p_i) \quad (4.43)$$

$$\sum_{k=0}^N D_{0,k} m_k(t) = 0 \quad (4.44)$$

Finally, the pseudo-pressure equation, Eq. 4.31, can be defined as follows:

$$m(p_{wf}(t^{n+1})) = m_N^{n+1} - \frac{As}{hx_{max}(t^{n+1})} \sum_{k=0}^N D_{N,k} m_k(t) \quad (4.45)$$

CHAPTER 5

A PERTURBATION SOLUTION

Perturbation technique is one of the common approaches to solve nonlinear problems. In this approach, small disturbances are introduced to the exact solution of the linear problem to find an approximate solution of the nonlinear problem (Ahmadi, 2012). In this chapter, following Barreto et al. (2012), a perturbation formulation will be presented for 1D, linear flow of real gases in porous media for variable-rate-production condition. Because the perturbation approach breaks the nonlinear problem into a series of linear problems, the solutions of the linear problems for variable-rate-production are obtained by using the Green's function approach. The solution leads to the definition of the correct superposition time discussed in Chapter 7 to be used in the analysis of gas-well performances when the viscosity-compressibility product is a function of pressure.

5.1 Problem Formulation

The diffusion equation in terms of pseudo-pressure is given by:

$$\frac{\partial^2 m}{\partial x^2} = (1 + \omega) \frac{1}{\eta_i} \frac{\partial m}{\partial t} \quad (5.1)$$

where

$$\omega = \omega(x, t) = \frac{\eta_i - \eta}{\eta} = \frac{(\phi\mu c_t)_i - (\phi\mu c_t)}{(\phi\mu c_t)} \quad (5.2)$$

and

$$\eta = \frac{6.328 \times 10^{-3} k}{\phi\mu c_t} \quad (5.3)$$

The initial and boundary conditions are given by:

$$m(x, t \rightarrow 0) = 0 \quad (5.4)$$

$$m(x \rightarrow \infty, t) = 0 \quad (5.5)$$

and

$$\frac{\partial m}{\partial x}(x = 0, t) = -\frac{1422\pi qT}{2khx_f} \quad (5.6)$$

Let us express Eq. 5.1 as a perturbation equation:

$$\frac{\partial^2 m}{\partial x^2} = (1 + \varepsilon \omega) \frac{1}{\eta_i} \frac{\partial m}{\partial t} \quad (5.7)$$

where

$$\varepsilon = \begin{cases} 0 & \text{Linear} \\ 1 & \text{Non-Linear} \end{cases} \quad (5.8)$$

The solution of Eq. 5.7 can be assumed in the following form:

$$m = m^0 + \sum_{k=1}^{\infty} \varepsilon^k m^k \quad (5.9)$$

Substituting Eq. 5.9 into Eq. 5.7, we obtain

$$\begin{aligned} & \left(\frac{\partial^2 m^0}{\partial x^2} - \frac{1}{\eta_i} \frac{\partial m^0}{\partial t} \right) + \varepsilon \left(\frac{\partial^2 m^1}{\partial x^2} - \frac{1}{\eta_i} \frac{\partial m^1}{\partial t} - \frac{\omega^0}{\eta_i} \frac{\partial m^0}{\partial t} \right) \\ & + \varepsilon^2 \left(\frac{\partial^2 m^2}{\partial x^2} - \frac{1}{\eta_i} \frac{\partial m^2}{\partial t} - \frac{\omega^1}{\eta_i} \frac{\partial m^1}{\partial t} \right) + \dots = 0 \end{aligned} \quad (5.10)$$

Eq. 5.10 suggests that $\Delta m^0, \Delta m^1, \Delta m^2, \dots$, are the solutions of

$$\begin{aligned} & \frac{\partial^2 m^0}{\partial x^2} - \frac{1}{\eta_i} \frac{\partial m^0}{\partial t} = 0 \\ & \frac{\partial^2 m^1}{\partial x^2} - \frac{1}{\eta_i} \frac{\partial m^1}{\partial t} - \frac{\omega^0}{\eta_i} \frac{\partial m^0}{\partial t} = 0 \\ & \frac{\partial^2 m^2}{\partial x^2} - \frac{1}{\eta_i} \frac{\partial m^2}{\partial t} - \frac{\omega^1}{\eta_i} \frac{\partial m^1}{\partial t} = 0 \\ & \vdots \\ & \frac{\partial^2 m^k}{\partial x^2} - \frac{1}{\eta_i} \frac{\partial m^k}{\partial t} - \frac{\omega^{k-1}}{\eta_i} \frac{\partial m^{k-1}}{\partial t} = 0 \end{aligned} \quad (5.11)$$

5.2 Solution of the Perturbation Problem

Consider the 0th order perturbation (the linear problem):

$$\frac{\partial^2 m^0}{\partial x^2} - \frac{1}{\eta_i} \frac{\partial m^0}{\partial t} = 0 \quad (5.12)$$

$$m^0(x, t \rightarrow 0) = 0 \quad (5.13)$$

$$m^0(x \rightarrow \infty, t) = 0 \quad (5.14)$$

and

$$\left(\frac{\partial m^0}{\partial x} \right)_{x=0} = -\frac{2844\pi q(t)T}{2x_f kh} = \frac{2844\pi \tilde{q}(t)T}{k} \quad (5.15)$$

The Green's function solution of the linear problem (Eqs. 5.12-5.15) is given by:

$$m^0(x, t) = \frac{2844T\pi}{k} \eta_i \int_0^t \tilde{q}(t') S(x, t-t') dt' \quad (5.16)$$

where

$$S = \frac{1}{2\sqrt{\pi\eta_i(t-t')}} \exp\left[-\frac{x^2}{4\eta_i(t-t')}\right] \quad (5.17)$$

So that

$$m^0(x, t) = \frac{1422T\sqrt{\pi\eta_i}}{k} \int_0^t \frac{\tilde{q}(t')}{\sqrt{t-t'}} \exp\left[-\frac{x^2}{4\eta_i(t-t')}\right] dt' \quad (5.18)$$

If $\tilde{q} = \text{constant} = q / (2x_f h)$, then

$$\begin{aligned} m^0(x, t) &= \frac{1422qT\sqrt{\pi\eta_i}}{2x_f kh} \int_0^t \frac{1}{\sqrt{t-t'}} \exp\left[-\frac{x^2}{4\eta_i(t-t')}\right] dt' \\ &= \frac{1422qT}{kh} \left[\sqrt{\frac{\pi\eta_i t}{x_f^2}} \exp\left(-\frac{x^2}{4\eta_i t}\right) - \frac{\pi x}{2x_f} \operatorname{erfc}\left(\frac{x}{2\sqrt{\eta_i t}}\right) \right] \end{aligned} \quad (5.19)$$

Let us now consider the 1st order perturbation:

$$\frac{\partial^2 m^1}{\partial x^2} - \frac{1}{\eta_i} \frac{\partial m^1}{\partial t} - \frac{\omega^0 \partial m^0}{\partial t} = 0 \quad (5.20)$$

$$m^1(x, t \rightarrow 0) = 0 \quad (5.21)$$

$$m^1(x \rightarrow \infty, t) = 0 \quad (5.22)$$

and

$$\left(\frac{\partial m^1}{\partial x} \right)_{x=0} = 0 \quad (5.23)$$

The Green's function solution of the problem in Eqs. 5.20 through 5.23 is given by:

$$m^1(x, t) = -\eta_i \int_0^t \int_0^\infty \left[G \left(\frac{\partial^2 \Delta m^1}{\partial x'^2} - \frac{\omega^0}{\eta_i} \frac{\partial \Delta m^0}{\partial t'} \right) - \Delta m^1 \frac{\partial^2 G}{\partial x'^2} \right] dx' dt' \quad (5.24)$$

Because, from Eq. 5.12

$$\frac{\partial m^0}{\partial t} = \eta_i \frac{\partial^2 m^0}{\partial x^2} \quad (5.25)$$

We can write Eq. 5.24 as:

$$m^1(x, t) = -\eta_i \int_0^t \int_0^\infty \left[\left(G \frac{\partial^2 m^1}{\partial x'^2} - m^1 \frac{\partial^2 G}{\partial x'^2} \right) - G \left(\omega^0 \frac{\partial^2 m^0}{\partial x'^2} \right) \right] dx' dt' \quad (5.26)$$

Using Green's second identity,

$$\int_D (\phi \nabla^2 \psi - \psi \nabla^2 \phi) dD = \int_\Gamma (\phi \bar{\nabla} \psi - \psi \bar{\nabla} \phi) \cdot \bar{n} d\Gamma \quad (5.27)$$

Eq. 5.26 becomes:

$$\begin{aligned} m^1(x, t) &= -\eta_i \int_0^t \left[\int_{x \in \Gamma} \left(G \frac{\partial m^1}{\partial y} - m^1 \frac{\partial G}{\partial x} \right) - \int_0^\infty G \left(\omega^0 \frac{\partial^2 m^0}{\partial x'^2} \right) dx' \right] dt' \\ &= \eta_i \int_0^t \int_0^\infty G \left(\omega^0 \frac{\partial^2 m^0}{\partial x'^2} \right) dx' dt' \end{aligned} \quad (5.28)$$

Consider,

$$\frac{\partial^2}{\partial x^2} (\omega^0 m^0) = \omega^0 \frac{\partial^2 m^0}{\partial x^2} + 2 \frac{\partial \omega^0}{\partial m^0} \left(\frac{\partial m^0}{\partial x} \right)^2 + m^0 \frac{\partial^2 \omega^0}{\partial x^2} \quad (5.29)$$

Then, we can write Eq. 28 as follows:

$$\begin{aligned} m^1(x, t) &= \eta_i \int_0^t \int_0^\infty \left[G \frac{\partial^2 (\omega^0 m^0)}{\partial x'^2} - 2G \frac{\partial \omega^0}{\partial x} \left(\frac{\partial m^0}{\partial x} \right)^2 - G m^0 \frac{\partial^2 \omega^0}{\partial x'^2} \right] dx' dt' \\ &= \eta_i \int_0^t \int_0^\infty \left[G \frac{\partial^2 (\omega^0 m^0)}{\partial x'^2} - G m^0 \frac{\partial^2 \omega^0}{\partial x'^2} \right] dx' dt' - 2\eta_i \left[\frac{\partial \omega^0}{\partial m^0} \left(\frac{\partial m^0}{\partial x} \right)^2 \right]_{x,t} \end{aligned} \quad (5.30)$$

where we have used

$$\int_0^t \int_0^\infty G(x-x', t-t') \frac{\partial \omega^0}{\partial m^0} \left(\frac{\partial m^0}{\partial x} \right)^2 dx' dt' = \left[\frac{\partial \omega^0}{\partial m^0} \left(\frac{\partial m^0}{\partial x} \right)^2 \right]_{x,t} \quad (5.31)$$

From Green's second identity (Eq. 5.27), we have

$$\begin{aligned} \int_0^\infty \left[G \frac{\partial^2 (\omega^0 m^0)}{\partial x'^2} - (\omega^0 m^0) \frac{\partial^2 G}{\partial x'^2} \right] dx' &= \left[S \frac{\partial (\omega^0 m^0)}{\partial x} - (\omega^0 m^0) \frac{\partial G}{\partial x} \right]_{x \in \Gamma} \\ &= \left[S \left(\omega^0 \frac{\partial m^0}{\partial x'} + m^0 \frac{\partial \omega^0}{\partial x'} \right) \right]_{x \in \Gamma} \\ &= \left[S \left(\omega^0 + \frac{\partial \omega^0}{\partial \ln m^0} \right) \frac{\partial m^0}{\partial x'} \right]_{x \in \Gamma} \end{aligned} \quad (5.32)$$

Using Eq. 5.32, we can write Eq. 5.30 as follows

$$\begin{aligned} m^1(x, t) &= \eta_i \int_0^t \left\{ \left[S \left(\omega^0 + \frac{\partial \omega^0}{\partial \ln m^0} \right) \frac{\partial m^0}{\partial x'} \right]_{x \in \Gamma} \right. \\ &\quad \left. + \int_0^\infty \left[(\omega^0 m^0) \frac{\partial^2 G}{\partial x'^2} - G m^0 \frac{\partial^2 \omega^0}{\partial x'^2} \right] dx' dt' \right\} - 2\eta_i \left[\frac{\partial \omega^0}{\partial m^0} \left(\frac{\partial m^0}{\partial x} \right)^2 \right]_{x,t} \end{aligned} \quad (5.33)$$

Because

$$\left(\frac{\partial m^0}{\partial x'} \right)_{x' \in \Gamma} = - \frac{2844\pi \tilde{q}(t') T}{k} \quad (5.34)$$

We can also write

$$\begin{aligned} m^1(x, t) &= - \frac{2844T\pi}{k} \eta_i \int_0^t \left[\tilde{q}(t') \left(\omega^0 + \frac{\partial \omega^0}{\partial \ln m^0} \right) S \right]_{x \in \Gamma} \\ &\quad + \eta_i \int_0^t \int_0^\infty m^0 \left(\omega^0 \frac{\partial^2 G}{\partial x'^2} - G \frac{\partial^2 \omega^0}{\partial x'^2} \right) dx' dt' - 2\eta_i \left[\frac{\partial \omega^0}{\partial m^0} \left(\frac{\partial m^0}{\partial x} \right)^2 \right]_{x,t} \end{aligned} \quad (5.35)$$

Because

$$\begin{aligned}
\int_0^\infty m^0 \left(\omega^0 \frac{\partial^2 G}{\partial x'^2} - G \frac{\partial^2 \omega^0}{\partial x'^2} \right) dx' &= \overline{m^0} \int_0^\infty \left(\omega^0 \frac{\partial^2 G}{\partial x'^2} - G \frac{\partial^2 \omega^0}{\partial x'^2} \right) dx' \\
&= \overline{m^0} \left(\omega^0 \frac{\partial G}{\partial x'} - G \frac{\partial \omega^0}{\partial x'} \right)_{x' \in \Gamma} \\
&= -\overline{m^0} \left(S \frac{\partial \omega^0}{\partial x'} \right)_{x' \in \Gamma} = -\overline{m^0} \left(S \frac{\partial \omega^0}{\partial m^0} \frac{\partial m^0}{\partial x'} \right)_{x' \in \Gamma} \\
&= \frac{1422T\pi}{k} \tilde{q}(t') \left[\left(\frac{\overline{m^0}}{m^0} \frac{\partial \omega^0}{\partial \ln m^0} \right) S \right]_{x' \in \Gamma}
\end{aligned} \tag{5.36}$$

Eq. 5.35 can be written as

$$m^1(x, t) = \frac{2844T\pi}{k} \eta_i \int_0^t \tilde{q}(t') \kappa^1(t') S(x, t-t') dt' - 2\eta_i \left[\frac{\partial \omega^0}{\partial m^0} \left(\frac{\partial m^0}{\partial x} \right)^2 \right]_{x, t} \tag{5.37}$$

where we have defined

$$\kappa^1(t') = \kappa^1(x=0, t') = - \left[\omega^0 + \left(1 - \frac{\overline{m^0}}{m^0} \right) \right] \frac{\partial \omega^0}{\partial \ln m^0} \tag{5.38}$$

Now consider the 2nd order perturbation:

$$\frac{\partial^2 m^2}{\partial x^2} - \frac{1}{\eta_i} \frac{\partial m^2}{\partial t} - \frac{\omega^1}{\eta_i} \frac{\partial m}{\partial t} = 0 \tag{5.39}$$

$$m^2(x, t \rightarrow 0) = 0 \tag{5.40}$$

$$m^2(x \rightarrow \infty, t) = 0 \tag{5.41}$$

and

$$\left(\frac{\partial m^2}{\partial x} \right)_{x=0} = 0 \tag{5.42}$$

The Green's function solution of the problem in Eqs. 5.39 through 5.42 is given by

$$m^2(x, t) = -\eta_i \int_0^t \int_0^\infty \left[G \left(\frac{\partial^2 m^2}{\partial x'^2} - \frac{\omega'}{\eta_i} \frac{\partial m^1}{\partial t'} \right) - m^2 \frac{\partial^2 G}{\partial x'^2} \right] dx' dt' \quad (5.43)$$

Because, from Eq. 5.20

$$\frac{\partial^2 m^1}{\partial x^2} - \omega \frac{\partial^2 m^0}{\partial x^2} = \frac{1}{\eta_i} \frac{\partial m^1}{\partial t} \quad (5.44)$$

we can write Eq. 5.43 as

$$m^2(x, t) = -\eta_i \int_0^t \int_0^\infty \left[\left(G \frac{\partial^2 m^2}{\partial x'^2} - m^2 \frac{\partial^2 G}{\partial x'^2} \right) - G \omega' \left(\frac{\partial^2 m^1}{\partial x'^2} - \omega^0 \frac{\partial^2 m^0}{\partial x'^2} \right) \right] dx' dt' \quad (5.45)$$

and, using Green's second identity (Eq. 5.27), Eq. 5.45 becomes

$$\begin{aligned} m^2(x, t) &= -\eta_i \int_0^t \left[\left(G \frac{\partial m^2}{\partial x'} - m^2 \frac{\partial G}{\partial x'} \right)_{x' \in \Gamma} \right. \\ &\quad \left. - \int_0^\infty G \omega^1 \left(\frac{\partial^2 m^1}{\partial x'^2} - \omega^0 \frac{\partial^2 m^0}{\partial x'^2} \right) dx' \right] dt' \\ &= \eta_i \int_0^t \int_0^\infty G \left(\omega^1 \frac{\partial^2 m^1}{\partial x'^2} - \omega^1 \omega^0 \frac{\partial^2 m^0}{\partial x'^2} \right) dx' dt' \end{aligned} \quad (5.46)$$

Consider

$$\frac{\partial^2}{\partial x^2} (\omega^1 m^1) = \omega^1 \frac{\partial^2 m^1}{\partial x^2} + 2 \frac{\partial \omega^1}{\partial m^1} \left(\frac{\partial m^1}{\partial x} \right)^2 + m^1 \frac{\partial^2 \omega^1}{\partial x^2} \quad (5.47)$$

and

$$\frac{\partial^2}{\partial x^2} (\omega^1 \omega^0 m^0) = \omega^1 \omega^0 \frac{\partial^2 m^0}{\partial x^2} + 2 \omega^1 \frac{\partial \omega^0}{\partial m^0} \left(\frac{\partial m^0}{\partial x} \right)^2 + m^0 \frac{\partial^2 (\omega^1 \omega^0)}{\partial x^2} \quad (5.48)$$

Then, we can write Eq. 5.46 as follows:

$$\begin{aligned}
m^2(x,t) = & \eta_i \int_0^t \int_0^\infty \left\{ \left[G \frac{\partial^2(\omega^1 m^1)}{\partial x'^2} - G m^1 \frac{\partial^2 \omega^1}{\partial x'^2} \right] \right. \\
& - \left. \left[G \frac{\partial^2(\omega^1 \omega^0 m^0)}{\partial x'^2} - G m^0 \frac{\partial^2(\omega^1 \omega^0)}{\partial x'^2} \right] \right\} dx' dt' \\
& - 2\eta_i \left\{ \left[\frac{\partial \omega^1}{\partial m^1} \left(\frac{\partial m^1}{\partial x} \right)^2 \right]_{x,t} - \left[\omega^1 \frac{\partial \omega^0}{\partial m^0} \left(\frac{\partial m^0}{\partial x} \right)^2 \right]_{x,t} \right\}
\end{aligned} \tag{5.49}$$

where we have used

$$\int_0^t \int_0^\infty G(x-x', t-t') \frac{\partial \omega^1}{\partial m^1} \left(\frac{\partial m^1}{\partial x'} \right)^2 dx' dt' = \left[\frac{\partial \omega^1}{\partial m^1} \left(\frac{\partial m^1}{\partial x} \right)^2 \right]_{x,t} \tag{5.50}$$

and

$$\int_0^t \int_0^\infty G(x-x', t-t') \frac{\partial(\omega^1 \omega^0)}{\partial m^0} \left(\frac{\partial m^0}{\partial x'} \right)^2 dx' dt' = \left[\omega^1 \frac{\partial \omega^0}{\partial m^0} \left(\frac{\partial m^0}{\partial x} \right)^2 \right]_{x,t} \tag{5.51}$$

From Green's second identity (Eq. 5.27), we have

$$\begin{aligned}
\int_0^\infty \left[G \frac{\partial^2(\omega^1 m^1)}{\partial x'^2} - (\omega^1 m^1) \frac{\partial^2 G}{\partial x'^2} \right] dx' &= \left[G \frac{\partial(\omega^1 m^1)}{\partial x'} - (\omega^1 m^1) \frac{\partial G}{\partial x'} \right]_{x' \in \Gamma} \\
&= \left[G \left(\omega^1 + m^1 \frac{\partial \omega^1}{\partial \Delta m^1} \right) \cancel{\frac{\partial m^1}{\partial x'}} - (\omega^1 m^1) \cancel{\frac{\partial G}{\partial x'}} \right]_{x' \in \Gamma} = 0
\end{aligned} \tag{5.52}$$

and

$$\begin{aligned}
\int_0^\infty \left[G \frac{\partial^2(\omega^1 \omega^0 m^0)}{\partial x'^2} - (\omega^1 \omega^0 m^0) \frac{\partial^2 G}{\partial x'^2} \right] dx' \\
= \left[G \frac{\partial(\omega^1 \omega^0 m^0)}{\partial x'} - (\omega^1 \omega^0 m^0) \frac{\partial G}{\partial x'} \right]_{x' \in \Gamma} \\
= \left[G \left(\omega^1 \omega^0 + m^0 \frac{\partial \omega^1 \omega^0}{\partial m^0} \right) \cancel{\frac{\partial m^0}{\partial x'}} - (\omega^1 \omega^0 m^0) \cancel{\frac{\partial G}{\partial x'}} \right]_{x' \in \Gamma}
\end{aligned} \tag{5.53}$$

that is,

$$G \frac{\partial^2 (\omega^1 m^1)}{\partial x'^2} = \omega^1 m^1 \frac{\partial^2 G}{\partial x'^2} \quad (5.54)$$

and

$$\int_0^\infty \left[G \frac{\partial^2 (\omega^1 \omega^0 m^0)}{\partial x'^2} \right] dx' = \int_0^\infty (\omega^1 \omega^0 m^0) \frac{\partial^2 G}{\partial x'^2} dx' - \frac{2844T\pi}{k} \tilde{q}(t') \left[\omega^1 \left(\omega^0 + \frac{\partial \omega^0}{\partial \ln m^0} \right) S \right]_{x' \in \Gamma} \quad (5.55)$$

where we have used Eq. 5.34. Then, Eq. 5.49 becomes

$$\begin{aligned} m^2(x, t) = & \frac{2844T\pi}{k} \eta_i \int_0^t \tilde{q}(t') \left[\omega^1 \left(\omega^0 + \frac{\partial \omega^0}{\partial \ln m^0} \right) \right]_{x' \in \Gamma} S(x, t-t') dt' \\ & + \eta_i \int_0^t \int_0^\infty \left\{ m^1 \left[\omega^1 \frac{\partial^2 G}{\partial x'^2} - G \frac{\partial^2 \omega^1}{\partial x'^2} \right] \right. \\ & \left. - m^0 \left[(\omega^1 \omega^0) \frac{\partial^2 G}{\partial x'^2} - G \frac{\partial^2 (\omega^1 \omega^0)}{\partial x'^2} \right] \right\} dx' dt' \\ & - 2\eta_i \left\{ \left[\frac{\partial \omega^1}{\partial m^1} \left(\frac{\partial m^1}{\partial x} \right)^2 \right]_{x,t} - \left[\omega^1 \frac{\partial \omega^0}{\partial m^0} \left(\frac{\partial m^0}{\partial x} \right)^2 \right]_{x,t} \right\} \end{aligned} \quad (5.56)$$

Consider

$$\begin{aligned} \int_0^\infty m^1 \left[\omega^1 \frac{\partial^2 G}{\partial x'^2} - G \frac{\partial^2 \omega^1}{\partial x'^2} \right] dx' &= \overline{m^1} \int_0^\infty \left[\omega^1 \frac{\partial^2 G}{\partial x'^2} - G \frac{\partial^2 \omega^1}{\partial x'^2} \right] dx' \\ &= \overline{m^1} \left[\omega^1 \frac{\cancel{\partial G}}{\cancel{\partial x'}} - G \frac{\partial \omega^1}{\partial m^1} \frac{\cancel{\partial m^1}}{\cancel{\partial x'}} \right]_{x' \in \Gamma} = 0 \end{aligned} \quad (5.57)$$

and

$$\begin{aligned}
\int_0^\infty m^0 \left[(\omega^1 \omega^0) \frac{\partial^2 G}{\partial x'^2} - G \frac{\partial^2 (\omega^1 \omega^0)}{\partial x'^2} \right] dx' &= \overline{m^0} \int_0^\infty \left[(\omega^1 \omega^0) \frac{\partial^2 G}{\partial x'^2} - G \frac{\partial^2 (\omega^1 \omega^0)}{\partial x'^2} \right] dx' \\
&= \overline{\Delta m^0} \left[(\omega^1 \omega^0) \frac{\partial G}{\partial x'} - S \omega^1 \frac{\partial \omega^0}{\partial m^0} \frac{\partial m^0}{\partial x'} \right]_{x' \in \Gamma} \\
&= - \left[S \omega^1 \frac{\overline{m^0}}{m^0} \frac{\partial \omega^0}{\partial \ln m^0} \frac{\partial m^0}{\partial x'} \right]_{x' \in \Gamma} = \frac{2844 \tilde{q}(t') T \pi}{k} \left[S \omega^1 \frac{\overline{m^0}}{m^0} \frac{\partial \omega^0}{\partial \ln m^0} \right]_{x' \in \Gamma}
\end{aligned} \tag{5.58}$$

where we have used Eq. 5.34. Then, we can write Eq. 5.56 as follows:

$$\begin{aligned}
m^2(x, t) &= \frac{2844 T \pi}{k} \eta_i \int_0^t \tilde{q}(t') \kappa^2(t') S(x, t-t') dt' \\
&\quad - 2\eta_i \left\{ \left[\frac{\partial \omega^1}{\partial m^1} \left(\frac{\partial m^1}{\partial x} \right)^2 \right]_{x, t} - \left[\omega^1 \frac{\partial \omega^0}{\partial m^0} \left(\frac{\partial m^0}{\partial x} \right)^2 \right]_{x, t} \right\}
\end{aligned} \tag{5.59}$$

where we have defined

$$\kappa^2(t') = \kappa^2(x=0, t') = \omega^1 \left[\omega^0 + \left(1 - \frac{\overline{m^0}}{m^0} \right) \frac{\partial \omega^0}{\partial \ln m^0} \right]_{x=0} = -\omega^1 \kappa^1(t') \tag{5.60}$$

If we now consider the k^{th} order perturbation, for $k \geq 3$, we have

$$\frac{\partial^2 m^k}{\partial x^2} - \frac{1}{\eta_i} \frac{\partial m^k}{\partial t} - \frac{\omega^{k-1}}{\eta_i} \frac{\partial m^{k-1}}{\partial t} = 0 \tag{5.61}$$

$$m^k(x, t \rightarrow 0) = 0 \tag{5.62}$$

$$m^k(x \rightarrow \infty, t) = 0 \tag{5.63}$$

and

$$\left(\frac{\partial m^k}{\partial x} \right)_{x=0} = 0 \tag{5.64}$$

The Green's function solution of the problem in Eqs. 5.61 through 5.64 is given by

$$m^k(x, t) = -\eta_i \int_0^t \int_0^\infty \left[G \left(\frac{\partial^2 m^k}{\partial x'^2} - \frac{\omega^{k-1}}{\eta_i} \frac{\partial m^{k-1}}{\partial t'} \right) - m^k \frac{\partial^2 G}{\partial x'^2} \right] dx' dt' \tag{5.65}$$

Because,

$$\frac{\partial^2 m^{k-1}}{\partial x^2} - \omega^{k-2} \frac{\partial^2 m^{k-2}}{\partial x^2} = \frac{1}{\eta_i} \frac{\partial m^{k-1}}{\partial t} \quad (5.66)$$

We can write Eq. 5.65 as

$$m^k(x, t) = -\eta_i \int_0^t \int_0^\infty \left[\left(G \frac{\partial^2 m^k}{\partial x'^2} - m^k \frac{\partial^2 G}{\partial x'^2} \right) - G \omega^{k-1} \left(\frac{\partial^2 m^{k-1}}{\partial x'^2} - \omega^{k-2} \frac{\partial^2 m^{k-2}}{\partial x'^2} \right) \right] dx' dt' \quad (5.67)$$

Using Green's second identity (Eq. 5.27), Eq. 5.67 becomes

$$\begin{aligned} m^k(x, t) &= -\eta_i \int_0^t \int_\Gamma \left(G \frac{\partial m^k}{\partial x'} - m^k \frac{\partial G}{\partial x'} \right) d\Gamma \\ &\quad - \int_0^\infty G \omega^{k-1} \left(\frac{\partial^2 m^{k-1}}{\partial x'^2} - \omega^{k-2} \frac{\partial^2 m^{k-2}}{\partial x'^2} \right) dx' dt' \\ &= \eta_i \int_0^t \int_0^\infty G \left(\omega^{k-1} \frac{\partial^2 m^{k-1}}{\partial x'^2} - \omega^{k-1} \omega^{k-2} \frac{\partial^2 m^{k-2}}{\partial x'^2} \right) dx' dt' \end{aligned} \quad (5.68)$$

Consider

$$\frac{\partial^2}{\partial x^2} (\omega^{k-1} m^{k-1}) = \omega^{k-1} \frac{\partial^2 m^{k-1}}{\partial x^2} + 2 \frac{\partial \omega^{k-1}}{\partial m^1} \frac{\partial m^{k-1}}{\partial x} + m^{k-1} \frac{\partial^2 \omega^{k-1}}{\partial x^2} \quad (5.69)$$

and

$$\begin{aligned} \frac{\partial^2}{\partial x^2} (\omega^{k-1} \omega^{k-2} m^{k-2}) &= \omega^{k-1} \omega^{k-2} \frac{\partial^2 m^{k-2}}{\partial x^2} + 2 \frac{\partial(\omega^{k-1} \omega^{k-2})}{\partial x} \frac{\partial m^{k-2}}{\partial x} \\ &\quad + m^{k-2} \frac{\partial^2 (\omega^{k-1} \omega^{k-2})}{\partial x^2} \end{aligned} \quad (5.70)$$

Then, we can write Eq. 5.68 as follows:

$$\begin{aligned}
m^k(x, t) = & \eta_i \int_0^t \int_0^\infty \left\{ \left[G \frac{\partial^2 (\omega^{k-1} m^{k-1})}{\partial x'^2} - G m^{k-1} \frac{\partial^2 \omega^{k-1}}{\partial x'^2} \right] \right. \\
& - \left. \left[G \frac{\partial^2 (\omega^{k-1} m^{k-1})}{\partial x'^2} - G m^{k-1} \frac{\partial^2 \omega^{k-1}}{\partial x'^2} \right] \right\} dx' dt' \\
& - 2\eta_i \left\{ \left[\frac{\partial \omega^{k-1}}{\partial m^{k-1}} \left(\frac{\partial m^{k-1}}{\partial x} \right)^2 \right]_{x,t} - \left[\omega^{k-1} \frac{\partial \omega^{k-2}}{\partial m^{k-2}} \left(\frac{\partial m^{k-2}}{\partial x} \right)^2 \right]_{x,t} \right\}
\end{aligned} \tag{5.71}$$

where we have used

$$\int_0^t \int_0^\infty G(x-x', t-t') \frac{\partial \omega^{k-1}}{\partial x'} \frac{\partial m^{k-1}}{\partial x'} dx' dt' = \left[\frac{\partial \omega^{k-1}}{\partial m^{k-1}} \left(\frac{\partial m^{k-1}}{\partial x} \right)^2 \right]_{x,t} \tag{5.72}$$

and

$$\int_0^t \int_0^\infty G(x-x', t-t') \frac{\partial (\omega^{k-1} \omega^{k-2})}{\partial x} \frac{\partial m^{k-2}}{\partial x} dx' dt' = \left[\omega^{k-1} \frac{\partial \omega^{k-2}}{m^{k-2}} \left(\frac{\partial m^{k-2}}{\partial x} \right)^2 \right]_{x,t} \tag{5.73}$$

From Green's second identity (Eq. 5.27), we have

$$\begin{aligned}
& \int_0^\infty \left[G \frac{\partial^2 (\omega^{k-1} m^{k-1})}{\partial x'^2} - (\omega^{k-1} m^{k-1}) \frac{\partial^2 G}{\partial x'^2} \right] dx' \\
& = \int_\Gamma \left[G \frac{\partial (\omega^{k-1} m^{k-1})}{\partial x'} - (\omega^{k-1} m^{k-1}) \frac{\partial G}{\partial x'} \right] d\Gamma \\
& = \int_\Gamma \left[G \left(\omega^{k-1} \frac{\partial m^{k-1}}{\partial x} + m^{k-1} \frac{\partial \omega^{k-1}}{\partial x} \right) \right] d\Gamma = \int_\Gamma G m^{k-1} \frac{\partial \omega^{k-1}}{\partial x} d\Gamma \\
& = \left(m^{k-1} \frac{\partial \omega^{k-1}}{\partial x'} S \right)_{x'=0} = \left(m^{k-1} \frac{\partial \omega^{k-1}}{\partial m^{k-1}} \frac{\partial m^{k-1}}{\partial x'} S \right)_{x'=0} = 0
\end{aligned} \tag{5.74}$$

and

$$\begin{aligned}
& \int_0^\infty \left[G \frac{\partial^2 (\omega^{k-1} \omega^{k-2} m^{k-2})}{\partial x'^2} - (\omega^{k-1} \omega^{k-2} m^{k-2}) \frac{\partial^2 G}{\partial x'^2} \right] dx' \\
&= \int_\Gamma \left[G \frac{\partial (\omega^{k-1} \omega^{k-2} m^{k-2})}{\partial x'} - (\omega^{k-1} \omega^{k-2} m^{k-2}) \frac{\partial G}{\partial x'} \right] d\Gamma \\
&= \int_\Gamma \left[G \frac{\partial (\omega^{k-1} \omega^{k-2} m^{k-2})}{\partial x'} \right] d\Gamma = \frac{\partial (\omega^{k-1} \omega^{k-2} m^{k-2})}{\partial x'} S \quad (5.75) \\
&= \left[\left(\omega^{k-1} \omega^{k-2} \frac{m^{k-2}}{\partial x'} + m^{k-2} \frac{\partial \omega^{k-1} \omega^{k-2}}{\partial x'} \right) S \right]_{x=0} \\
&= \left\{ \left[\omega^{k-1} \left(\omega^{k-2} + m^{k-2} \frac{\partial \omega^{k-2}}{\partial m^{k-2}} \right) \frac{m^{k-2}}{\partial x'} \right] S \right\}_{x=0} = 0
\end{aligned}$$

Using Eqs. 5.73 and 5.74, we can write Eq. 5.70 as follows

$$m^k(x, t) = -2\eta_i \left\{ \left[\frac{\partial \omega^{k-1}}{\partial m^{k-1}} \left(\frac{\partial m^{k-1}}{\partial x} \right)^2 \right]_{x,t} - \left[\omega^{k-1} \frac{\partial \omega^{k-2}}{\partial m^{k-2}} \left(\frac{\partial m^{k-2}}{\partial x} \right)^2 \right]_{x,t} \right\} \quad (5.76)$$

We can now summarize the solution of Eq. 5.11 as follows:

$$m^0(x, t) = \frac{2844T\pi}{k} \eta_i \int_0^t \tilde{q}(t') S(x, t-t') dt' \quad (5.77)$$

$$m^1(x, t) = \frac{2844T\pi}{k} \eta_i \int_0^t \tilde{q}(t') \kappa^1(t') S(x, t-t') dt' - 2\eta_i \left[\frac{\partial \omega^1}{\partial m^1} \left(\frac{\partial m^1}{\partial x} \right)^2 \right]_{x,t} \quad (5.78)$$

$$\begin{aligned}
m^2(x, t) &= \frac{2844T\pi}{k} \eta_i \int_0^t \tilde{q}(t') \kappa^2(t') S(x, t-t') dt' \\
&\quad - 2\eta_i \left\{ \left[\frac{\partial \omega^1}{\partial m^1} \left(\frac{\partial m^1}{\partial x} \right)^2 \right]_{x,t} - \left[\omega^1 \frac{\partial \omega^0}{\partial m^0} \left(\frac{\partial m^0}{\partial x} \right)^2 \right]_{x,t} \right\} \\
&\quad \vdots \quad (5.79)
\end{aligned}$$

$$m^k(x,t) = -2\eta_i \left\{ \left[\frac{\partial \omega^{k-1}}{\partial m^{k-1}} \left(\frac{\partial m^{k-1}}{\partial x} \right)^2 \right]_{x,t} - \left[\omega^{k-1} \frac{\partial \omega^{k-2}}{\partial m^{k-2}} \left(\frac{\partial m^{k-2}}{\partial x} \right)^2 \right]_{x,t} \right\} \quad k \geq 3 \quad (5.80)$$

where

$$S = S(x, t - t') = \frac{1}{2\sqrt{\pi\eta_i(t-t')}} \exp\left[-\frac{x^2}{4\eta_i(t-t')}\right] \quad (5.81)$$

Therefore, using Eq. 5.9, the solution of Eq. 5.7 is given by

$$\begin{aligned} m(x,t) &= m^0 + m^1 + m^2 + \sum_{k=3}^{\infty} m^k \\ &= \frac{2844T\pi}{k} \eta_i \int_0^t \tilde{q}(t') [1 + \kappa(t')] S(x, t - t') dt' - 2\eta_i \left[\frac{\partial \omega^1}{\partial m^1} \left(\frac{\partial m^1}{\partial x} \right)^2 \right]_{x,t} \\ &\quad - 2\eta_i \sum_{k=2}^{\infty} \left\{ \left[\frac{\partial \omega^{k-1}}{\partial m^{k-1}} \left(\frac{\partial m^{k-1}}{\partial x} \right)^2 \right]_{x,t} - \left[\omega^{k-1} \frac{\partial \omega^{k-2}}{\partial m^{k-2}} \left(\frac{\partial m^{k-2}}{\partial x} \right)^2 \right]_{x,t} \right\} \end{aligned} \quad (5.82)$$

where

$$\begin{aligned} \kappa(t) &= \kappa^1(t) + \kappa^2(t) = \left(1 - \omega^1\right)_{x=0} \kappa^1(t) \\ &= \left\{ \left(\omega^1 - 1\right) \left[\omega^0 + \left(1 - \frac{\overline{m^0}}{m^0}\right) \frac{\partial \omega^0}{\partial \ln m^0} \right] \right\}_{x=0} \end{aligned} \quad (5.83)$$

Consider Eq. 5.82 on the fracture plane ($x = 0$):

$$\begin{aligned} m(0,t) &= \frac{2844T\pi}{k} \eta_i \int_0^t \tilde{q}(t') [1 + \kappa(t')] S(0, t - t') dt' \\ &\quad + 2\eta_i \left[\frac{\omega^1}{m^0} \frac{\partial \omega^0}{\partial \ln m^0} \left(\frac{\partial m^0}{\partial x} \right)^2 \right]_{0,t} \\ &= \frac{2844T\sqrt{\pi\eta_i}}{2k} \int_0^t \tilde{q}(t') [1 + \kappa(t')] \frac{dt'}{\sqrt{(t-t')}} \\ &\quad + 2\eta_i \left(\frac{2844T\pi}{k} \right)^2 \left(\frac{\omega^1}{m^0} \frac{\partial \omega^0}{\partial \ln m^0} \right)_{0,t} [\tilde{q}(t)]^2 \end{aligned} \quad (5.84)$$

Let us consider the sequence of time $0 = t_0 < t_1 < t_2 \cdots < t_n < t_{n+1} = t$ and write Eq. 5.84 as

$$\begin{aligned}
m(0,t) &= \frac{2844T\sqrt{\pi\eta_i}}{2k} \sum_{i=1}^n \int_{t_i}^{t_{i+1}} \tilde{q}(t') [1 + \kappa(t')] \frac{dt'}{\sqrt{(t-t')}} \\
&\quad + 2\eta_i \left(\frac{2844T\pi}{k} \right)^2 \left(\frac{\omega^1}{m^0} \frac{\partial \omega^0}{\partial \ln m^0} \right)_{0,t} [\tilde{q}(t)]^2
\end{aligned} \tag{5.85}$$

For $t_i < t' < t_{i+1}$, if we approximate

$$\tilde{q}(t') [1 + \kappa(t')] \approx \tilde{q}(t_{i+1}) [1 + \kappa(t_{i+1})] \equiv \tilde{q}_{i+1} (1 + \kappa_{i+1}) \equiv \frac{q_{i+1}}{2x_f h} (1 + \kappa_{i+1}) \tag{5.86}$$

where $q(t)$ is the flow rate from the entire surface of the fracture, Eq. 5.85 becomes

$$\begin{aligned}
m(0,t) &= \frac{2844T\sqrt{\pi\eta_i}}{2x_f kh} \sum_{i=1}^n q_{i+1} (1 + \kappa_{i+1}) \int_{t_i}^{t_{i+1}} \frac{dt'}{\sqrt{(t-t')}} \\
&\quad + \frac{\eta_i}{2} \left(\frac{2844T\pi}{x_f kh} \right)^2 \left(\frac{\omega^1}{m^0} \frac{\partial \omega^0}{\partial \ln m^0} \right)_{0,t} [q(t)]^2 \\
&= \frac{2844T\sqrt{\pi\eta_i}}{2x_f kh} \sum_{i=1}^n q_{i+1} (1 + \kappa_{i+1}) (\sqrt{t-t_i} - \sqrt{t-t_{i+1}}) \\
&\quad + \frac{\eta_i}{2} \left(\frac{2844T\pi}{x_f kh} \right)^2 \left(\frac{\omega^1}{m^0} \frac{\partial \omega^0}{\partial \ln m^0} \right)_{0,t} [q(t)]^2
\end{aligned} \tag{5.87}$$

Expanding

$$\begin{aligned}
m(0,t) &= \frac{2844T\sqrt{\pi\eta_i}}{2x_f kh} \left[q_1 (1 + \kappa_1) (\sqrt{t-t_0} - \sqrt{t-t_1}) \right. \\
&\quad + q_2 (1 + \kappa_2) (\sqrt{t-t_1} - \sqrt{t-t_2}) \\
&\quad + q_3 (1 + \kappa_3) (\sqrt{t-t_2} - \sqrt{t-t_3}) \\
&\quad \vdots \\
&\quad + q_n (1 + \kappa_n) (\sqrt{t-t_{n-1}} - \sqrt{t-t_n}) \\
&\quad \left. + q_{n+1} (1 + \kappa_{n+1}) (\sqrt{t-t_n} - \sqrt{t-t_{n+1}}) \right] \\
&\quad + \frac{\eta_i}{2} \left(\frac{2844T\pi}{x_f kh} \right)^2 \left(\frac{\omega^1}{m^0} \frac{\partial \omega^0}{\partial \ln m^0} \right)_{0,t} [q(t)]^2
\end{aligned} \tag{5.88}$$

Because $t_0 = 0$ and $t_{n+1} = t$, we can rearrange Eq. 5.88 as follows:

$$m(0,t) = \frac{2844T\sqrt{\pi\eta_i}}{2x_f kh} \left\{ q_1(1+\kappa_1)\sqrt{t} + \sum_{i=1}^n [q_{i+1}(1+\kappa_{i+1}) - q_i(1+\kappa_i)]\sqrt{t-t_i} \right\} + \frac{\eta_i}{2} \left(\frac{2844T\pi}{x_f kh} \right)^2 \left(\frac{\omega^1}{m^0} \frac{\partial \omega^0}{\partial \ln m^0} \right)_{0,t} [q(t)]^2 \quad (5.89)$$

or,

$$m(0,t) = \frac{200.5T}{(x_f\sqrt{k})h\sqrt{(\phi c_t \mu)_i}} \left\{ q_1(1+\kappa_1)\sqrt{t} + \sum_{i=1}^n [q_{i+1}(1+\kappa_{i+1}) - q_i(1+\kappa_i)]\sqrt{t-t_i} \right\} + \frac{\eta_i}{2} \left(\frac{2844T\pi}{x_f kh} \right)^2 \left(\frac{\omega^1}{m^0} \frac{\partial \omega^0}{\partial \ln m^0} \right)_{0,t} [q(t)]^2 \quad (5.90)$$

Dividing by $q(t) = q(t_{n+1}) = q_{n+1}$

$$\frac{m(0,t)}{q(t)} = \frac{2844T\sqrt{\pi\eta_i}}{2x_f kh} \left\{ \frac{q_1}{q(t)}(1+\kappa_1)\sqrt{t} + \sum_{i=1}^n \left[\frac{q_{i+1}}{q(t)}(1+\kappa_{i+1}) - \frac{q_i}{q(t)}(1+\kappa_i) \right] \sqrt{t-t_i} \right\} + \frac{\eta_i}{2} \left(\frac{2844T\pi}{x_f kh} \right)^2 \left(\frac{\omega^1}{m^0} \frac{\partial \omega^0}{\partial \ln m^0} \right)_{0,t} q(t) \quad (5.91)$$

or,

$$\frac{m(0,t)}{q(t)} = \frac{200.5T}{(x_f\sqrt{k})h\sqrt{(\phi c_t \mu)_i}} \left\{ \frac{q_1}{q(t)}(1+\kappa_1)\sqrt{t} + \sum_{i=1}^n \left[\frac{q_{i+1}}{q(t)}(1+\kappa_{i+1}) - \frac{q_i}{q(t)}(1+\kappa_i) \right] \sqrt{t-t_i} \right\} + \frac{\eta_i}{2} \left(\frac{2844T\pi}{x_f kh} \right)^2 \left(\frac{\omega^1}{m^0} \frac{\partial \omega^0}{\partial \ln m^0} \right)_{0,t} q(t) \quad (5.92)$$

5.3 Computational Procedure

To numerically evaluate the solution in Eq. 5.92, we need to evaluate ω_0 and ω_1 . This requires that we compute m^0 and m^1 , convert pseudo-pressures to pressures, and evaluate ω_0 and ω_1 at these pressures. Let us first consider m^0 given in Eq. 5.77. Following the lines used in the derivation of Eq. 5.89, we can write,

$$m^0(0,t) = \frac{200.5T}{(x_f \sqrt{k}) h \sqrt{(\phi c_i \mu)_i}} \left[q_1 \sqrt{t} + \sum_{i=1}^n (q_{i+1} - q_i) \sqrt{t-t_i} \right] \quad (5.93)$$

Similarly, we can write Δm^1 in Eq. 5.78 as follows:

$$m^1(0,t) = \frac{200.5T}{(x_f \sqrt{k}) h \sqrt{(\phi c_i \mu)_i}} \left[q_1 \kappa_1^1 \sqrt{t} + \sum_{i=1}^n (q_{i+1} \kappa_{i+1}^1 - q_i \kappa_i^1) \sqrt{t-t_i} \right] \quad (5.94)$$

where

$$\kappa_i^1 = \kappa^1(t_i) = - \left[\omega_i^0 + \left(1 - \frac{\bar{m}^0}{m^0} \right)_i \left(\frac{\partial \omega^0}{\partial \ln m^0} \right)_i \right] = - \left[(\omega^0)_{\Delta m^0(t_i)} + \left(1 - \frac{\bar{m}^0(t_i)}{m^0(t_i)} \right) \left(\frac{\partial \omega^0}{\partial \ln m^0} \right)_{t_i} \right] \quad (5.95)$$

For an infinite reservoir, we can assume $\bar{m}^0(t) = \bar{m}^0(t=0) = 0$ and write Eq. 5.95 as follows:

$$\kappa_i^1 = \kappa^1(t_i) = - \left[\omega_i^0 + \left(\frac{\partial \omega^0}{\partial \ln m^0} \right)_i \right] = - \left[(\omega^0)_{m^0(t_i)} + \left(\frac{\partial \omega^0}{\partial \ln m^0} \right)_{t_i} \right] \quad (5.96)$$

The step-by-step computational procedure is the following:

1. Divide the range of the pressure, $14.7 \text{ psi} \leq p \leq p_i$, into K points ($K = 100$ is usually sufficient) and generate tables of p_k vs. m_k and p_k vs. Δm_k for $k = 1, 2, \dots, K$.
2. Compute $m^0(t_i)$ for $i = 1, 2, \dots, n+1$ from Eq. 5.93.
3. Convert $m^0(t_i)$ to $p^0(t_i)$ using the p_k vs. m_k table (use interpolation when the $m^0(t_i)$ value falls between m_k and m_{k+1}).
4. Compute ω_i^0 at $p^0(t_i)$ for $i = 1, 2, \dots, n+1$ by using the correlations for the gas viscosity and compressibility.
5. Make a table of ω_i^0 vs. $m^0(t_i)$ and evaluate $(\partial \omega^0 / \partial \ln m^0)_{t_i} = \left[m^0 (\partial \omega^0 / \partial m^0) \right]_{t_i}$ for $i = 1, 2, \dots, n+1$
6. Using the computed values of ω_i^0 and $(\partial \omega^0 / \partial \ln m^0)_{t_i}$, evaluate κ_i^1 from Eq. 5.96 for $i = 1, 2, \dots, n+1$
7. Using κ_i^1 , compute $m^1(t_i)$ for $i = 1, 2, \dots, n+1$ from Eq. 5.94.
8. Follow steps 3 and 4 to generate a table of ω_i^1 vs. $m^1(t_i)$.
9. Compute κ_i from Eq. 5.83 by assuming $\bar{m}^0(t) = \bar{m}^0(t=0) = 0$ as follows:

$$\kappa_i = \kappa(t_i) = (\omega_i^1 - 1) \left[\omega_i^0 + \left(\frac{\partial \omega^0}{\partial \ln m^0} \right)_i \right] = (1 - \omega_i^1) \kappa_i^1 \quad (5.97)$$

where κ_i^1 are the values computed in Step 6.

- Using κ_i , compute $m^0(0, t)$ or $m^0(0, t)/q(t)$ from Eq. 5.90 or 5.92, respectively.

CHAPTER 6

VERIFICATION OF THE SPECTRAL SOLUTION AND APPLICATIONS

This chapter verifies the spectral solution presented in Chapter 4 by considering asymptotic cases and comparing its results to numerical simulations. Applications of the spectral solution are also presented to emphasize the importance of taking into account the variation of the viscosity-compressibility product.

For the discussions in this chapter, the data in Table 6.1 are used. Different correlations can be chosen for the z-factor, gas compressibility, and gas viscosity (Lodono et al., 2002). In this research, the gas properties have been computed from the correlations shown in Fig. 6.1.

TABLE 6.1: RESERVOIR AND FLUID DATA	
Formation height, h , ft	37.15
Fracture half length, x_f , ft	70
Matrix permeability, k , md	3.584E-04
Matrix porosity, ϕ	0.08
Reservoir Length, L_e , ft	1000
Specific gas gravity, SG	0.57
Initial Reservoir Pressure, P_i , psia	9597
Initial Reservoir Temperature, T_i , °F	258

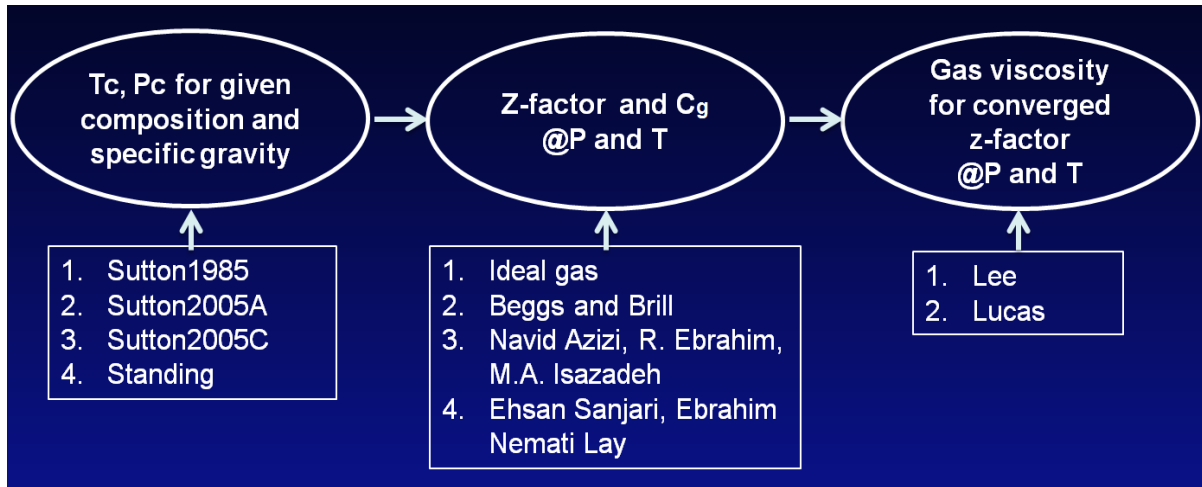


Figure 6.1: Gas property correlations used in this work.

To simulate different production scenarios, the wellbore boundary conditions shown in Table 6.2 will be used. The wellbore boundary conditions shown in Table 6.2 are based on statistical models (Veena et al., n.d.) and can be used to simulate various constant and variable pressure production conditions. Once the decline behavior is selected (Column 1), user can control the decline rate by changing the parameters a , b , c , and d .

TABLE 6.2: WELLBORE BOUNDARY CONDITION MODELS	
Constant Pressure	$p_{wf}(t) = a \quad (6.1)$
Rational Model	$p_{wf}(t) = \frac{(a + bt)}{(1 + ct + dt^2)} \quad (6.2)$
Morgan-Mercer-Flodin Model	$p_{wf}(t) = \frac{(ab + ct^d)}{(b + t^d)} \quad (6.3)$
Weibull Model	$p_{wf}(t) = a - b \exp(-ct^d) \quad (6.4)$
Polynomial Model	$p_{wf}(t) = a_0 + a_1t + a_2t^2 + a_3t^3 + a_4t^4 + \dots \quad (6.5)$
Error Function Model	$p_{wf}(t) = 0.5 \{1 - \text{erf} [a(t - t_s)]\} (p_{\max} - p_{\min}) + p_{\min} \quad (6.6)$

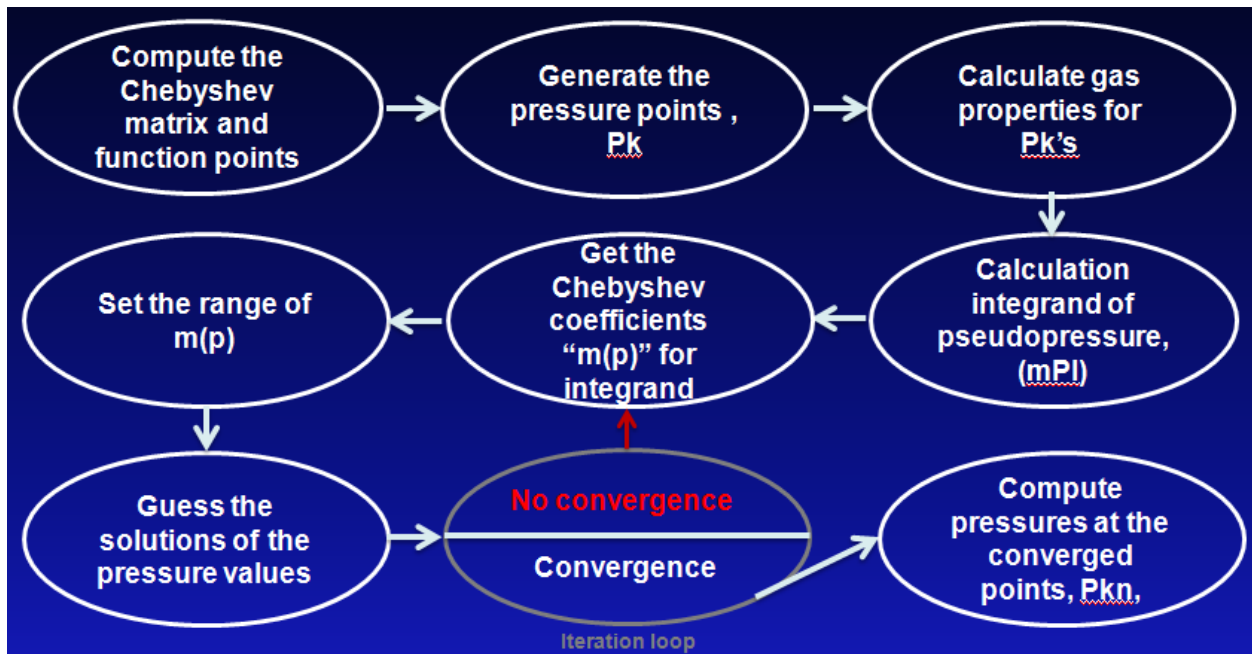


Figure 6.2: Spectral Solution Algorithm.

Figure 6.2 shows the workflow to compute the pressure and pseudo-pressure values by the spectral solution. The solution is faster than the conventional solutions for simple geometries due to the exact computation of the derivatives and the exponential convergence for smooth functions. In addition, the solution method approximates the solution as a linear combination of continuous functions that are generally nonzero throughout the domain (global approach). Besides all these advantages, the nonlinear terms are very easy to incorporate.

6.1 Comparison of the Analytical (Similarity) and Spectral Solutions

Thompson (2012) created analytical and numerical solutions for both constant and variable viscosity-compressibility product effects on constant and variable pressure production. Here the results of the analytical (similarity) and the spectral solutions will be compared.

Figure 6.3 compares the analytical and spectral results under constant-pressure-production condition for both constant and variable compressibility-viscosity production scenarios. The results are plotted in terms of rate-normalized pseudo-pressure versus square root of time in Fig. 6.3. Skin is not included in this example. The results obtained by the analytical and spectral solutions display excellent match verifying the accuracy of the spectral solution. As noted above, the spectral solution is much faster than the similarity solution.

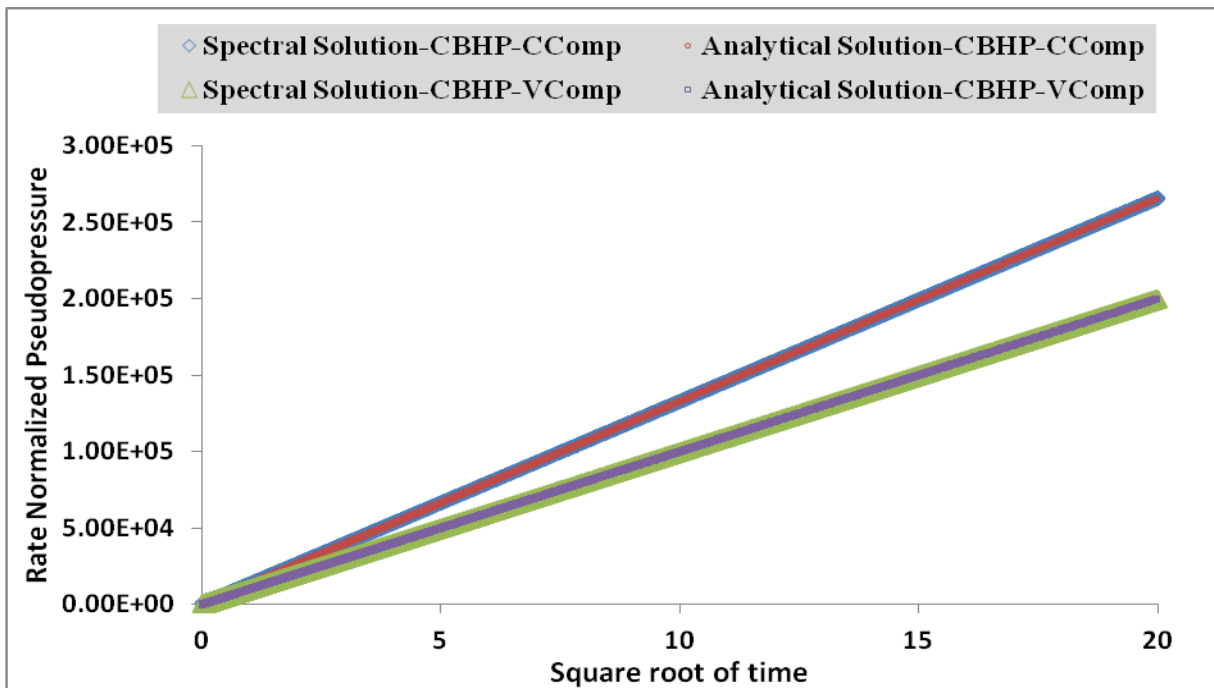


Figure 6.3: Spectral and Analytical Models match.

The comparison of the flow rates obtained by the analytical and spectral solution is shown on Fig. 6.4. As expected, although all solutions display the same trend, the solutions for the constant compressibility-viscosity condition yield lower flow rates than pressure-dependent compressibility-viscosity solution.

The comparison shown in Fig. 6.4 show some discrepancies between the analytical and spectral solutions at early times. This is a result of the relatively low number of collocation points used in the Chebyshev polynomial approximation (120 points for this case). Although the excellent match between the analytical and spectral solutions after 0.01 days is sufficient for the verification of the spectral solution, if necessary, the accuracy of the spectral solution at very early times ($t < 0.01$ days) can be improved by increasing the number of collocation points used in the spectral solution. Sensitivity analysis for the collocation points will be shown later in this chapter.

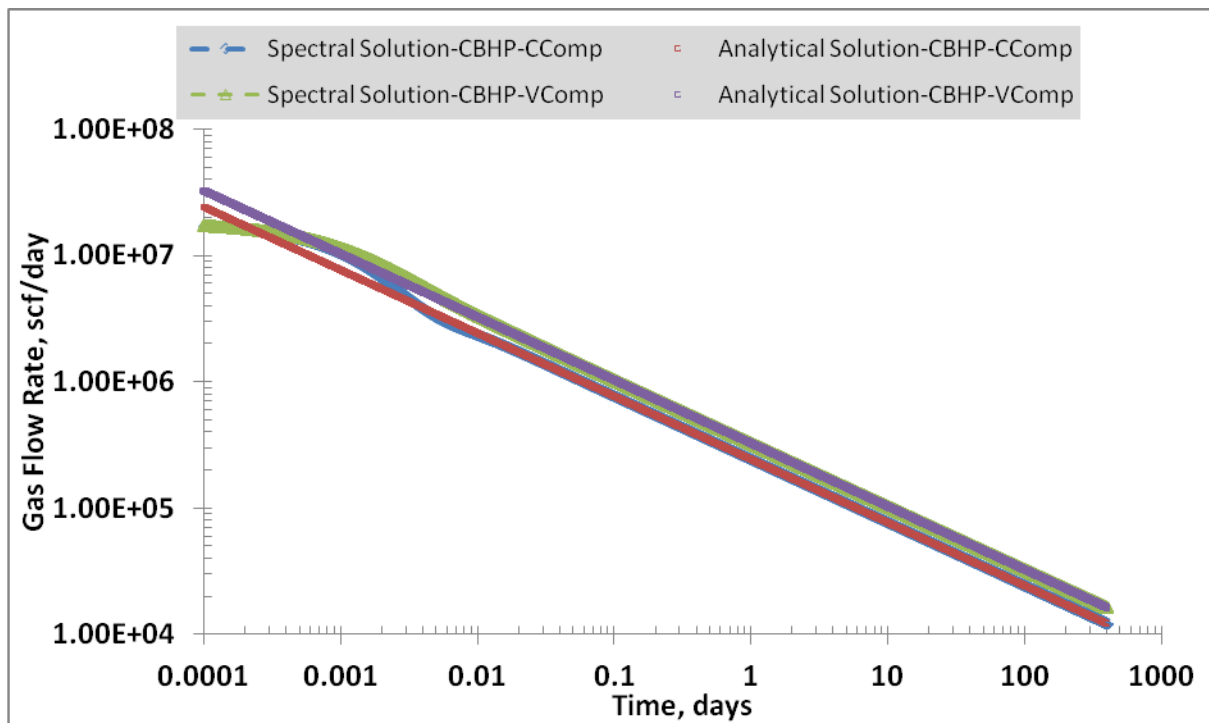


Figure 6.4: Gas flow rate vs. time obtained from the spectral and analytical solutions.

6.2 Comparison of the Spectral Solution with a Commercial Simulator

Numerical simulation is a common resort to deal with nonlinear flow problems. As noted earlier, one of the motivations of this work is to demonstrate that the spectral solution may be a more efficient alternative if the reservoir heterogeneity is not of concern. Having verified the

accuracy of the spectral solution in handling pressure-dependent viscosity-compressibility product, here we compare the spectral solution with a commercial simulator. In this study, we used Eclipse. It must be emphasized, however, that the conclusions drawn here are not about the particular choice of the simulator; our point is to show that finite-difference models may require excessive grid refinement to provide near-analytical accuracy of the spectral solution (Fig. 6.5).

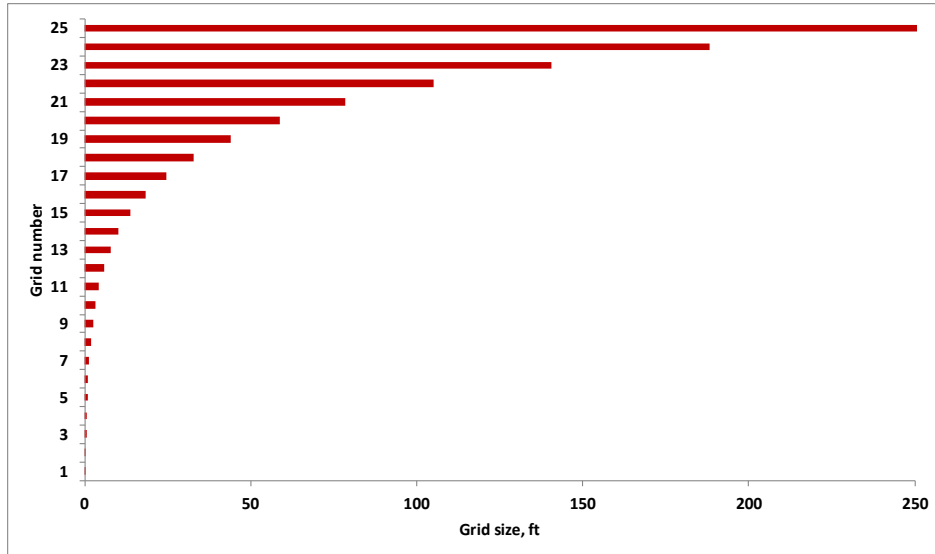


Figure 6.5: Logarithmic grid sizes of the Eclipse model.

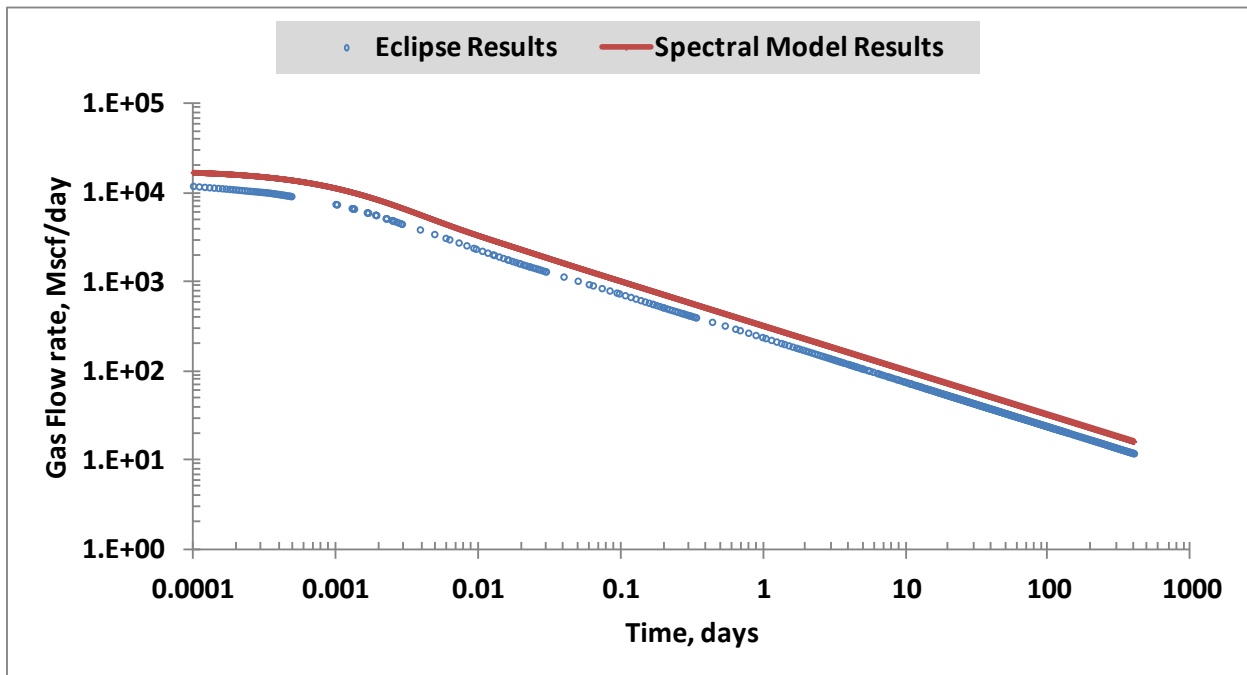


Figure 6.6: Eclipse vs. spectral model results for constant pressure production.

In Fig. 6.6, the same fluid and reservoir data are used to compare the two models under constant-pressure-production condition ($p_{wf} = 1000$ psia). Results in Fig. 6.6 show a similar rate decline behavior during the transient flow period for both Eclipse and spectral solution; however, the numerical simulator predicts lower rates (the spectral solution gives 13MMScf cumulative production while the simulator gives 9.46MMScf after 400 days). This supports our initial hypothesis that because of the grid size limitations, the finite difference simulator cannot capture the large changes in the viscosity-compressibility product in the near vicinity of the fracture face.

This gridding effect on the accuracy of the finite-difference simulation deteriorates when the complexity of the problem increases. In Fig. 6.6 no skin effect was considered around the fracture. Fig. 6.7 shows the pressure behavior for a variable-pressure-production scenario (Weibull model) with a skin zone ($s = 0.2$) around the fracture face. The corresponding rate decline behavior in Fig. 6.8 shows a larger discrepancy between the results of the spectral and numerical models at early times compared with the results of the constant-pressure-production case with no-skin shown in Fig. 6.6. The total gas productions in this case are 11.5MMScf and 8.4MMScf for the spectral and Eclipse models, respectively. Our numerical experiments have indicated that, due to excessive grid-refinement requirement, it would be almost impossible to improve the accuracy of the finite-difference model to the level of the spectral solution.

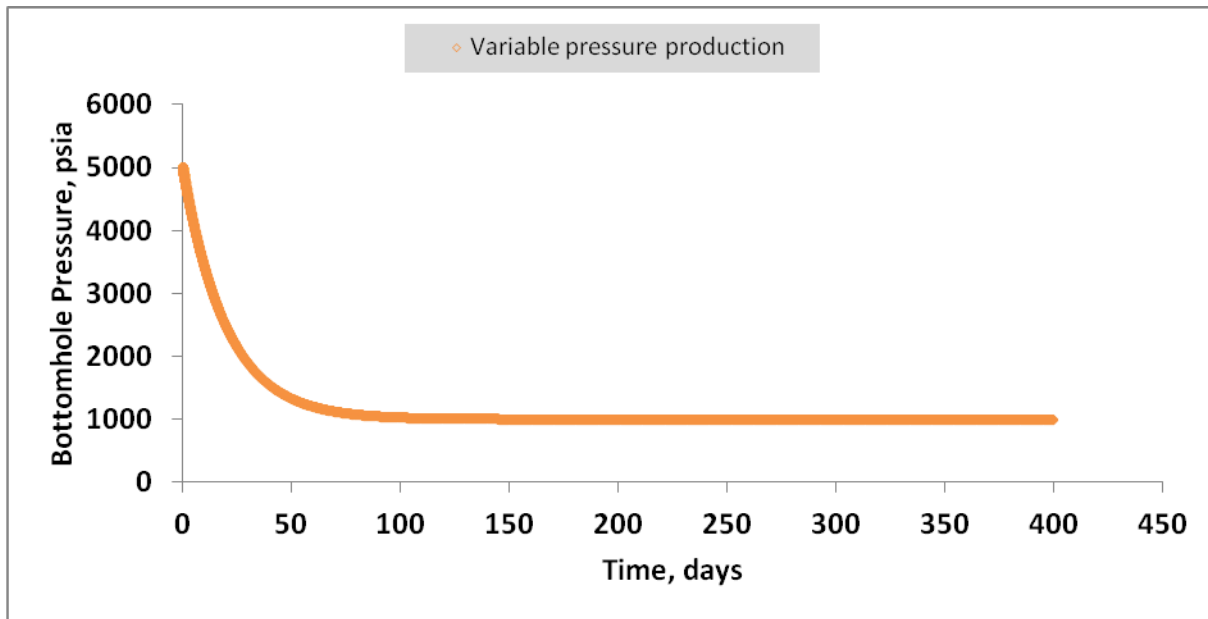


Figure 6.7: Bottomhole pressures for the variable-pressure-production scenario generated by the Weibull regression model.

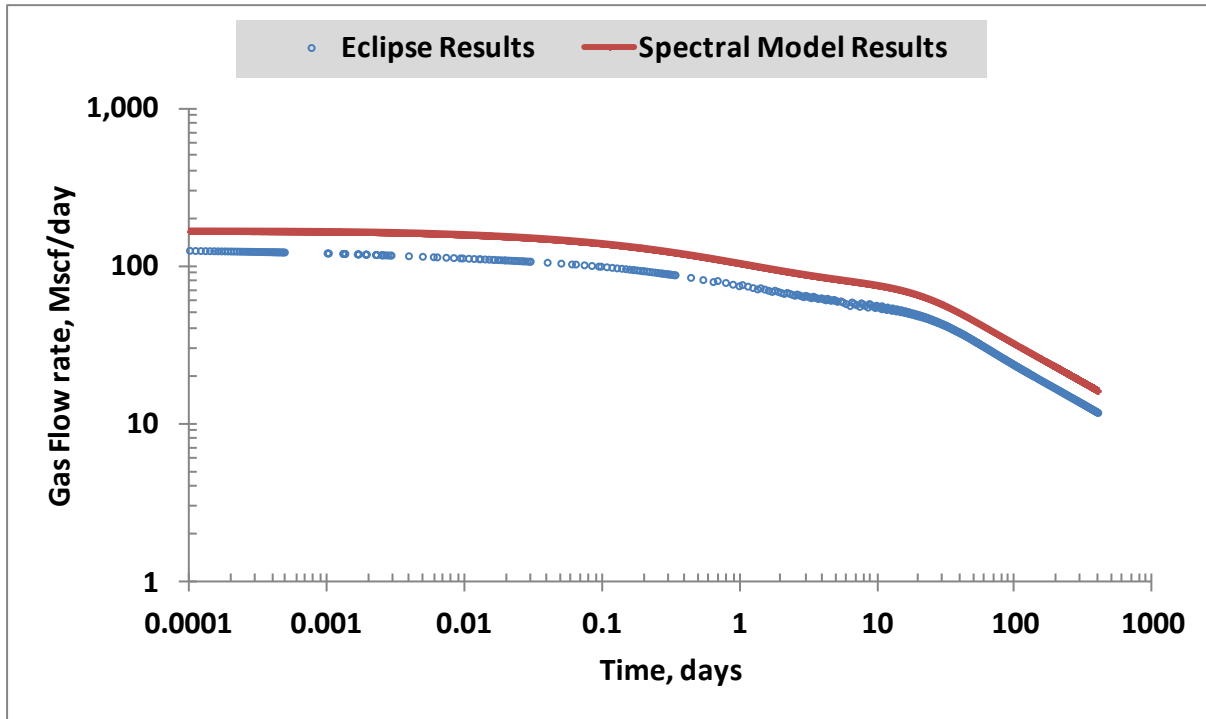


Figure 6.8: Comparison of the results of Eclipse and the spectral model for variable-pressure production with skin.

6.3 Comparison of Constant and Variable Viscosity-Compressibility product

As we mentioned earlier, pressure drops in fractures -especially in the vicinity of the wellbore- are very large to be neglected in tight-gas systems. Therefore, the main motivation of this research was to present new tools and approaches to improve the prediction and analysis of tight-gas-well responses when the viscosity-compressibility product displays strong variability with pressure. Here, we use the spectral solution to highlight the effect of variable viscosity and compressibility on the analysis of gas-well performances.

As shown in Fig. 6.9, the spectral solutions for transient flow period with and without variable viscosity-compressibility product assumptions follow similar linear-flow trends (a half-slope straight line); however, the constant viscosity-compressibility product solution yields lower rates than the variable compressibility-viscosity solution. This result is attributed to higher viscosity-compressibility changes around the fracture face due to large pressure drops, which cannot be taken into account by the constant compressibility and viscosity assumption.

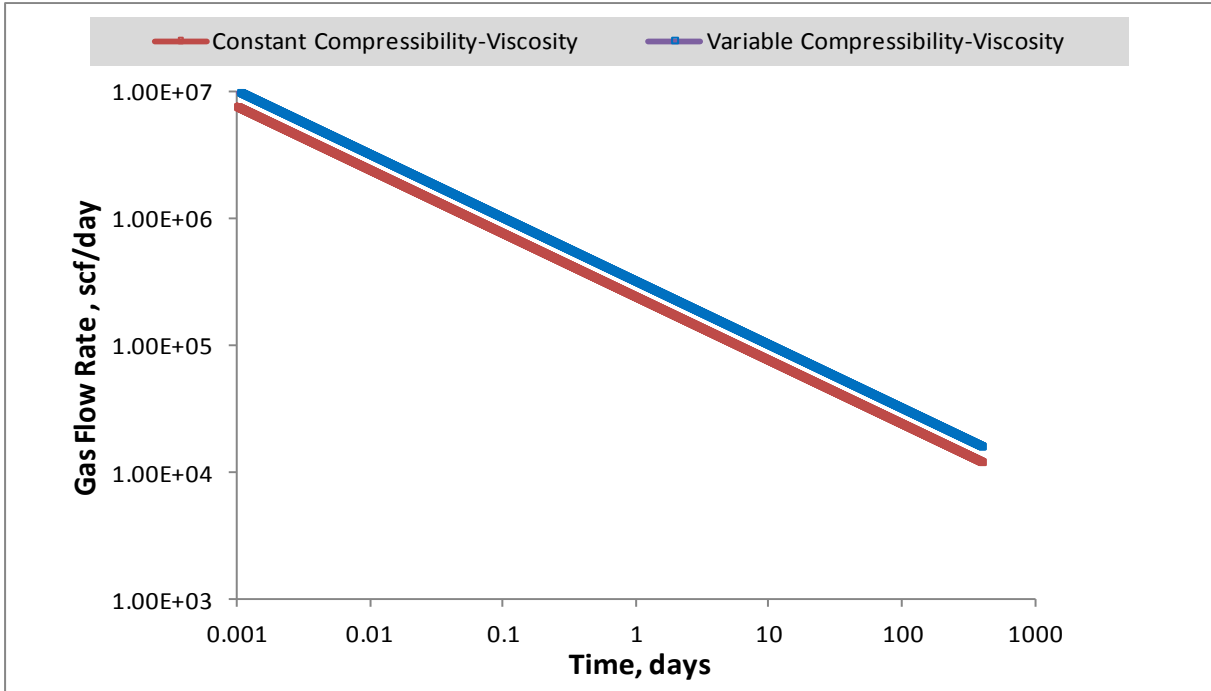


Figure 6.9: Constant vs. variable viscosity-compressibility product comparison for constant pressure production ($p_{wf}=1000$ psia).

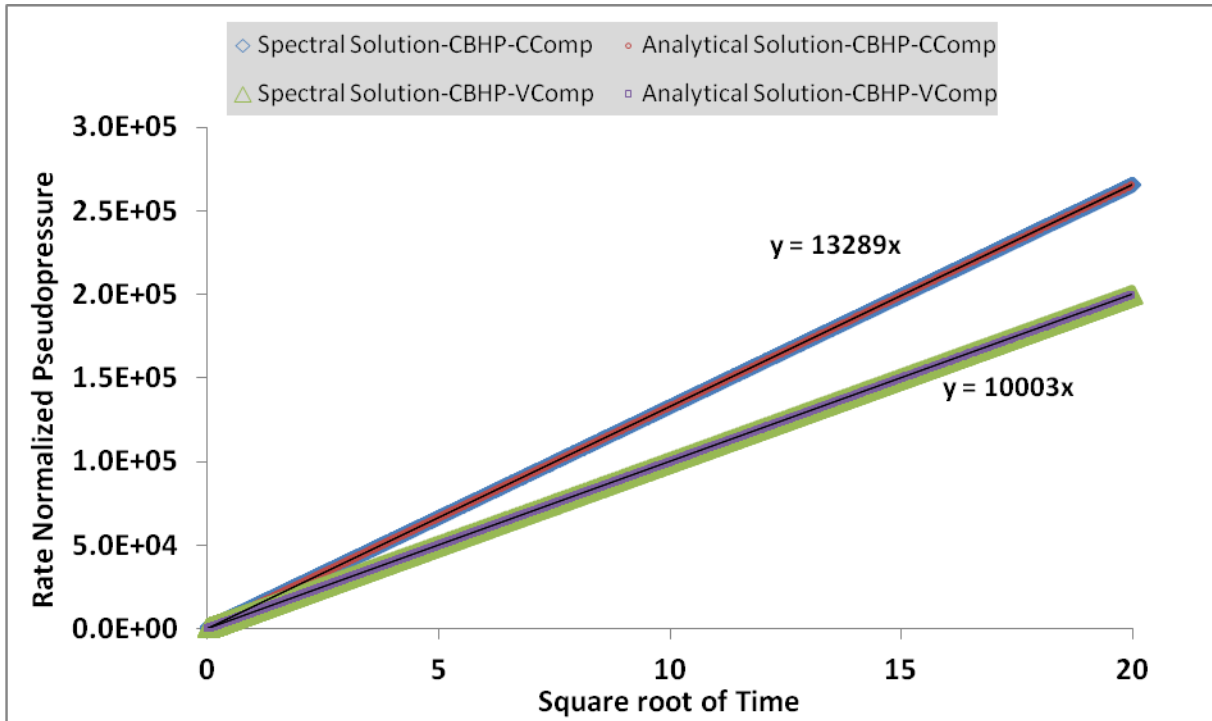


Figure 6.10: Rate-normalized pseudo-pressure vs. square root of time for constant and variable viscosity-compressibility product scenarios: Constant pressure production ($p_{wf}=1000$ psia).

Figure 6.10 shows the rate normalized pseudo-pressure, $m(p_{wf})_c / q_g$, vs. square root of time for the constant pressure production ($p_{wf} = 1000$ psia) scenario considered in Fig. 6.6. The results for both constant and variable viscosity-compressibility product scenarios display straight lines. Consideration of the variation in viscosity and compressibility, however, yields a straight line with smaller slope. As mentioned in Chapter 2, in the conventional analysis of the rate-normalized pseudo-pressure responses for constant-pressure production, an estimate of the permeability-cross sectional area product is obtained from the expected slope of the straight line given by Eq. 2.8.

In Fig. 6.10, the larger slope value corresponding to the constant viscosity-compressibility assumption gives $1.356 \text{ ft}\cdot\sqrt{\text{md}}$ for $x_f\sqrt{k}$ ($k = 3.58 \times 10^{-4} \text{ md}$). On the other hand, the smaller slope value for the variable viscosity-compressibility assumption gives $1.762 \text{ ft}\cdot\sqrt{\text{md}}$ ($k = 6.34 \times 10^{-4} \text{ md}$). Therefore, the use of the expected slope (Eq. 2.8) based on the constant viscosity-compressibility product assumption leads to the estimation of higher $x_f\sqrt{k}$ values if the viscosity-compressibility product is a function of pressure.

TABLE 6.3: SQUARE ROOT OF TIME ANALYSIS OF THE FOUR VARIABLE COMPRESSIBILITY-VISCOSITY PRODUCT SCENARIOS						
Constant Bottomhole Pressure, psia	$m(p_i)$ $p_i = 9597 \text{ psia}$	$m(p_{wf,c})$	$\psi_1(x=0)$	Slope m	kx_f	Error, %
$p_{wf,c}=1000$	3.31E+09	6.56E+07	5.815	2333.8	0.10753	9E-05
$p_{wf,c}=2000$	3.31E+09	2.55E+08	5.985	2406.2	0.10735	1E-03
$p_{wf,c}=3000$	3.31E+09	5.42E+08	6.438	2508.5	0.10668	7.8E-03
$p_{wf,c}=4000$	3.31E+09	8.96E+08	6.201	2591.6	0.10722	2.8E-03

To further verify the observations from Fig. 6.10, four more variable viscosity-compressibility product scenarios have been simulated for the constant bottomhole pressures of $p_{wf,c} = 1000, 2000, 3000,$ and 4000 psia. The results have been analyzed by using the slope relation indicated by the similarity solution of the variable viscosity-compressibility product problem given by Eq. 3.96 in Chapter 3. Table 6.3 summarizes the analysis and the estimates of

the kx_f product. The correct kx_f value for the cases in Table 6.3 is 0.10752 md-ft ($k = 3.584\text{E-}04$ md and $x_f = 300$) ft. The $y_1(x = 0)$ term in Table 6.3 represents the correction coefficient for the slope of the constant viscosity-compressibility case (Eq. 2.8) and is computed numerically by an iterative procedure discussed in Chapter 2.

6.4 Correction Factors for Square-Root-of-Time and Superposition-Time Analyses

Ibrahim and Wattenbarger (2006) presented a correction factor approach to improve the accuracy of the estimations of $\sqrt{kx_f}$ from the square-root-of-time and superposition-time analyses. Here, a brief introduction of the correction factor approach will be provided for infinite-acting flow conditions and it will be shown that Ibrahim and Wattenbarger's correction factors do not sufficiently improve the estimates of $\sqrt{kx_f}$ results. Then, using the data generated in this research, new corrections factors will be presented.

Ibrahim and Wattenbarger (2006) also presented a correction factor to improve the estimation of the distance to the boundary from the end of transient linear flow regime on the square root of time plot. An improved correction factor will also be presented here to be used for the variable viscosity-compressibility conditions.

6.4.1 Correction Factors for Infinite-Acting Reservoirs

We discuss the application of the correction factor approach for the square root of time analysis of the gas-well responses in infinite-acting systems first. Then, we consider and correction factor for the superposition time analysis.

6.4.1.1 Correction Factor for Square Root of Time Analysis

Ibrahim and Wattenbarger (2006) noted that high drawdowns could cause serious errors in the estimates of $\sqrt{kx_f}$ product by the transient linear-flow analysis of gas-well performances. To correct these errors, they proposed the use of the following corrected slope relation for the square-root-of-time analysis:

$$m = f_{\sqrt{t}} \frac{0.315}{h \sqrt{\phi(c_t \mu_g)_i}} \frac{T}{\sqrt{kx_f}} \quad (6.7)$$

where $f_{\sqrt{t}}$ is the correction factor given by

$$f_{\sqrt{t}} = 0.9895 - 0.0852D_D - 0.0857D_D^2 \quad (6.8)$$

and

$$D_D = \frac{[\tilde{m}(p_i) - \tilde{m}(p_{wf})]}{\tilde{m}(p_i)} \quad (6.9)$$

In Eq. 6.9, $\tilde{m}(p)$ is the pseudo-pressure defined by Ibrahim and Wattenbarger (2006) as follows:

$$\tilde{m}(p) = 2 \int_0^p \frac{p'}{\mu z} dp' = m(0) - m(p) \quad (6.10)$$

To demonstrate the application and the accuracy of the correction factor, in Fig. 6.11, rate-normalized pseudo-pressure defined by Eq. 6.10 is plotted against \sqrt{t} for four constant bottomhole pressures, $p_{wf,c} = 1000, 2000, 3000,$ and 4000 psia, and for a fracture half-length of 300 ft. Table 6.4 summarizes the input data and the estimation of $\sqrt{k}x_f$ by using the correction factor approach. As shown in the last column of Table. 6.4, the calculated $\sqrt{k}x_f$ values still include considerable error despite the use of the correction factor and the error is larger for higher drawdowns (lower bottomhole pressures).

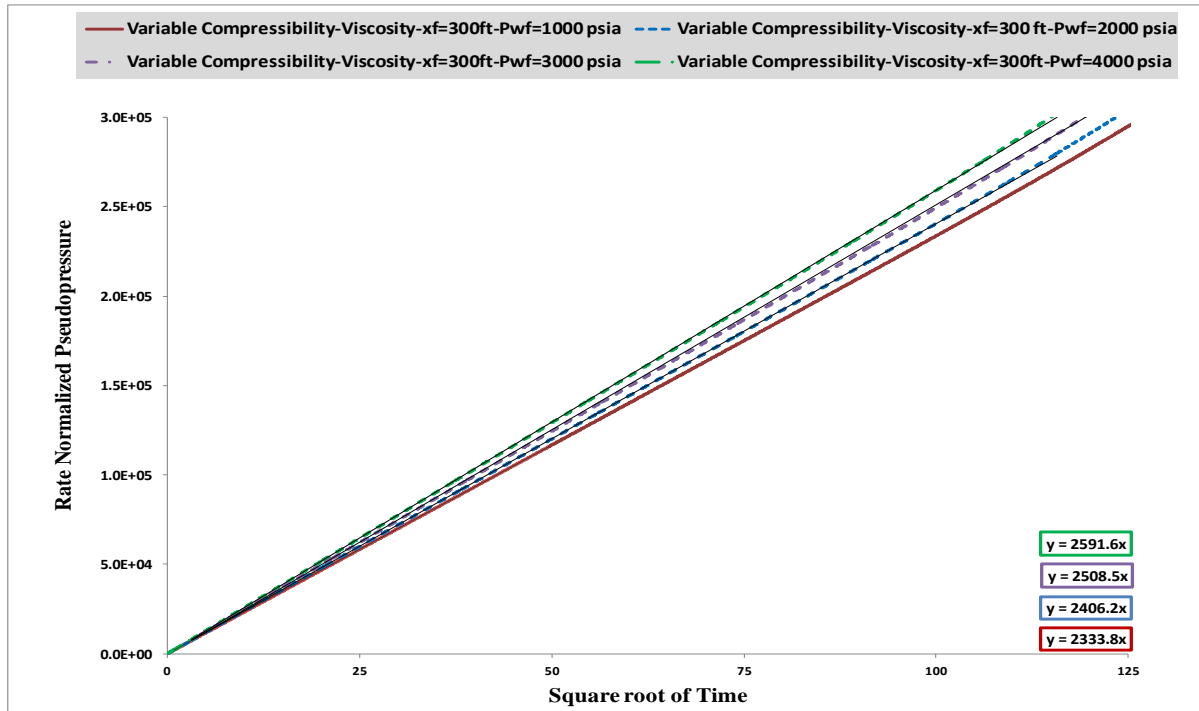


Figure 6.11: Square root of time plot to calculate $\sqrt{k}x_f$ for constant $p_{wf,c}$ values of 1000, 2000, 3000 and 4000 psia.

TABLE 6.4: CALCULATED kx_f VALUES AND ERROR PERCENTAGES WITH CORRECTION FACTOR PROPOSED BY IBRAHIM AND WATTENBARGER						
Constant Bottomhole Pressure, psia	$\tilde{m}(p_i)$ $p_i = 9597$ psia	$\tilde{m}(p_{wf,c})$	$f_{\sqrt{t}}$	Slope m	$\sqrt{kx_f}$	Error, %
$p_{wf,c}=1000$	3.31E+09	6.56E+07	0.863644	2333.8	6.52	14.8
$p_{wf,c}=2000$	3.31E+09	2.55E+08	0.859587	2406.2	6.29	10.7
$p_{wf,c}=3000$	3.31E+09	5.42E+08	0.853778	2508.5	5.99	5.6
$p_{wf,c}=4000$	3.31E+09	8.96E+08	0.847193	2591.6	5.76	1.6

Because Ibrahim and Wattenbarger's (2006) correction factor (Eq. 6.8) does not yield satisfactory results for the variable viscosity-compressibility product cases considered in this study, a new correction factor has been developed by applying Ibrahim and Wattenbarger's (2006) procedure to the data generated by the spectral solution for constant bottomhole pressures between $p_{wf,c} = 500$ and $p_{wf,c} = 6000$ psia. Figure 6.12 shows the new correction factor, $f_{\sqrt{t}-new}$, computed from the data given in Table 6.5 vs. D_D (Eq. 6.5). The second order polynomial fit through the data points in Fig. 6.12 yields the following new correction factor correlation:

$$f_{\sqrt{t}-new} = 0.9561 - 0.0528D_D - 0.1582D_D^2 \quad (6.11)$$

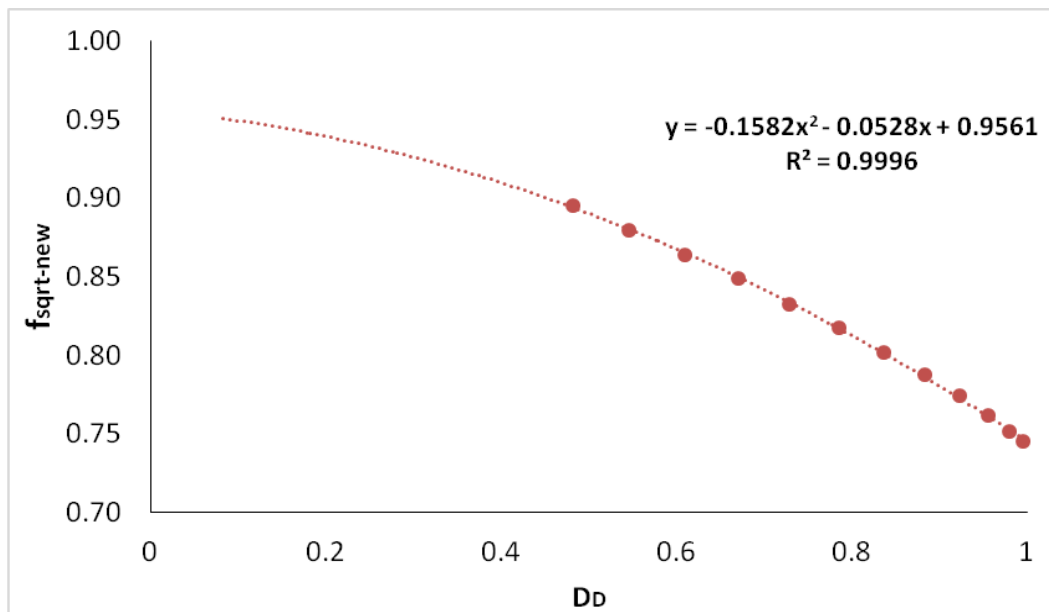


Figure 6.12: Correlation for the new correction factor for the square-root-of-time analysis.

TABLE 6.5: CALCULATED kx_f VALUES WITH THE NEW SQUARE ROOT OF TIME CORRECTION FACTOR					
Constant Bottomhole Pressure, psia	$\tilde{m}(p_i)$ $p_i = 9597$ psia	$\tilde{m}(p_{wf,c})$	Slope m	$f_{\sqrt{t}-new}$	$\sqrt{k}x_f$
$p_{wf,c} = 500$	3.31E+09	1.60E+07	2312.4	0.7448	5.678
$p_{wf,c} = 1000$	3.31E+09	6.56E+07	2334	0.7518	5.678
$p_{wf,c} = 1500$	3.31E+09	1.46E+08	2365.5	0.7619	5.678
$p_{wf,c} = 2000$	3.31E+09	2.55E+08	2402.9	0.7740	5.678
$p_{wf,c} = 2500$	3.31E+09	3.88E+08	2444.6	0.7874	5.678
$p_{wf,c} = 3000$	3.31E+09	5.42E+08	2489.6	0.8019	5.678
$p_{wf,c} = 3500$	3.31E+09	7.12E+08	2538	0.8175	5.678
$p_{wf,c} = 4000$	3.31E+09	8.96E+08	2585.2	0.8327	5.678
$p_{wf,c} = 4500$	3.31E+09	1.09E+09	2634.5	0.8486	5.678
$p_{wf,c} = 5000$	3.31E+09	1.29E+09	2682.8	0.8641	5.678
$p_{wf,c} = 5500$	3.31E+09	1.5E+09	2731.7	0.8799	5.678
$p_{wf,c} = 6000$	3.31E+09	1.71E+09	2778.7	0.8950	5.678

6.4.1.2 Correction Factor for Superposition-Time Analysis

As mentioned in previous chapters, another common approach to analyze tight-gas well performances is the use of superposition time. Ibrahim and Wattenbarger (2006) presented the following expression for the estimation of $\sqrt{k}x_f$ from the slope, m , of the superposition time plot:

$$\sqrt{k}x_f = f_{\text{super}} \frac{0.2007}{h\sqrt{\phi(c_t \mu_g)_i}} \frac{T}{m} \quad (6.12)$$

where f_{super} is the correction factor to minimize the errors in superposition time analysis of tight-gas well performances given by

$$f_{\text{super}} = 0.9833 - 0.0258D_D - 0.1512D_D^2 \quad (6.13)$$

Figure 6.13 shows the superposition-time plot for four constant bottomhole pressures of $p_{wf,c} = 1000, 2000, 3000$ and 4000 psia and Table 6.6 summarizes the calculation of f_{super} and $\sqrt{k}x_f$. The errors in $\sqrt{k}x_f$ estimates are documented in the last column of Table 6.6.

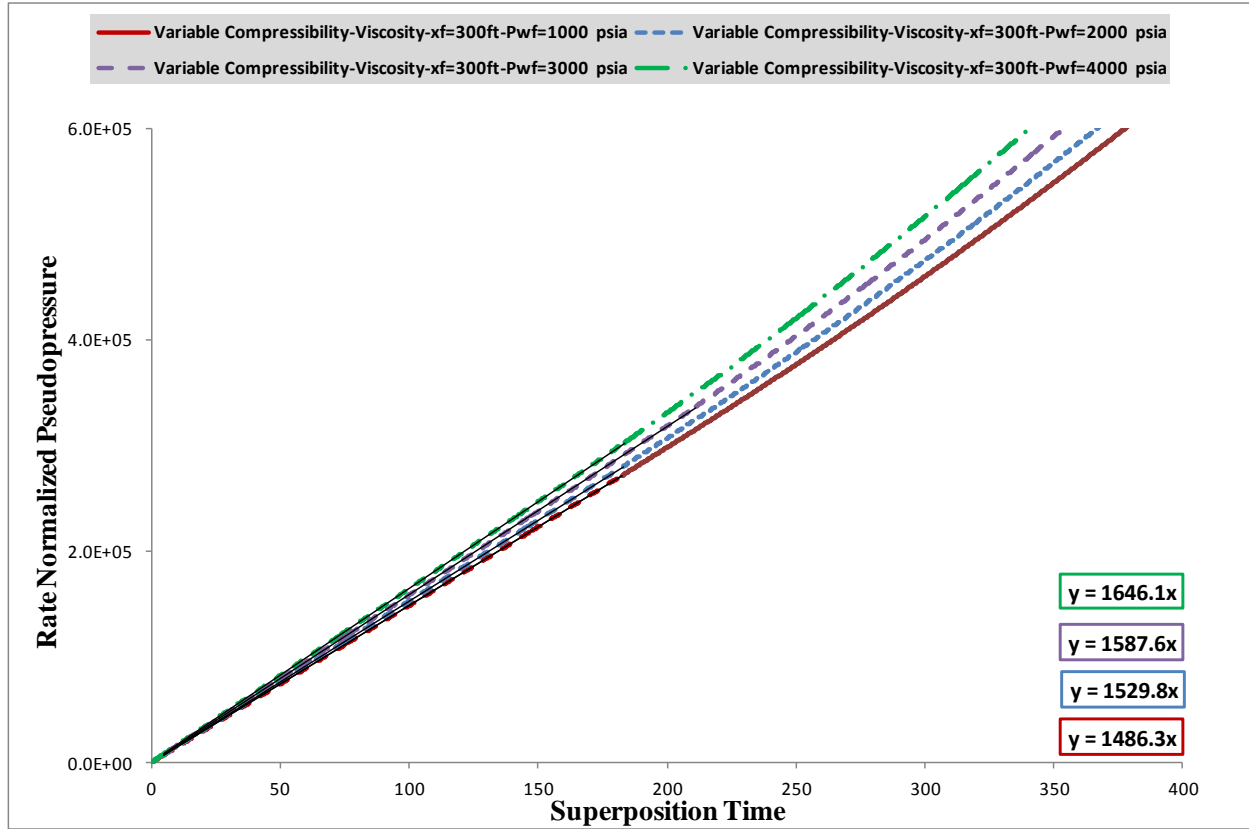


Figure 6.13: Superposition time plot to calculate $\sqrt{k}x_f$ for constant $p_{wf,c}$ values of 1000, 2000, 3000 and 4000 psia.

TABLE 6.6: CALCULATED kx_f VALUES AND ERROR PERCENTAGES WITH THE CORRECTION FACTOR PROPOSED BY IBRAHIM AND WATTENBARGER (2006)						
Constant Bottomhole Pressure, psia	$\tilde{m}(p_i)$ $p_i = 9597$ psia	$\tilde{m}(p_{wf,c})$	f_{super}	Slope m	$\sqrt{k}x_f$	Error, %
$p_{wf,c} = 1000$	3.31E+09	6.56E+07	0.8127	1486.3	7.56	33.15
$p_{wf,c} = 2000$	3.31E+09	2.55E+08	0.8307	1529.8	7.34	29.25
$p_{wf,c} = 3000$	3.31E+09	5.42E+08	0.8559	1587.6	7.07	24.49
$p_{wf,c} = 4000$	3.31E+09	8.96E+08	0.8841	1646.1	6.82	20.09

Errors shown in Table 6.6 indicate that Ibrahim and Wattenbarger's correction factor (Eq. 6.13) is not successful enough to improve the estimates of $\sqrt{kx_f}$ when the viscosity-compressibility product changes considerably with pressure. A new correction-factor correlation, $f_{\text{super-new}}$, for variable viscosity-compressibility cases has been developed from the data in Fig. 6.14 and is given by;

$$f_{\text{super-new}} = 0.9621 - 0.0673D_D - 0.1495D_D^2 \quad (6.14)$$

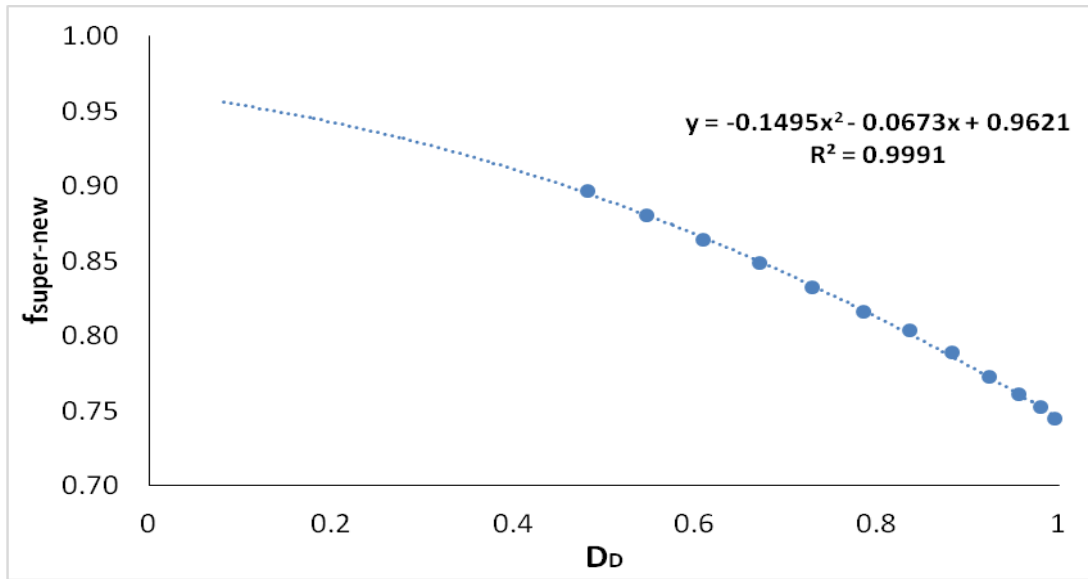


Figure 6.14: Calculation of new correction value for superposition time slope.

As shown in Table 6.7 for four example cases, the use of the new correction factor yields accurate results.

TABLE 6.7: CALCULATED kx_f VALUES WITH THE NEW SUPERPOSITION TIME CORRECTION FACTOR					
Constant Bottomhole Pressure, psia	$\tilde{m}(p_i)$ $p_i = 9597$ psia	$\tilde{m}(p_{wf,c})$	Slope m	$f_{\text{super-new}}$	$\sqrt{kx_f}$
$p_{wf,c} = 1000$	3.31E+09	6.56E+07	1486.3	0.7609	5.678
$p_{wf,c} = 2000$	3.31E+09	2.55E+08	1529.8	0.7730	5.678
$p_{wf,c} = 3000$	3.31E+09	5.42E+08	1587.6	0.8039	5.678
$p_{wf,c} = 4000$	3.31E+09	8.96E+08	1646.1	0.8327	5.678

6.4.2 Correction Factors for Bounded Reservoirs

In Figure 6.15, constant pressure production solutions for $p_{wf,c} = 1000, 2000, 3000$ and 4000 psia are plotted in terms of rate-normalized pseudo-pressure, $\tilde{m}(p_{wf,c})/q$ vs. square root of time. The parameter of interest in this case is the time for the end of the linear flow period.

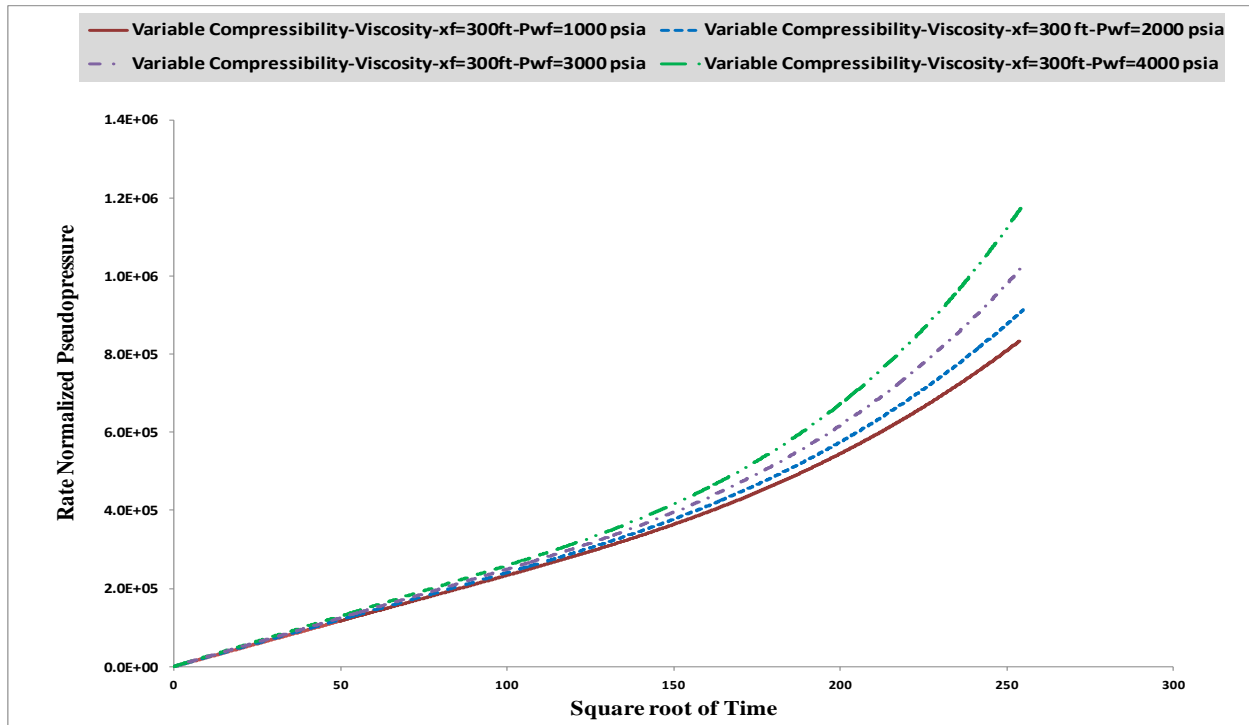


Figure 6.15: Boundary effects on square root of time plot.

Ibrahim and Wattenbarger (2006) proposed the following equation to calculate the drainage area, $A = 4x_f y_e$, or equivalently, the distance to the boundary, y_e , from the slope, m , and the time to the end of the straight line, t_{est} , on the square root of time plot:

$$A = \frac{0.2 \times T}{h(\phi c_t \mu_g)_i} \left(\frac{\sqrt{t_{est}}}{m} \right) \quad (6.15)$$

Table 6.8 shows the $\sqrt{t_{est}}$ values computed from Eq. 6.15 and read from Fig. 6.14 directly. Corrected values of $\sqrt{t_{est}}$ by using the corrected slope, m (Eq. 6.11), with the new correction factor, $f_{\sqrt{t}-new}$ (Eq. 6.11), are also given in Table 6.8.

TABLE 6.8: SQUARE ROOT OF TIME ANALYSIS FOR THE BOUNDED SYSTEM					
Constant Bottomhole Pressure, psia	Slope m	Calculated $\sqrt{t_{esl}}$	$f\sqrt{t}_{-new}$	Corrected $\sqrt{t_{esl}}$	Reading $\sqrt{t_{esl}}$
$p_{wf,c} = 1000$	2334	71.81	0.7518	95.52	115
$p_{wf,c} = 2000$	2402.9	73.93	0.7740	95.52	110
$p_{wf,c} = 3000$	2489.6	76.60	0.8019	95.52	105
$p_{wf,c} = 4000$	2585.2	79.54	0.8327	95.52	100
$p_{wf,c} = 5000$	2682.8	82.54	0.8641	95.52	100

Although the values read directly from Fig. 6.14 are closer to the corrected values of $\sqrt{t_{esl}}$, there is still a considerable difference between the two estimates. However, the error should be attributed to the accuracy of the graphical technique, which requires the determination of the time at which the data starts deviating from the straight-line behavior.

In the next figure, it can be seen that superposition time data deviates from the straight line behavior slightly for all production cases (Figure 6.16)

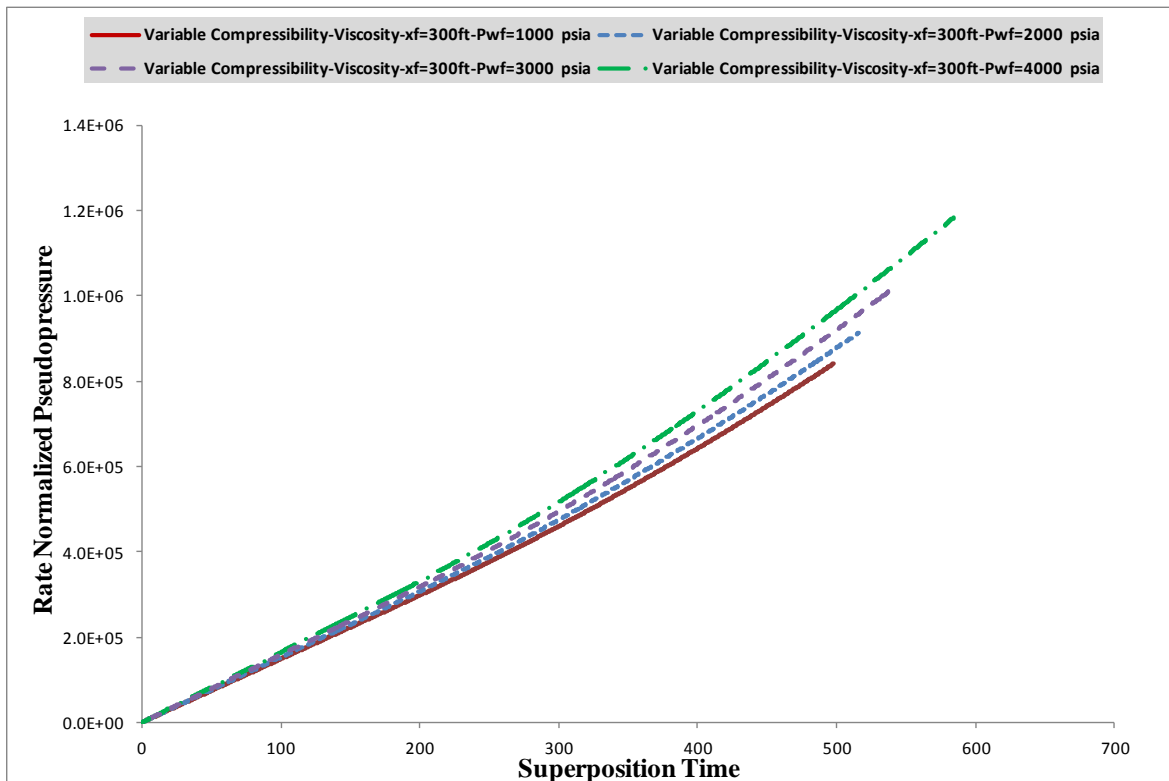


Figure 6.16: Boundary effects on superposition time plot.

6.5 Validity of Spectral Solution for Variable Pressure Production

In order to analyze variable pressure production, only one variable pressure production case has been used, and constant and pressure dependent compressibility-viscosity solution have been compared in flow, square root of time and superposition time plots.

In Figure 6.17, transient linear flow and boundary effects can be seen on the log-log plot of gas flow rate and time. Variable compressibility-viscosity solution produces with higher rates and also feels the boundaries later than constant compressibility viscosity solution, as it seen clearly in Figure 6.18.

In order to calculate $\sqrt{kx_f}$ values, Eq. 6.14 will be used again. However, this time correction factor can't be used, because $m(p_{wf})$ value is changing with time and that's make it impossible to calculate constant D_D value which is the only input of correction factor.

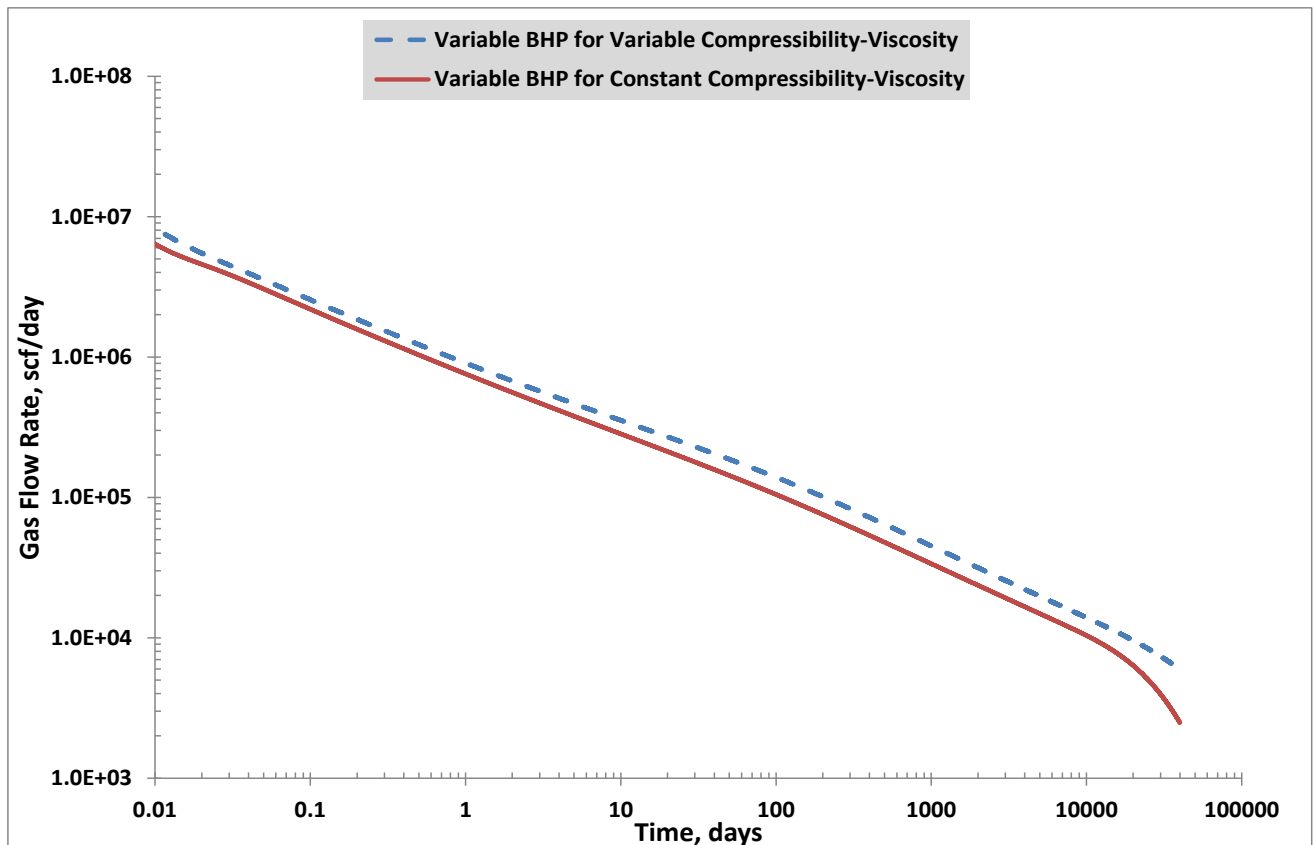


Figure 6.17: Boundary effects on square root of time plot.

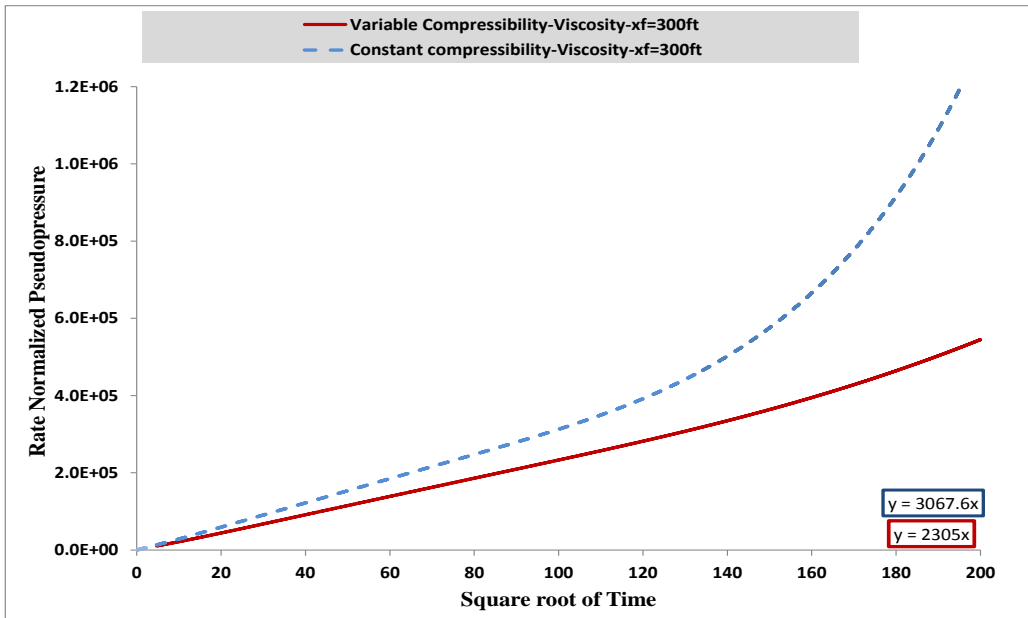


Figure 6.18: Square root of time plot for variable pressure production.

With these slope values, variable compressibility-viscosity solution gives 7.65 value for $\sqrt{k}x_f$ and constant product assumption gives 5.74 value. If these results are compared with input values (5.679), variable product solution's result contains 35%, constant product solution contains 1% error.

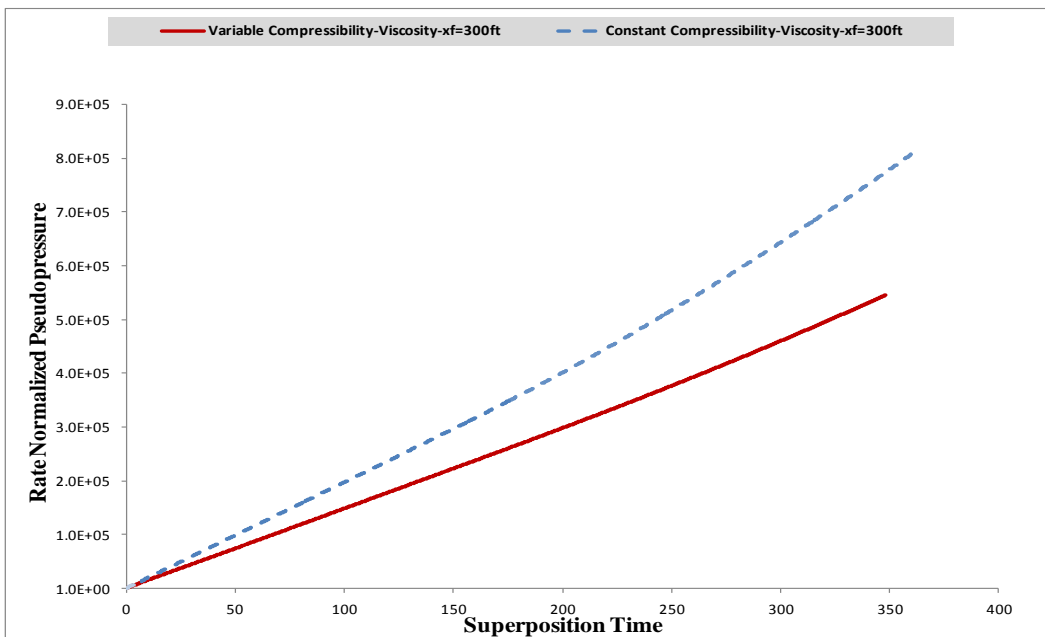


Figure 6.19: Superposition time plot variable pressure production.

Superposition time analysis gives the close results to square root of time results. Calculated slope values of Superposition time plot can be seen in Figure 6.19. With these slopes information, calculated $\sqrt{kx_f}$ values from Eq. 6.18 are 5.68 and 7.49 for constant and variable compressibility-viscosity solutions, respectively.

6.6 Sensitivity Analysis of Spectral Solution

As noted earlier, the accuracy of the spectral solution is sensitive to the number of the collocation points used in the Chebyshev spatial approximation. Collocation methods are similar to finite-difference methods in the sense of setting grid points, which are called collocation points (x_n) (Costa, 2004). In generating the spectral solution results presented thus far, 120 collocation points have been used. In this section, 10, 75 and 150 collocation points will be used to examine the sensitivity of the spectral solution for the variable-pressure production condition. In general, using fewer collocation points reduces the physical memory requirement and the computation time, but may cause convergence problems.

In the sensitivity analysis, a variable-pressure-production scenario according to the Weibull wellbore boundary condition model has been used (Fig. 6.20). Pressure-independent and pressure-dependent compressibility-viscosity solutions are considered separately in Figs. 6.21 and 6.22, respectively.

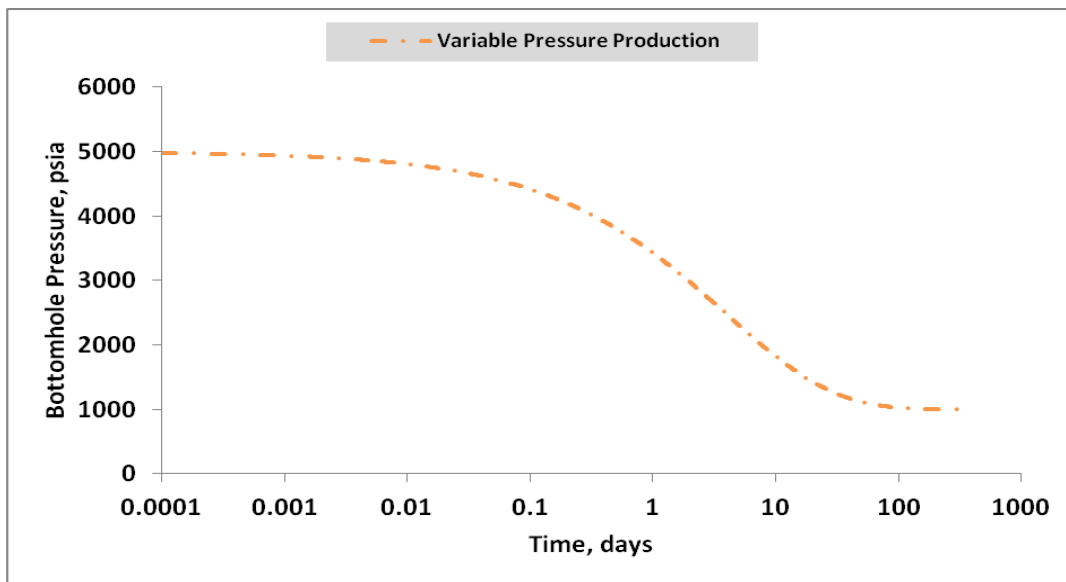


Figure 6.20: Variable Pressure production with Weibull regression model to analyze spectral solution sensitivity.

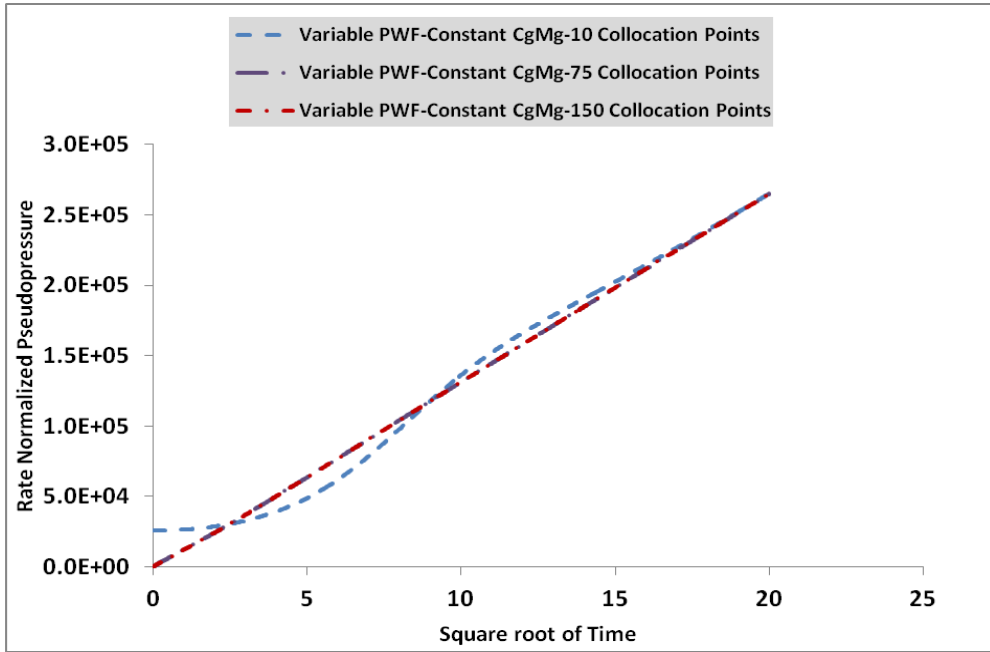


Figure 6.21: Constant viscosity-compressibility solution for 10, 75, and 150 collocation points for variable-pressure production case.

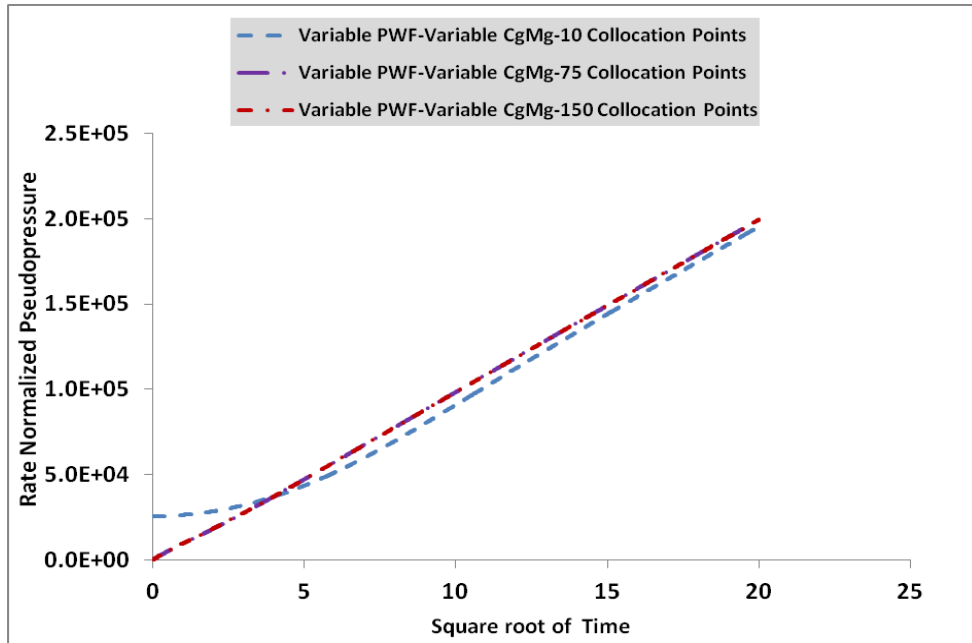


Figure 6.22: Variable viscosity-compressibility solution for 10, 75, and 150 collocation points for variable-pressure production.

In Fig. 6.21, 75 and 150 collocation points yield the same solution for the constant compressibility-viscosity product case; however the spectral solution with 10 collocation points converges to the solutions for the 75 and 150 collocation points after 225 days. Fig. 6.22 displays similar results to Fig. 6.21 for the variable viscosity-compressibility product case. In this case, the spectral solution with 10 collocation points converges to the solutions for the 75 and 150 collocation points much slower than the constant compressibility-viscosity product case (the convergence does not happen even even after 400 days).

CHAPTER 7

APPLICATIONS OF THE NEW SUPERPOSITION TIME

In this chapter, two synthetic examples are considered to demonstrate the application of the new gas superposition time. In each case, the rate-normalized pseudo-pressures are analyzed to obtain $\sqrt{k}x_f$ by using the square root of time, conventional superposition time, and the new gas superposition time to show the improvement of the analysis by the gas superposition time.

The following equations are used to obtain $\sqrt{k}x_f$ from the slopes, m_{srt} , m_{st} , and m_{gst} , corresponding to the Cartesian plots of the normalized pseudo-pressure vs. square-root-of-time, conventional superposition time, and the new gas superposition time, respectively:

$$\sqrt{k}x_f = \frac{315}{h\sqrt{\phi(c_t \mu_g)_i}} \frac{T}{m_{srt}} \quad (7.1)$$

$$\sqrt{k}x_f = \frac{200.5}{h\sqrt{\phi(c_t \mu_g)_i}} \frac{T}{m_{gst}} \quad (7.2)$$

$$\sqrt{k}x_f = \frac{200.5}{h\sqrt{\phi(c_t \mu_g)_i}} \frac{T}{m_{st}} \quad (7.3)$$

Eqs. 7.1 through 7.3 assume that the rate-normalized pseudo-pressures, m_{wf}/q_{sc} , are in $\text{psia}^2/\text{Mscf-cp}$.

Two sets of synthetic data have been generated for the analyses presented in this chapter by using the spectral solution presented in Chapters 4 and 6. For both examples, the reservoir is assumed to be infinite acting; that is, we have linear flow for all times. For the first case, the rational model given by Eq. 6.2 in Table 6.2 has been used for the inner boundary condition to generate the production-rate data. For Case 2, the production data have been computed by imposing the Weibull model as the inner boundary condition (Eq. 6.4 in Table 6.2). For both cases, the reservoir parameters have remained the same as in Table 6.1.

7.1 Case 1 - Linear Pressure Decline Based on the Rational Model

For the data used in this case, the wellbore boundary condition has been set up for a steep, linear pressure decline to test the limit of the new gas superposition time. Figure 7.1 presents the bottomhole pressure and flow rate as a function of time.

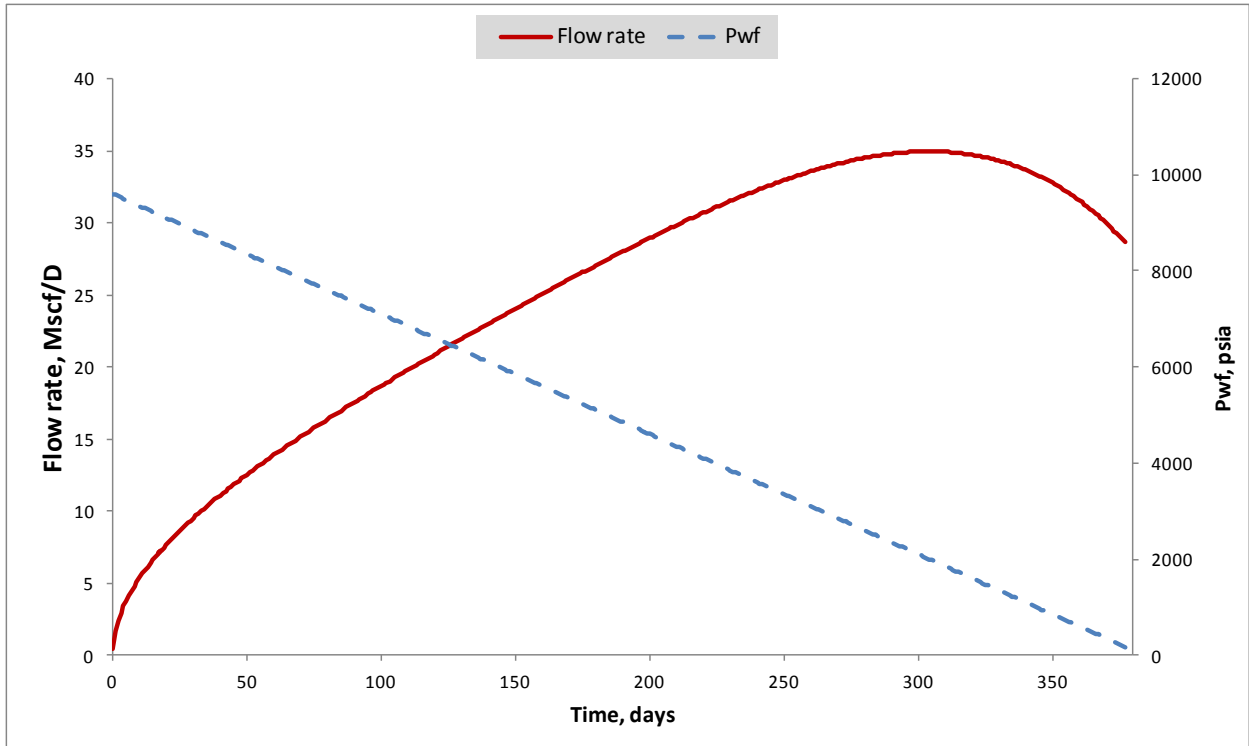


Figure 7.1: Wellbore pressure and flow rate as a function of time for Case 1.

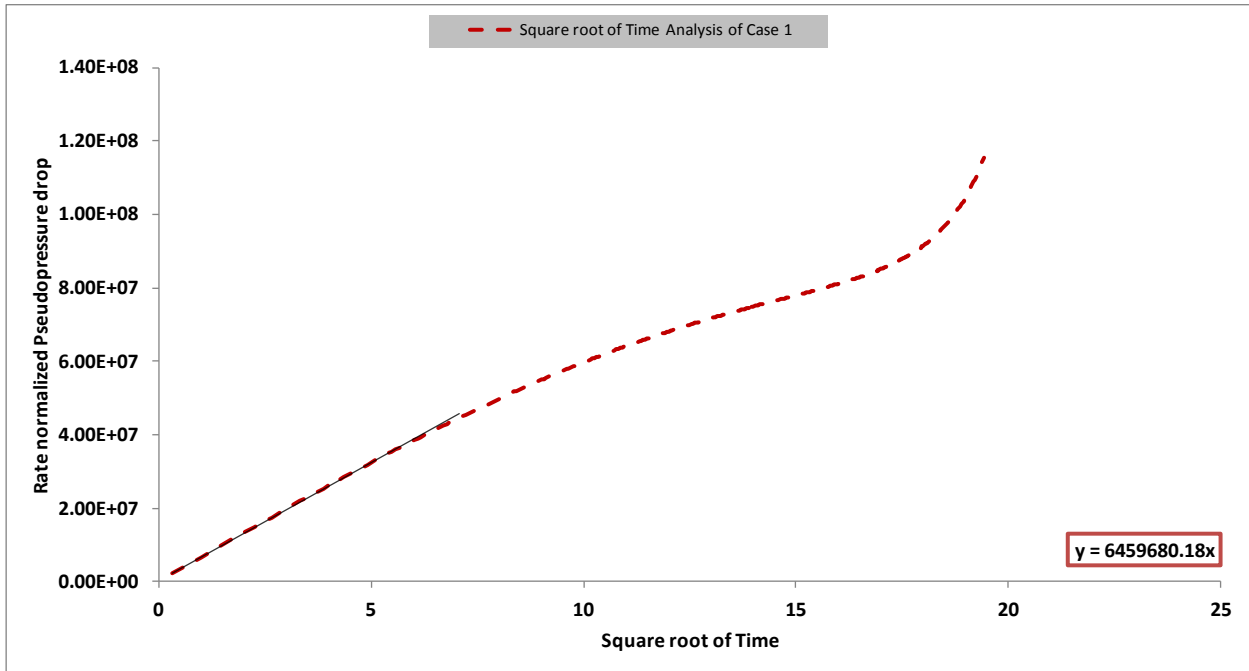


Figure 7.2: Square-root-of-time analysis of Case 1.

First, we analyze the data by plotting the normalized pseudo-pressure versus the conventional square root of time as shown in Fig. 7.2. Because the data have been generated for a linear-flow system, plotting pseudo-pressure versus square root of time would be expected to yield a straight line for all times if the flow rate were constant and the viscosity-compressibility product were not a function of pressure. As shown by Fig. 7.2, only the early portion of the plot displays a straight line because the rate is not constant and the viscosity-compressibility product changes with pressure. Using the slope of the straight line in Fig. 7.2 in Eq. 7.1, we obtain

$$\sqrt{k}x_f = 2.937 \sqrt{md}\text{-ft}$$

Next, we analyze the data by using the conventional superposition time and the new gas superposition time (Fig. 7.3). In this case, plotting normalized pseudo-pressure versus superposition time would be expected to account for the effects of variable rate (the data would form a straight line for all times) if the viscosity-compressibility product were constant. Fig. 7.3 shows that the pressure dependency of the viscosity-compressibility product causes normalized pseudo-pressure versus superposition time plot (blue line) to deviate from the straight-line behavior after the early times. On the other hand, the use of the new gas superposition time (dashed red line) makes the data to display a perfect straight-line trend for all times. This is an indication of the success of the new gas superposition time.

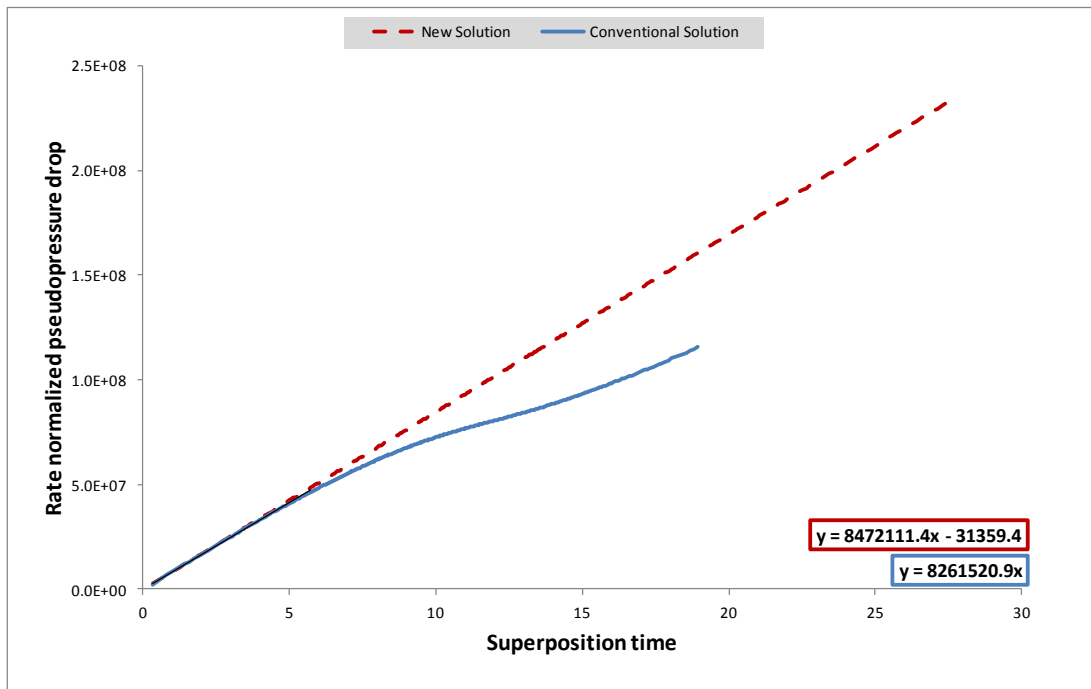


Figure 7.3: Comparison of the conventional and new, gas superposition time analyses - Case 1.

Using the slopes of the straight lines fitted to the blue and red dashed lines in Fig. 7.3, and the data given in Table 6.1, we obtain $\sqrt{k}x_f = 1.36$ and $1.324 \sqrt{md} - ft$, respectively from Eqs. 7.2 and 7.3. Comparisons of these results are summarized in the Table 7.1. As expected, the error in the square-root-of time analysis is very large because the bottomhole pressures are not constant or nearly constant. The error in the $\sqrt{k}x_f$ estimate from the conventional superposition time approach is 2.5% while it is only 0.07% for the new gas superposition time approach.

Solution Method	<i>Calculated values</i>	<i>Original inputs</i>	<i>Error, %</i>
<i>Square Root of Time</i>	$\sqrt{k}x_f = 2.937$	$\sqrt{k}x_f = 1.325$	121.6
<i>Conventional Superposition time</i>	$\sqrt{k}x_f = 1.358$	$\sqrt{k}x_f = 1.325$	2.48
<i>New Superposition time</i>	$\sqrt{k}x_f = 1.3243$	$\sqrt{k}x_f = 1.325$	0.07

7.2 Case 2 – Nonlinear Decline

Another variable pressure production scenario has been set up by using the Weibull bottomhole pressure model (Eq. 6.4 in Table 6.2). As shown in Fig. 7.4, the bottomhole pressure vs. time behavior resembles a sigmoid curve in this case. Also shown in Fig. 7.4 is the production rate vs. time corresponding to the specified bottomhole pressures. Same reservoir parameters as in Case 1 have been used in this example with the only exception of the fracture half-length ($x_f = 100$ ft).

The superposition time and square-root-of-time plots for this case are shown in Figs. 7.5 and 7.6 with the summary of the analyses given in Table 7.2. Similar to Case 1, in this case, the square-root-of-time plot does not yield acceptable estimates. Even though the conventional superposition-time plot displays a better straight-line trend, the error in the result is higher than the corresponding case in Case 1 (Table 7.1). Similarly, the new gas superposition time solution yields an almost perfect straight-line trend with a high rate of accuracy.

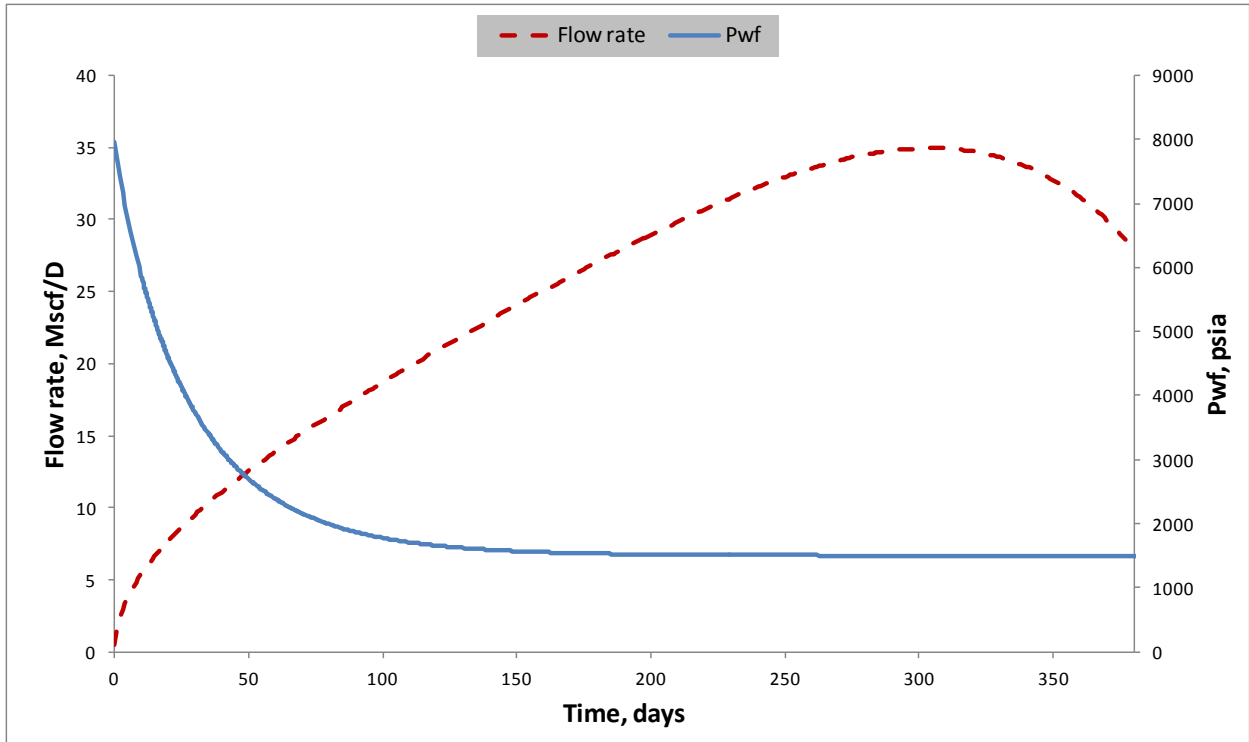


Figure 7.4: The bottomhole pressures from the Weibull model and the corresponding flow rate trend - Case 2.

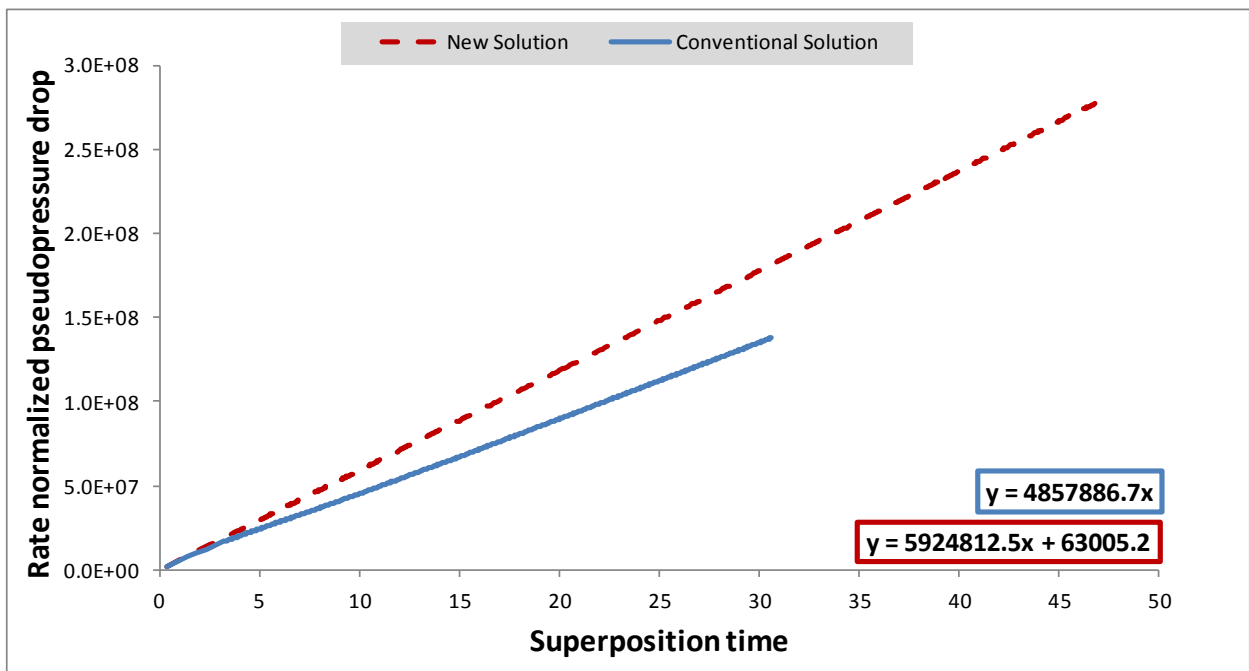


Figure 7.5: Comparison of the new and conventional superposition time solution - Case 2.

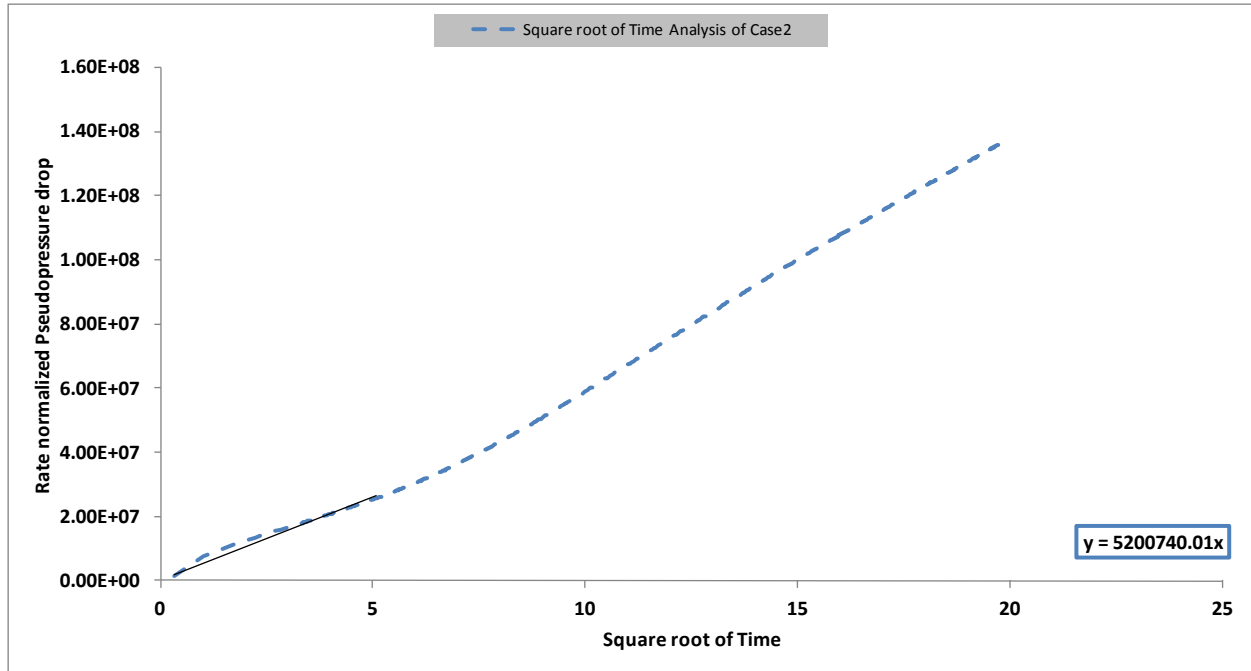


Figure 7.6: Square root of time analysis - Case 2.

TABLE 7.2: COMPARISON OF THE SPECILAZED SOLUTIONS AND THE NEW METHOD-CASE 2			
Solution Method	<i>Calculated values</i>	<i>Original inputs</i>	<i>Error, %</i>
<i>Square Root of Time</i>	$\sqrt{k}x_f = 3.388$	$\sqrt{k}x_f = 1.89314$	78.9
<i>Conventional Superposition Time</i>	$\sqrt{k}x_f = 2.309$	$\sqrt{k}x_f = 1.89314$	21.9
<i>New Superposition Time</i>	$\sqrt{k}x_f = 1.8932$	$\sqrt{k}x_f = 1.89314$	0.03

CHAPTER 8

CONCLUSIONS AND RECOMMENDATIONS

The main goal of this study was to investigate the effect of large compressibility-viscosity variations on tight-gas well performances. Different analysis techniques have been used in this study to demonstrate the shortcomings of the existing techniques and to highlight the need for improvements. Moreover, a new superposition time method has been presented and its results were compared with the results of the conventional analysis methods.

8.1 Conclusions

After documenting the challenges encountered in the analysis of tight-gas wells and presenting the semianalytical solutions that overcome the nonlinearity of gas-flow in these systems, the following conclusions were drawn:

- The validity of the spectral solution has been proved by the comparison of the results with the analytical solutions for both infinite and bounded systems. The spectral solution's accuracy has been tested and verified for both constant and variable pressure production cases.
- It has been shown that neglecting variable compressibility-viscosity conditions leads to underestimation of the flow rates in tight gas wells. The reason for this phenomenon is the underestimation of the gas compressibility, which is actually significantly higher than its in-situ values.
- Comparison of the finite-difference and spectral solution showed that the spectral solution yields higher accuracy with less computational time and effort. The finite-difference solutions require much smaller grid blocks than usual to capture the effect of the pressure dependent compressibility-viscosity changes.
- Spectral methods are less expensive than finite-difference methods for simple geometries. However, complex geometries may increase the complexity of the spectral solution and erode its advantages over finite-difference solutions.
- The conventional square-root-of-time analysis leads to the estimation of lower permeability values. Moreover, increasing drawdown causes larger errors.

- The use of the conventional superposition time does not sufficiently reduce the error in the estimates of $\sqrt{k}x_f$. Similarly, the correction factor method is incapable of improving the analysis for variable rate, variable pressure production conditions.
- Optimization of the run-time and the accuracy of the spectral solution require finding the optimal number of the collocation points. For simple geometries and homogenous reservoirs, 75 collocation points are normally sufficient.
- The use of the new superposition time defined in this study has yielded up to 99% accuracy in the estimation of $\sqrt{k}x_f$ in synthetic examples.

8.2 Recommendations for Future Work

In this work, all solutions were derived assuming a linear, homogenous, infinite system. Furthermore, infinite-conductive hydraulic fractures were assumed. To analyze more realistic cases, additional complexities should be incorporated into the models and tested. The following suggestions may help future research:

- The perturbation solution should be extended to apply under boundary dominated flow conditions
- Pressure dependent permeability and the Klinkenberg effect should be incorporated into the solutions.
- The effects of skin and finite fracture conductivity should also be investigated in future studies.

WORKS CITED

- Abate, J. and Valkó, P.P., 2004. Multi-precision Laplace transform inversion, *International Journal for Numerical Methods in Engineering*, Vol. 60 (Iss. 5-7) 2004, pp 979–993.
- Agarwal, R.G. 1980. A New Method to Account for Producing Time Effects When Drawdown Type Curves Are Used to Analyze Pressure Buildup and Other Test Data. Paper SPE 9289 presented at the SPE Annual Technical Convention and Exhibition, Dallas, TX, 21-24 Sep.
- Agarwal, R.G., Gardner, D.C., Kleinstieber, S.W., and Fussell, D.D., 1999. Analyzing Well Production Data Using Combined-Type-Curve and Decline-Curve Analysis Concepts. Paper SPE 49222 presented at the SPE Annual Technical Conference and Exhibition held in New Orleans, Louisiana, 27-30 September 1998
- Ahmadi, M. 2012. Laplace Transform Deconvolution and Its Application to Perturbation Solution of Nonlinear Diffusivity Equation. PhD Dissertation. Colorado School of Mines, Golden, Colorado.
- Al-Hussainy, R., Ramey, H.J., Crawford, P.B. 1965. The Flow of Real Gases Through Porous Media. *Journal of Petroleum Technology*, May 1966, pp 624-636
- Barreto, A. B., Peres, A., and Pires, A. P. 2012. A Variable-Rate Solution to the Nonlinear Diffusivity Gas Equation by Use of Green's Function Method. Paper SPE 145468 presented at the 2011 SPE Annual Technical Conference and Exhibition. Denver, Colorado, 30 October-2 November.
- Carslaw, H.S. and Jaeger, J.C. 1959. *Conduction of Heat in Solids*. Second Edition, Oxford University Press, Oxford, England.
- Cartwright, D. J. 2001. *Underlying Principles of the Boundary Element Method*. WIT Press. Southampton, UK.
- Cinco-Ley, H. and Samaniego, F.V. 1989. Use and Misuse of the Superposition Time Function in Well Test Analysis. Paper SPE 19817 presented at the 1989 SPE Annual Technical Conference and Exhibition, San Antonio, Texas, 8-11 October.
- Costa, B. 2004, *Spectral Methods for Partial Differential Equations*. CUBO A Mathematical Journal, Vol 6, No. 4, pp 1-32, December 2004
- Dalen, V. 1979. Simplified Finite-Element Models for Reservoir Flow Problems. *Society of Petroleum Engineers Journal*, pp 333-343, October 1979.
- Divo, E.A. and Kassab, A.J. 2003. *Boundary Element Methods for Heat Conduction: With*

- Applications in Non-Homogeneous Media. WIT Press, Southampton, UK.
- Durlofsky, L.J. and Chien M.C.H. 1993. Development of a Mixed Finite-Element-Based Compositional Reservoir Simulator. Paper SPE 25253 presented at the SPE Symposium on Reservoir Simulation, 28 February-3 March, New Orleans, Louisiana
- El-Banbi, A.H. and Wattenbarger, R.A. 1998. Analysis of Linear Flow in Gas Well Production. Paper SPE 39972 presented at the 1998 SPE Gas Technology Symposium, Calgary, 15-18 March.
- Gupta, K.C., Andsager, R.L. 1967. Application of Variable Rate Analysis Technique to Gas Wells. Paper SPE 1836 presented at the 42nd Annual Fall Meeting of Petroleum Engineers of AIME, Houston, Texas, 1-4 October 1967.
- Fetkovich, M. J. and Vienot, M. E. 1984. Rate Normalization of Buildup Pressure by Using Afterflow Data. JPT (Dec.): 2211-2224.
- Forsyth, P.A. 1990. A Control-Volume Finite-Element Method for Local Mesh Refinement. Paper SPE 18145 SPE Reservoir Engineering Journal, pp 561-566, November 1990.
- Fung, L.S., Hiebert, A.D. and Nghiem, L.X. 1991. Reservoir Simulation with a Control-Volume Finite Element Method. Paper SPE 21224 presented at the 11th Symposium on Reservoir Simulation, Anaheim, CA. 17-20, Feb.
- Ibrahim, M.H. 2004. History matching pressure response functions from production data. PhD Dissertation. Texas A&M University, College Station, Texas.
- Ibrahim, M. and Wattenbarger, R.A. 2006. Analysis of Rate Dependence in Transient Linear Flow in Tight Gas Wells. Paper SPE 100836 presented at the 2006 Abu Dhabi International Petroleum Exhibition and Conference held in Abu Dhabi, United Arab Emirates, 5-8 November.
- Kale, D. and Mattar, L., 1980. Solution of a nonlinear gas flow equation by the perturbation technique, JCPT, PETSOC 80-04-06, pp. 63-67.
- Kikani, J. and Horne, R.N. 1992. Pressure-Transient Analysis of Arbitrarily Shaped Reservoirs With the Boundary-Element Method. Paper SPE 18159 SPE Formation Evaluation Journal, pp 53 – 60, March 1992
- Kohlhaas, C. A., del Giudice, C., and Abbott, W. A. 1982. Application of Linear and Spherical Flow Analysis Techniques to Field Problems-Case Studies. Society of Petroleum Engineers. Paper SPE 11088 presented at SPE Annual Technical Conference and

- Exhibition, 26-29 September, New Orleans, Louisiana
- Krogstad, S., Hauge, V.L., and Gulbransen, A. 2011. Adjoint Multiscale Mixed Finite Elements. Paper SPE 119112 presented at the SPE Reservoir Simulation Symposium held in The Woodlands, Texas, 2-4 February 2009
- Liang, P., Mattar, L., Moghadam, S. 2011. Analyzing Variable Rate/Pressure Data in Transient Linear Flow in Unconventional Gas Reservoirs. Paper CSUG/SPE 149472 presented at the Canadian Unconventional Resources Conference, Calgary, Alberta, Canada, 15-17 November 2011.
- Lodono, F.E., Archer, R.A., Blasingame, T.A. 2002. Simplified Correlations for Hydrocarbon Gas Viscosity and Gas Density-Validation and Correlation of Behavior Using a Large-Scale Database. Paper SPE 75721 presented at the SPE Gas Technology Symposium held in Calgary, Alberta, Canada, 30 April-2 May 2002.
- Miller, E.E. 1956. Physical theory for capillary flow phenomena. *Journal Application Physics*, 27, pp 324-332.
- Muskat, M. 1937. *The Flow of Homogeneous Fluid Through Porous Media*. McGraw-Hill, New York
- Palacio, J.C. and Blasingame, T.A. 1993. Decline-Curve Analysis Using Type Curves – Analysis of Gas Well Production Data. Paper SPE 25909, presented at the SPE Joint Rocky Mountain Regional and Low Permeability Reservoir Symposium, April 26-28, Denver Colorado.
- Peres, A.M.M., Serra, K.V., Reynolds, A.C., 1989. Toward a Unified Theory of Well Testing for Nonlinear-Radial-Flow Problems With Applications to Interference Tests. Paper SPE 18113, appeared in a *Society of Petroleum Engineering Journal* 1989
- Poe, B.D. 2002. Effective Well and Reservoir Evaluation Without the Need for Well pressure History. Paper SPE 77691, presented at the SPE Annual Technical Conference and Exhibition, 29 September – 2 October, San Antonio, Texas.
- Press, W.H., Teukolsky, S.A., Vetterling, W.T. et al., 2007. *Numerical Recipes-The Art of Scientific Computing*, third edition. Cambridge University Press
- Raghavan, R. 1993. *Well Test Analysis*, Prentice-Hall, New Jersey.
- Samaniego, F., and Cinco-Ley, H. 1991. Transient pressure analysis for variable rate testing of gas wells, Low Permeability Reservoirs Symposium, Denver, Colorado, SPE Paper 21831

- Sato, K. and Horne, R.N. 1993a. Perturbation Boundary Element Method for Heterogeneous Reservoirs: Part 1-Steady-State Flow Problems. Paper SPE 25299 SPE Formation Evaluation Journal, pp 306 – 314, December 1993
- Sato, K. and Horne, R.N. 1993b. Perturbation Boundary Element Method for Heterogeneous Reservoirs: Part 2-Transient Flow Problems. Paper SPE 25300 SPE Formation Evaluation Journal, pp 315 – 322,
- Schlumberger, Eclipse Reference Manual. 2013. Version 2013.1
- Stright, D.H. and Gordon, J.I. 1983. Decline Curve Analysis in Fractured Low Permeability Gas Wells in the Piceance Basin. Paper SPE/DOE 11640 presented at the SPE/DOE Low Permeability Symposium, Denver, Co, 14-16 March 1983
- Thompson, L. 2012. Flow to a Vertically Fractured Well in a Tight Gas Reservoir. Personal Communication.
- Thompson, L. 2012. Characterization of Flow in Fractured Tight Gas Reservoirs. Personal Communication.
- Thompson, L. 2014. “Spectral Solution Code for Tight Gas Flow Analysis” Personal Communication
- Trefethen, Lloyd N. 2000. Spectral Methods in Matlab. Society for Industrial and Applied Mathematics, Philadelphia.
- Walker, A.C. 1968. Estimating Reservoir Pressure using the Principle of Superposition. Second Regional Technical Symposium in 1968, Society of Petroleum Engineers of AIME.
- Wattenbarger, R.A., El-Banbi, A.H., Villegas, M.E., and Maggard, J.B. 1998. Production Analysis of Linear Flow into Fractured Tight Gas Wells. Paper SPE 39931 presented at the 1998 SPE Rocky Mountain Regional/Low Permeability Reservoirs Symposium and Exhibition, Denver, 5-8 April.
- Whitson, C.H. and Sognesand S.1986. Application of the Van Evendingen-Meyer Method for Analyzing Variable-Rate Well Tests. Paper SPE 15482 presented at the 1986 SPE Annual Technical Conference and Exhibition, New Orleans, 5-8 October.
- Van Everdingen, A.F. and Hurst, W. 1949. The Application of the Laplace Transformation to Flow Problems in Reservoirs. Paper T.P. 2732 presented at the AIME Annual Meeting in San Francisco, February 13-17, 1949

- Veena, R., Megeri, S.N., Patil, S.J., Bhat, A.R.S., n.d. Statistical Models to Predict the Height of Different Tree Species in the Agroforestry System. <http://www.share-pdf.com/e67e1d68d5624be5aaa6ba41151c3718/E-Journal%20Artical.htm> , (downloaded 8 August 2014).
- Young, L.C. 1981. A Finite-Element Method for Reservoir Simulation. Society of Petroleum Engineers Journal, pp 115-128, February 1981
- Zhou, W., Samson, B., Krishnamurthy, S., Tilke, P., Banerjee, R., Spath, J., and Thambynayagam, M. 2013. Analytical Reservoir Simulation and Its Applications to Conventional and Unconventional Resources. Paper SPE 164882, presented at the EAGE Annual Conference and Exhibition incorporating SPE Europec, 10-13 June, London, UK.